

การศึกษาพฤติกรรมแอสฟัลติกคอนกรีตโดยการทดสอบและการวิเคราะห์เชิงตัวเลขภายใต้
สภาพแวดล้อมเขตร้อน



นายฉนกร ชมภูรัตน์

ศูนย์วิทยทรัพยากร

วิทยานิพนธ์นี้เป็นส่วนหนึ่งของการศึกษาตามหลักสูตรปริญญาวิศวกรรมศาสตรดุษฎีบัณฑิต

สาขาวิชาวิศวกรรมโยธา ภาควิชาวิศวกรรมโยธา

คณะวิศวกรรมศาสตร์ จุฬาลงกรณ์มหาวิทยาลัย

ปีการศึกษา 2552

ลิขสิทธิ์ของจุฬาลงกรณ์มหาวิทยาลัย

AN EXPERIMENTAL AND NUMERICAL STUDY OF ASPHALTIC CONCRETE
UNDER TROPICAL ENVIRONMENTS

Mr. Thanakorn Chompoorat




ศูนย์วิทยทรัพยากร
จุฬาลงกรณ์มหาวิทยาลัย

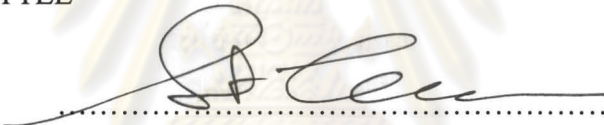
A Dissertation Submitted in Partial Fulfillment of the Requirements
for the Degree of Doctor of Philosophy in Civil Engineering
Department of Civil Engineering
Faculty of Engineering
Chulalongkorn University
Academic Year 2009
Copyright of Chulalongkorn University

Thesis Title AN EXPERIMENTAL AND NUMERICAL STUDY OF ASPHALTIC
CONCRETE UNDER TROPICAL ENVIRONMENTS
By Mr. Thanakorn Chompoorat
Field of Study Civil Engineering
Thesis Advisor Assistant Professor Suched Likitlersuang, D.Phil

Accepted by the Faculty of Engineering, Chulalongkorn University in Partial
Fulfillment of the Requirements for the Doctoral Degree


..... Dean of the Faculty of Engineering
(Associate Professor Boonsom Lerdhirunwong, Dr.Ing.)


THESIS COMMITTEE


..... Chairman
(Associate Professor Supot Teachavorasinskun, D.Eng.)


..... Thesis Advisor
(Assistant Professor Suched Likitlersuang, D.Phil)

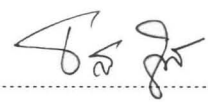
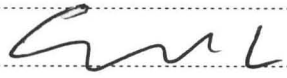

..... Examiner
(Associate Professor Boonchai Ukritchon, Sc.D.)


..... Examiner
(Associate Professor Tirawat Boonyatee, D.Eng.)


..... External Examiner
(Assistant Professor Kunnawee Kanitpong, Ph.D.)

ธนกร ชมภูรัตน์: การศึกษาพฤติกรรมแอสฟัลติกคอนกรีตโดยการทดสอบและการวิเคราะห์เชิงตัวเลขภายใต้สภาพแวดล้อมเขตร้อน. (An experimental and numerical study of asphaltic concrete under tropical environments) อ. ที่ปรึกษาวิทยานิพนธ์หลัก: ผศ. ดร. สุเชษฐ์ ถิचितเลอสรวง, 108 หน้า.

แอสฟัลติกคอนกรีตเป็นวัสดุก่อสร้างที่สำคัญในงานก่อสร้างถนนแบบยึดหยุ่น โดยพฤติกรรมของวัสดุแอสฟัลติกคอนกรีตมีความซับซ้อนมากโดยเฉพาะพฤติกรรมที่ขึ้นกับการเปลี่ยนแปลงของอุณหภูมิและ/หรืออัตราความเครียด สำหรับการออกแบบโครงสร้างถนนในประเทศไทยยังคงอ้างอิงมาตรฐานการออกแบบของต่างประเทศ มาตรฐานการออกแบบส่วนมากมักพัฒนามาจากฐานข้อมูลการทดสอบที่ทำในสภาพแวดล้อมของประเทศนั้น ๆ ซึ่งอาจไม่เหมาะสมถ้าจะนำข้อมูลผลการทดสอบตลอดจนวิธีการออกแบบของต่างประเทศมาใช้กับประเทศไทย ดังนั้นงานวิจัยฉบับนี้มุ่งเน้นศึกษาพฤติกรรมของแอสฟัลติกคอนกรีตภายใต้การเปลี่ยนแปลงของอุณหภูมิและการเปลี่ยนแปลงอัตราที่สอดคล้องกับการใช้งานในประเทศเขตร้อนอย่างประเทศไทย การศึกษานี้แบ่งออกเป็น 2 ส่วน คือ การศึกษาพฤติกรรมแอสฟัลติกคอนกรีตในห้องปฏิบัติการ และการวิเคราะห์ผลการทดสอบและจำลองพฤติกรรมแอสฟัลติกคอนกรีต การศึกษาในส่วนแรกประกอบไปด้วยการทดสอบ 4 ชนิด คือ การทดสอบแรงดึงทางอ้อมทั้งแบบสถิตและแบบวัฏจักร และการทดสอบกำลังรับแรงอัดแกนเดี่ยวทั้งแบบสถิตและแบบวัฏจักร หลังจากนั้นนำผลการทดสอบทั้งหมดมาวิเคราะห์โดยใช้หลักเกณฑ์ทั่วไปทางวิศวกรรมผิวทาง และวิเคราะห์ด้วยหลักการซ้อนทับกันระหว่างเวลากับอุณหภูมิ โดยผลการวิเคราะห์ทั้งหมดสามารถนำไปสร้างเป็นฐานข้อมูลสำหรับนำไปใช้ในการออกแบบภายในประเทศต่อไป สำหรับการศึกษานี้ในส่วนที่สองจะทำการจำลองพฤติกรรมแอสฟัลติกคอนกรีตด้วยการใช้แบบจำลองความสัมพันธ์ความเค้นและความเครียดที่อ้างอิงทฤษฎีไฮเพอร์พลาสติกซิตี โดยจุดเด่นของทฤษฎีไฮเพอร์พลาสติกซิตีคือการนิยามกฎความเค้นและความเครียดของวัสดุกระทำได้ด้วยการกำหนดค่าสมการพลังงานและสมการการไหลเพียงสองสมการ นอกจากนั้นแบบจำลองดังกล่าวได้ผนวกเอาหลักการโคเนมาติกฮาร์ดเดนนิงและหลักการพลาสติกซิตีแบบขึ้นกับอัตรามาใช้ด้วย จากแบบจำลองที่อ้างอิงทฤษฎีและหลักการข้างต้นที่พัฒนาขึ้น เราสามารถนำมาสอบเทียบกับผลการทดลองเพื่อสรุปค่าพารามิเตอร์ของแบบจำลองนี้ ซึ่งอาจสามารถนำไปประยุกต์ใช้กับการวิเคราะห์เชิงตัวเลขต่อไปในอนาคตได้

ภาควิชา _____ วิศวกรรมโยธา _____ ลายมือชื่อนิสิต 
 สาขาวิชา _____ วิศวกรรมโยธา _____ ลายมือชื่อ อ.ที่ปรึกษาวิทยานิพนธ์หลัก 
 ปีการศึกษา _____ 2552 _____

497 18135 21: MAJOR CIVIL ENGINEERING

KEYWORDS: ASPHALTIC CONCRETE / TEMPERATURE AND STRAIN RATE EFFECTS / EXPERIMENTAL TESTS / TIME-TEMPERATURE SUPERPOSITION / HYPERPLASTICITY

THANAKORN CHOMPOORAT: AN EXPERIMENTAL AND NUMERICAL STUDY OF ASPHALTIC CONCRETE UNDER TROPICAL ENVIRONMENTS. THESIS ADVISOR: ASST. PROF. SUCHED LIKITLERSUANG, D.Phil., 108 pp.

The asphaltic concrete is an essential material for flexible pavement construction. Its behaviour is however so complicated, especially the behaviour depended on the change of temperature and/or strain rate. The pavement design of Thailand has been still based on the standard of foreign countries. In fact most of them were created and developed based on the database observed under their environments. Those databases and methods from foreign countries may not be suitable to the condition of Thailand thereby this research focuses on the asphaltic concrete behaviour under the various temperatures and the changing rates which relate to the environment in the tropical countries such as Thailand. This study consists of two main parts which are to study the asphaltic concrete behaviour based on the laboratory test and to analyse the test result and then to model the asphaltic concrete behaviour. The former is composed of four tests which are the static and the cyclic indirect tensile tests and the static and the cyclic unconfined compress tests. All test results are analysed using the conventional pavement engineering method such as analyses result employing the time-temperature superposition. By all results of analysis they can be next used to produce the database for the road design in Thailand. The later studied the behaviour of asphaltic concrete can be used to validate the constitutive model based on the hyperplasticity theory. The main feature of this theory is that it enables to define the constitutive law by setting the potential energy equation and the flow potential equation. This constitutive model also relies on the kinematic hardening plasticity and the rate-dependent plasticity principle. Following this study both the model and the parameters can be future benefits to numerical application in the pavement analysis and design.

Department : Civil Engineering Student's Signature T. Chompoorat
 Field of Study : Civil Engineering Advisor's Signature Suched Likitlersuang
 Academic Year : 2009

ACKNOWLEDGEMENTS

This thesis would not have been smooth without the significant supports, the valuable advices and the guidance of my advisor, Assistant Professor Suched Likitlersuang. I would profoundly like to appreciate his great and eternal efforts to me.

I would like to extend my intense thankfulness to Associate Professor Tirawat Boonyatee for his suggestion of use of data collecting system and the advice of use of software programme to evaluate the testing data. I am obliged to the scholarship of Professor Dr. Supradit Bunnag funds for my research expense. I am also very thankful for all my lecturers at Geotechnical Engineering Chulalongkorn University for providing the knowledge. I am furthermore particularly grateful to Miss Roajjane Manvongvirot who gave me the best supports, the immortal willpower and her patience. Especially, it was very kind of her on the correction throughout my English writing. I also want to thank Mr. Nattawut Hematurin for all his assistance and the materials supplied on my study. I take this opportunity to thank all my friends at Chulalongkorn University.

Last but not least, I would like to give my special thanks to my family. Without their continuous supports, encouragement and love, I could not have successfully gone through all the difficulty I faced.

ศูนย์วิทยทรัพยากร
จุฬาลงกรณ์มหาวิทยาลัย

TABLE OF CONTENTS

| | Page |
|--|------|
| ABSTRACT (IN THAI) | iv |
| ABSTRACT (IN ENGLISH) | v |
| ACKNOWLEDGEMENTS | vi |
| TABLE OF CONTENTS | vii |
| LIST OF TABLES | x |
| LIST OF FIGURES | xi |
| LIST OF SYMBOLS | xv |
| CHAPTERS | |
| 1 Introduction | |
| 1.1 Research background | 1 |
| 1.2 Research objectives..... | 3 |
| 1.3 Research methodology | 4 |
| 1.4 Research expected contribution | 5 |
| 2 Literature review | |
| 2.1 Introduction..... | 6 |
| 2.2 Flexible pavement structure | 6 |
| 2.3 Failure criteria in flexible pavement | 8 |
| 2.3.1 Permanent deformation | 8 |
| 2.3.2 Thermal cracking or Horizontal cracking | 9 |
| 2.3.3 Fatigue cracking or Alligator cracking | 10 |
| 2.4 Problem and Improvement..... | 10 |
| 2.5 Critical stress/strain of flexible pavement..... | 11 |
| 2.6 Asphaltic concrete behaviour..... | 13 |
| 2.7 Characteristic of asphaltic concrete | 15 |
| 2.7.1 Resilient modulus..... | 15 |
| 2.7.2 Permanent deformation | 17 |
| 2.8 Constitutive model for asphaltic concrete..... | 20 |
| 2.8.1 Viscoelastic model | 20 |

| | Page |
|---|------|
| 2.8.2 Viscoelastic damage model..... | 23 |
| 2.8.3 Elasto-visco-plastic model..... | 24 |
| 2.8.4 Elasto-visco-plastic model (Schapry continuum model) | 25 |
| 2.9 Time-temperature superposition | 26 |
| 2.10 Rate process theory | 28 |
| 2.11 Hyperplasticity approach | 29 |
| 2.12 Summary | 32 |
| 3 Experimental programme | |
| 3.1 Introduction..... | 33 |
| 3.2 Material properties | 33 |
| 3.3 Specimen preparations | 34 |
| 3.4 Test apparatuses | 35 |
| 3.5 Experimental procedures | 37 |
| 3.5.1 Static and cyclic indirect tensile tests | 37 |
| 3.5.2 Static and cyclic unconfined compression tests..... | 40 |
| 3.6 Experimental results..... | 41 |
| 3.6.1 Static indirect tensile test (S-IDT) | 41 |
| 3.6.2 Static unconfined compression test (S-UC)..... | 45 |
| 3.6.3 Cyclic indirect tensile test (C-IDT)..... | 47 |
| 3.6.4 Cyclic unconfined compression test (C-UC) | 48 |
| 3.7 Summary | 50 |
| 4 Analysis of experimental result | |
| 4.1 Introduction..... | 51 |
| 4.2 Static indirect tensile test (S-IDT) | 51 |
| 4.3 Static unconfined compression test (S-UC)..... | 53 |
| 4.4 Cyclic indirect tensile test (C-IDT)..... | 56 |
| 4.5 Cyclic unconfined compression test (C-UC) | 58 |
| 4.6 Time-temperature superposition | 61 |
| 4.7 Summary | 62 |
| 5 Development of new constitutive model for asphaltic concrete | |
| 5.1 Introduction..... | 63 |

| | Page |
|--|------|
| 5.2 Constitutive equations..... | 63 |
| 5.3 Model calibration and effect of temperature..... | 65 |
| 5.4 Summary | 75 |
| 6 Numerical prediction | |
| 6.1 Introduction..... | 78 |
| 6.2 Numerical implementation..... | 78 |
| 6.3 Model prediction of static condition..... | 81 |
| 6.4 Model prediction of cyclic condition..... | 86 |
| 6.5 Summary | 90 |
| 7 Concluding and remarks | |
| 7.1 Introduction..... | 91 |
| 7.1 Numerical implementation..... | 91 |
| 7.2 Experimental tests..... | 92 |
| 7.3 Time-temperature superposition | 93 |
| 7.3 Future study | 93 |
| REFERENCE | 95 |
| APPENDIX | 98 |
| BIOGRAPHY | 108 |

ศูนย์วิทยทรัพยากร
จุฬาลงกรณ์มหาวิทยาลัย

LIST OF TABLES

| | Page |
|---|------|
| Table 3.1 Testing programme for the indirect tensile test | 39 |
| Table 3.2 Testing programme for the unconfined compression test..... | 41 |
| Table 4.1 Summarise of stress-strain-strength values from S-IDT tests..... | 52 |
| Table 4.2 Summarise of stress-strain-strength values from S-UC tests..... | 54 |
| Table 5.1 Fitted parameter values of the viscoelastic damage model at different temperatures | 68 |
| Table 5.2 Curve fitted function parameters of the viscoelastic damage model at different temperatures | 68 |
| Table 5.3 Fitted parameter values of the rate-dependent hyperplasticity model at different temperatures ($\alpha_0 = 0.02$ and $a = 3.0$)..... | 70 |
| Table 5.4 Derived parameter values of the rate-dependent hyperplasticity model as functions of temperature ($\alpha_0 = 0.02$ and $a = 3.0$) | 70 |
| Table 5.5 List of experimental programme for model parameter determination based on unconfined compression test..... | 77 |
| Table 6.1 Summarised parameters of the rate-dependent hyperplasticity model for S-IDT and S-UC tests..... | 81 |
| Table 6.2 Summarised parameters of the rate-dependent hyperplasticity model for C-IDT and S-IDT tests..... | 87 |

LIST OF FIGURES

| | Page |
|--|------|
| Figure 2.1 Tropical cross section of a flexible pavement..... | 7 |
| Figure 2.2 (a) Distress of rutting (b) Distress of shoving..... | 9 |
| Figure 2.3 (a) Distress of thermal cracking (b) Distress of fatigue cracking | 10 |
| Figure 2.4 Critical stress and strain at each layer of flexible pavement..... | 12 |
| Figure 2.5 Asphaltic concrete affected of temperature and strain rate..... | 14 |
| Figure 2.6 Definition of resilient modulus | 15 |
| Figure 2.7 Resilient Modulus of short term oven aged SSDA and SSGDA mixes at 6.0% binder content (Meor and Teoh, 2008) | 16 |
| Figure 2.8 Result of the average of resilient modulus: five regions in Thailand (Phromsorn <i>et al.</i> , 2003) | 17 |
| Figure 2.9 (a) Typical relationship between total cumulative plastic strain and loading cycles (b) Regression constants <i>a</i> and <i>b</i> | 18 |
| Figure 2.10 Permanent deformation at 6500 cycles and stiffness (Jahromi and Khodaii, 2008)..... | 19 |
| Figure 2.11 Result of the accumulated strain of loading pulses (Thammavong and Lavansiri, 2003) | 19 |
| Figure 2.12 Mechanical models for viscoelastic materials | 21 |
| Figure 2.13 Elasto-visco-plastic model..... | 25 |
| Figure 2.14 Data shifting to construct master curve | 26 |
| Figure 2.15 Schematic of time-temperature superposition principle by using cross plot | 28 |
| Figure 2.16 Imitation of the activated energy of soil when it is forced by shear | 29 |
| Figure 3.1 Gradation of aggregate..... | 34 |
| Figure 3.2 Superpave gyratory compactor | 35 |
| Figure 3.3 (a) Instron UTM-1.2MN (b) Controls UTM-14kN..... | 36 |
| Figure 3.4 (a) Schematic of S-IDT test setup (b) Instruments for S-IDT test | 38 |
| Figure 3.5 Schematic of C-IDT test setup | 39 |
| Figure 3.6 Shape and condition of loading..... | 39 |

| | Page |
|--|------|
| Figure 3.7 (a) Schematic of S-UC test setup (b) Schematic of C-UC test setup | 41 |
| Figure 3.8 Stress-strain behaviour of S-IDT tests with different strain rates at 10°C..... | 42 |
| Figure 3.9 Stress-strain behaviour of S-IDT tests with different strain rates at 25°C..... | 43 |
| Figure 3.10 Stress-strain behaviour of S-IDT tests with different strain rates at 40°C..... | 43 |
| Figure 3.11 Stress-strain behaviour of S-IDT test at 55°C..... | 44 |
| Figure 3.12 Example of failure mechanism of asphaltic concrete under S-IDT test at (a) 10°C and strain rate of 0.0083/sec (b) 55°C and strain rate of 0.0008/sec | 44 |
| Figure 3.13 Stress-strain behaviour of S-UC tests with different strain rates at 10°C..... | 45 |
| Figure 3.14 Stress-strain behaviour of S-UC tests with different strain rates at 25°C..... | 46 |
| Figure 3.15 Stress-strain behaviour of S-UC tests with different strain rates at 40°C..... | 46 |
| Figure 3.16 Stress-strain behaviour of S-UC tests with different strain rates at 55°C..... | 47 |
| Figure 3.17 Typical failure mechanism of asphaltic concrete under S-UC test | 47 |
| Figure 3.18 Variation of resilient modulus with temperatures..... | 48 |
| Figure 3.19 Relation of strain and number of cycle for prediction the FN at 25°C..... | 49 |
| Figure 3.20 Relation of strain and number of cycle for prediction the FN at 40°C..... | 49 |
| Figure 3.21 Relation of strain and number of cycle for prediction the FN at 55°C..... | 50 |
| Figure 4.1 Variation of E^{50} with temperature of S-IDT tests..... | 52 |
| Figure 4.2 Variation of σ_{max} with temperature of S-IDT tests | 53 |
| Figure 4.3 Variation of ε_{peak} with temperature of S-IDT tests..... | 53 |

| | Page |
|--|------|
| Figure 4.4 Variation of E^{50} with temperature of S-UC tests..... | 55 |
| Figure 4.5 Variation of σ_{max} with temperature of S-UC tests | 55 |
| Figure 4.6 Variation of ε_{peak} with temperature of S-UC tests | 56 |
| Figure 4.7 Parametric study for C-IDT test..... | 57 |
| Figure 4.8 Relation of stress-strain at last cycle under C-IDT test | 57 |
| Figure 4.9 Relation of strain and number of cycle for producing the classic power-law model at 25°C | 58 |
| Figure 4.10 Relation of strain and number of cycle for producing the classic power-law model at 40°C | 59 |
| Figure 4.11 Relation of strain and number of cycle for producing the classic power-law model at 55°C | 59 |
| Figure 4.12 Variation of a parameter with temperature | 60 |
| Figure 4.13 Variation of b parameter with temperature | 60 |
| Figure 4.14 Stress-reduce time master curve from S-IDT and S-UC tests | 61 |
| Figure 4.15 Time-temperature shift function from S-UC and S-IDT tests | 62 |
| Figure 5.1 Curve fitting of series function of relaxation modulus | 66 |
| Figure 5.2 Material damage function $C(S)$ at 5°C | 66 |
| Figure 5.3 Material damage function $C(S)$ at 25°C | 67 |
| Figure 5.4 Material damage function $C(S)$ at 40°C | 67 |
| Figure 5.5 Material damage function $C(S)$ at 60°C | 68 |
| Figure 5.6 Variation of μ with temperature | 70 |
| Figure 5.7 Variation of μr with temperature..... | 71 |
| Figure 5.8 Variation of E_0 with temperature | 71 |
| Figure 5.9 Variation of k_0 with temperature..... | 72 |
| Figure 5.10 Stress-strain curve of asphaltic concrete at 5°C for different strain rates | 73 |
| Figure 5.11 Stress-strain curve of asphaltic concrete at 25°C for different strain rates | 73 |

| | Page |
|---|------|
| Figure 5.12 Stress-strain curve of asphaltic concrete at 40°C for different strain rates | 74 |
| Figure 5.13 Stress-strain curve of asphaltic concrete at 60°C for different strain rates | 74 |
| Figure 5.14 Comparisons of experimentally observed and theoretically predicted value (a) peak strength; (b) strain at peak strength | 75 |
| Figure 6.1 Calculation flow chart for rate-dependent hyperplasticity model | 80 |
| Figure 6.2 Shape and condition of loading in the calculation | 80 |
| Figure 6.3 Stress-strain curves of asphaltic concrete under S-IDT test at 10°C..... | 82 |
| Figure 6.4 Stress-strain curves of asphaltic concrete under S-IDT test at 25°C..... | 82 |
| Figure 6.5 Stress-strain curves of asphaltic concrete under S-IDT test at 40°C..... | 83 |
| Figure 6.6 Stress-strain curves of asphaltic concrete under S-IDT test at 55°C..... | 83 |
| Figure 6.7 Stress-strain curves of asphaltic concrete under S-UC test at 10°C | 84 |
| Figure 6.8 Stress-strain curves of asphaltic concrete under S-UC test at 25°C | 84 |
| Figure 6.9 Stress-strain curves of asphaltic concrete under S-UC test at 40°C | 85 |
| Figure 6.10 Stress-strain curves of asphaltic concrete under S-UC test at 55°C | 85 |
| Figure 6.11 Stress-strain curves of asphaltic concrete under C-IDT test at 10°C..... | 87 |
| Figure 6.12 Stress-strain curves of asphaltic concrete under C-IDT test at 25°C..... | 88 |
| Figure 6.13 Stress-strain curves of asphaltic concrete under C-IDT test at 40°C..... | 88 |
| Figure 6.14 Stress-strain curves of asphaltic concrete under C-IDT test at 55°C..... | 89 |
| Figure 6.15 Comparison of stress-strain curve between experimental test and rate-dependent hyperplasticity model in the last cycle | 89 |

LIST OF SYMBOLS

| | |
|-------------------------------------|---|
| θ | absolute temperature |
| E_a | activated energy |
| λ | arbitrary non-negative multiplier |
| k | Boltzmann's constant (1.38×10^{-23} J/K) |
| k | coefficient of friction |
| μ | coefficient of viscosity |
| E^* | complex modulus |
| r | constant with the dimensions of strain rate |
| α | cumulative total plastic strain |
| q | deviator stress |
| P | dynamic load |
| E_i | elastic modulus associated with relaxation time |
| w | flow potential |
| f | frequency |
| χ_{ij} | generalized stress |
| g | Gibbs free energy |
| E_0 | initial stiffness |
| k_0 | initial strength value |
| η | internal coordinate |
| $\hat{\alpha} = \hat{\alpha}(\eta)$ | internal parameter (or plastic strain) with internal coordinate |
| α_{ij} | internal variable (or plastic strain) tensor |
| $\hat{H} = \hat{H}(\eta)$ | kernel function |
| ε_{ve} | linear visco-elastic strain |
| E_∞ | long-time equilibrium modulus |
| $\langle \rangle$ | Macaulay brackets |
| m | material constant for the transition of modulus |
| A, p | material constants for Schapery continuum model |

| | |
|---------------------|---|
| $C(S)$ | material damage function of single damage parameter |
| α | material-dependent constant for damage function |
| B, q | material properties for Schapery continuum model |
| N | number of loading cycles |
| ε_p | permanent strain or plastic strain |
| h | Planck's constant (6.624×10^{-32} J/s) |
| $\dot{\alpha}_{ij}$ | plastic strain rate |
| ν | Poisson's ratio |
| ε^R | pseudo strain |
| W^R | pseudo strain energy density function |
| ε_r | recoverable strain |
| t_R | reduced time |
| E_R | reference modulus or initial modulus |
| k_1 | reference strength parameter |
| θ_E | reference temperature of E term |
| θ_k | reference temperature of k term |
| a and b | regression constant |
| $E(t)$ | relaxation modulus |
| T_0, ρ_i | relaxation time |
| M_r | resilient modulus |
| T_1 | retardation time |
| α_0 | reference strain |
| E_1 | reference Young's modulus |
| a | shape parameter |
| G^* | shear dynamic modulus |
| $S(x)$ | signum function |
| S | single damage parameter |
| d | specimen thickness |
| E | spring constant |

| | |
|---------------------|---|
| ε | strain |
| ε_d | strain due to microstructure damage |
| $\dot{\varepsilon}$ | strain rate |
| ε_{ij} | strain tensor |
| k | strength parameter |
| σ | stress |
| σ_{ij} | stress tensor |
| A, B, C | temperature constant for rate-dependent hyperplasticity model |
| $a_T(T)$ | temperature shift parameter |
| $a_{Td}(T)$ | temperature shift parameter for microstructure damage |
| $a_{Tve}(T)$ | temperature shift parameter for visco-elastic |
| $a_{Tvp}(T)$ | temperature shift parameter for visco-plastic |
| t | time |
| δ | total recoverable deformation |
| ε_t | total strain |
| ε_{vp} | total viscoplastic strain |
| R | universal gas constant (8.3114 J/(K.mol)) |
| $g(\sigma)$ | uniaxial stress loading function |
| X | various constant |
| ε_{vp} | visco-plastic strain |
| σ_{visc} | viscous material the stress |

CHAPTER 1

Introduction

1.1 Research background

The high progress of economy and population lead to an increase in a demand of road infrastructure. To support the large amount of traffic, the pavement construction is now enlarged, and the increase of capacity of the pavement structure is also focused on. Whether the pavement structure will favourably support an abundance of traffic or not, it depends on the design approach and its material assumption. The appropriate design assumption is important for producing not only the durable pavement but the economical pavement as well. There are two general approaches for the flexible pavement or asphalt pavement design. The former is an empirical method which involves a lot of experiences and data both from laboratory and field test. The latter is an analytical method which depends on the characteristic of stress-strain-strength existing in the pavement material.

The empirical method was widely used in 1950-1980 owing to the simplicity and the rapidity. By this method, the design parameter is easily understood; however, the stress-strain of materials can not be explicitly evaluated. This may be the weakness because those previous properties are necessary for calculating in design. Moreover, the development of design chart normally comes from the load repetitions data which is not more than 10 MSA (Million Single Axle). If the amount of traffic used for design is higher than 10 MSA, the designed data from design chart is extremely inexact. In addition to this method, it is not suitable for Thailand since the data employed for design chart developed is not from the same material or environment in country.

Many researches in United State of America and Europe then persevered in developing procedures for the design of analytical method. In 1962 the valuable article "The Application of Elastic Theory to Flexible Pavement", which explains the

reasons supporting the elastic analysis theory for the flexible pavement design, was represented by Whiffin and Lister (1962). The elastic theory has been used in place of an old way because of the fact that it can be employed to analyse the lifetime of application. In addition, this method leads to the development of new techniques both in soil mechanics and asphalt technology and brings the chance to be able to choose the materials with high quality for a pavement construction.

Afterwards the methods for analysing flexible pavement material known as a numerical method was tried to analyse for an explanation of the behaviour of flexible pavement material. For instance, the asphaltic concrete is based on the basic elasto-viscoelastic principles to clarify the viscous behaviour happened in the material (Huang, 2004). This assumption of analytical and numerical methods can be used to assume only that the pavement materials can behave as elastic and/or viscoelastic. In fact these materials however have the behaviours which are more sophisticated than these above behaviours. Consequently, both of previous methods may not be appropriate for predicting the actual behaviours of pavement materials.

An asphaltic concrete can be theoretically categorised as a thermorheologically (or linear visco-elastic in a particular temperature) material. Consequently, many researches tried to prove that the asphaltic concrete also exhibits the thermo-visco-elasto-plastic behaviour. This is because the stress-strain-strength characteristic of asphaltic concrete will be changed when the temperature and/or strain rate are transformed. At any temperature, the asphaltic concrete will deform slowly and permanently if a load is slowly applied. On the other hand, if a higher rate of loading is applied, the asphaltic concrete will behave much stiffer and might subject to fracture or crack. Furthermore, the asphaltic concrete will relax differently when there is the temperature changing at any strain rate.

This research focuses on the development of a new constitutive model to explain sophisticated behaviour of asphaltic concrete under the effects of both strain rate and temperature. The developed constitutive model namely rate-dependent hyperplasticity model (Likitlersuang *et al.*, 2009) can exhibit the thermo-elasto-viscoplastic behaviour of asphaltic concrete under shear loading. This model is based

on the principle of continuous hyperplasticity framework (Houlsby and Puzrin, 2006). The model is verified against both the experimental data from laboratory and is compared with existing constitutive model for asphaltic concrete. More analytical studies for evaluation of conventional pavement engineering properties such as resilient modulus, rutting curve and temperature shift function are also carried out with consideration of the temperature effect. In addition, the time-temperature superposition analysis the principle of time-temperature superposition with growing damage (Schwartz *et al.*, 2002) is used to demonstrate the effect of time and temperature on asphaltic concrete behaviour.

1.2 Research objectives

This research aims to conduct a rigorous evaluation of asphaltic concrete behaviour in proposed performance and mechanistic behaviour. The main studies can be categorised three sections as follows:

(1) The constitutive model for asphaltic concrete based on a rate-dependent hyperplasticity model (Houlsby and Puzrin, 2003) is developed.

(2) To prove that the developed constitutive model can be used to predict the asphaltic concrete behaviour under the changes of temperature and strain rate.

(3) The asphaltic concrete is tested to study the strength and plastic deformation characteristic. The tests consist of the static and cyclic indirect tensile tests (S-IDT and C-IDT) and the static and cyclic unconfined compression tests (S-UC and C-UC). Two factors affecting the asphaltic concrete, which are temperature and strain rate, are studied.

(4) The test results are firstly analysed by a conventional pavement engineering knowledge such as regression analysis of resilient modulus and permanent deformation (rutting). The time-temperature superposition with growing damage developed by Schwartz *et al.* (2002) is moreover used for studying and explaining the effect of temperature and strain rate resulting in the asphaltic concrete.

1.3 Research methodology

The main procedure for achieving previous objective comprises the numerical analysis, experimental testing, and the conventional analysis of experimental results. The details of these three parts are clarified as shown in the following items.

(1) In numerical analysis, the rate-dependent hyperplasticity model for predicting the asphaltic concrete under the effect of temperature and strain rate is developed. This model is then calibrated against viscoelastic damage model and experimental data (Schwartz *et al.*, 2002). After calibration, this model is predicted to compare with the IDT and UC test results of this research.

(2) In experimental study, the behaviour of asphaltic concrete are studied under S-IDT and C-IDT tests and S-UC and C-UC tests. The tested specimens of both static and cyclic tests are designed with 5.5% by aggregate weight of AC 60/70 based on Marshall Method. They are produced by means of controlling the density using Superpave Gyratory Compactor (SGC). Two factors observed in static load test are the various temperatures and the diverse rates of loading. These different temperatures which are 10, 25, 40, and 55°C are used for both S-IDT and S-UC tests. For the selected rate of loading, the specimens of S-IDT test are studied at 0.0008, 0.0025, 0.0083, and 0.0250 s⁻¹, and the specimens of S-UC tests is studied at 0.0006, 0.0017, 0.0056, and 0.0167 s⁻¹. For the factor studied in cyclic load test, the specimens of which have rate of loading 1 Hz (1:9), is tested at similarly temperature as static scheme.

(3) In the analysis of experiment, the database and/or empirical formula to analyse are created under various temperatures and strain rates. This process is based on the conventional pavement engineering method and the principle of time-temperature superposition with growing damage.

1.4 Research expected contribution

According to the whole research composing of a numerical implementation, an experimental testing, and a conventional analysis of experimental test, the expected contribution is concluded as follows:

(1) The rate-dependent hyperplasticity model relied on the hyperplasticity approach were produced for an attainable prediction under the principles of continuous hyperplasticity framework, the kinematic hardening plasticity, and the rate-dependent plasticity. The thermo-elasto-viscoplastic behaviour would be shown clearly by numerical study that the numerical method can provide an accurate prediction closer to the actual behaviour of materials than the empirical method and analytical method. This introduces the usefulness and the new alternative to apply to the finite element program for the pavement problem. In addition, this research may lead to the increase in concern of numerical study on the pavement material work.

(2) Following the experimental testing and analyse of experimental testing, the result can be used for evaluation of asphaltic concrete properties. The outcome can be the material database of the asphaltic concrete and also to design for the pavement construction in tropical countries especially Thailand. For example, the maximum stress (σ_{\max}), the strain at maximum stress (ϵ_{peak}), and the secant Young's modulus at 50% of the maximum stress (E^{50}) under different temperatures and strain rates can be estimated by means of the testing results of the static test. As for the value of resilient modulus (M_r) from C-IDT test it can be used to design the layer of the asphaltic concrete. In C-UC test, the simple equation obtained from this test can be employed for rutting prediction of pavement structure. Additionally, the indirect tensile stress/strength and the unconfined compression stress/strength at changed temperatures and strain rates are able to be estimated by the analysis of time-temperature superposition.

CHAPTER 2

Literature review

2.1 Introduction

This literature review can be categorised into three parts: (1) conventional of pavement engineering knowledge, (2) constitutive modelling for asphaltic concrete and time-temperature superposition, and (3) rate process theory and hyperplasticity approach. In the first part, the flexible pavement structure, the failure criteria, the critical stress/strain of flexible pavement, the asphaltic concrete behaviour, and the asphaltic concrete characteristic are discussed. In the second part, the famous constitutive model such as a viscoelastic model and an elasto-visco-plastic model are reviewed. The time-temperature superposition reported by Schwartz *et al.* (2002) is also looked over. In the last part, the rate process theory is reviewed to completely understand the asphaltic concrete behaviour. The hyperplasticity approach is briefly described. The development of rate dependent hyperplasticity model is also reviewed. In addition, the summary of the literature review is presented at the end of this chapter.

2.2 Flexible pavement structure

A typical flexible pavement structure is made up of layers each of which comprises different material and superimposes together as shown in Figure 2.1. The better-qualified material is located on higher layers due to the fact that they must sustain a higher value of stress. Besides, by the reason of sustaining lower stress, a inferior materials are beneath. The meaning and function of each layer are indicated as follows:

(1) Seal coat: A seal coat is a thin asphalt surface treatment. It makes use of the skid resistance because the aggregates in the surface probably could slip by the polishing of the traffic. In addition, it is used to waterproof the surface.

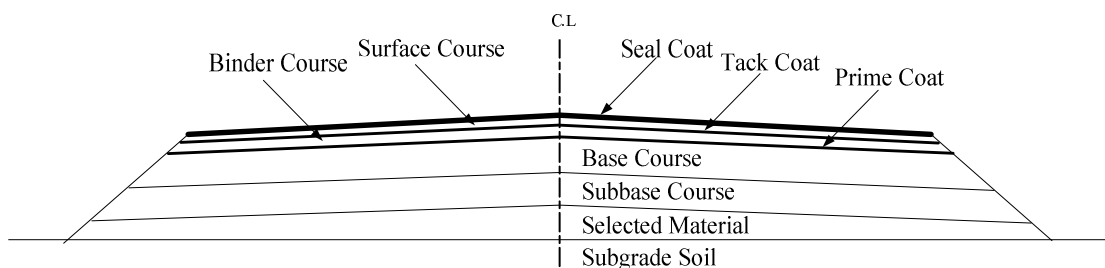


Figure 2.1 Tropical cross section of a flexible pavement

(2) Surface course (Wearing course): The surface course is the top course of asphalt pavement, which is normally constructed of the dense grade hot mix asphalt (HMA). This course is used for the purpose of resisting the distortion under the traffic and providing a smooth and skid-resistant riding surface. It is also employed to protect the entire pavement and subgrade soil from water which is a cause of its weakness. Therefore, the toughness and waterproofing are the essential properties of surface course.

(3) Binder course (Asphalt base course): It is the asphalt layer below the surface course. In order to fulfill the surface course, the binder course is produced. Since the thickness of hot mix asphalt is too much, the hot mix asphalt is hard to be compacted in one layer. Thus, it must be placed in two layers. Furthermore, for more economical design, a part of surface course is replaced by the binder course. Accordingly, the binder course does not need high quality as the surface course, and it generally consists of the larger aggregates and less asphalt.

(4) Tack coat and Prime coat: A tack coat is an extremely light application of asphalt, which is regularly diluted with water to be asphalt emulsion. Because it is necessary to bind each layer of an asphalt to the layer below, a tack coat is used for not only ensuring a bond between the surface being paved and the overlying course but also binding the asphalt layer to an old asphalt pavement. A prime coat is an application of low-viscous cutback asphalt to an absorbent surface. It is useful to bind between the granular base and an asphalt layer.

(5) Base course and Subbase course: A base course is the layer of material suddenly below the surface or binder course. It plays an important role in distributing

the traffic load safely to the subgrade soil. Its component can be the crushed rocks and gravels, including cement-stabilized base material. For the subbase course, it is the layer of the material beneath the base course. The materials of subbase course usually consist of an economical material which is available in local area. Its functions are truly similar to the base course. However, the slight difference to be economical is that it regularly comprises the weaker and cheaper material than the base material.

(6) Selected materials: The selected materials are generally composed of the marginal material in local area. This layer is produced where the pavement is heavily loaded or where the subgrade soil is very weak.

(7) Subgrade soil: This soil is the natural soil underlying the pavement about one meter. On the other hand, the subgrade soil is approximately one-meter deep part beneath the finished level of embankment. It is also the one-meter part below the excavated surface in case of cut. Moreover, the stabilized or treated soil replacing unsuitable natural soil is counted as the subgrade soil.

2.3 Failure criteria in flexible pavement

For the development of design approach at present, the majority of failure usually occurred in the asphaltic concrete surface is mainly focused. The failures mentioned next are arisen from the properties of an asphaltic concrete, the environment, and the repeated traffic loads. It is noticed that each failure on the surface may be appeared similarly, although the cause of each failure may be different. The failure problems normally happened in the asphaltic concrete surface can be separated as follows:

2.3.1 Permanent deformation

The pavement change found in the shape of surface layer or layer of a pavement structure is called permanent deformation. This deformation generally occurs in wheel path where the vehicle loads pass along or the areas where the vehicle stop frequently. Permanent deformation can occur only in the surface layer or only in the layer of pavement structure, or it can also occur in both surface layer and layer of

pavement of structure. This problem results from losing the sustaining of layer of material used in construction. This situation leads to the deformation caused by a pavement sedimentation or flowing of this layer.

The deformation normally has two types: (1) permanent deformation occurred in the wheel path of traffic loads and paralleled the traffic direction is called rutting as shown in Figure 2.2(a). (2) permanent deformation existed in the area where the vehicles stop frequently or move the traffic direction slowly and perpendicularly is call shoving as illustrated in Figure 2.2(b). The rutting of permanent deformation is mostly found in the rural highways because the traffic can be more quickly. Both rutting and shoving are generally discovered in the urbanized roads especially at the intersection and zones of traffic jam.



Figure 2.2 (a) Distress of rutting (b) Distress of shoving

2.3.2 Thermal cracking or Horizontal cracking

Temperature change is the cause for the thermal cracking in an asphalt pavement as displayed in Figure 2.3(a). When the rates of tensile stresses caused by low temperatures are more than the rates of tensile strengths of asphaltic concrete mixture, thermal cracking exists horizontally. This problem in the asphalt pavement is mainly caused by the properties of asphalt at low temperature because of the fact that under low temperature an asphalt becomes stiff and fragile. The behaviour possibly happens according to grade, crude source, age, and strain rate of each asphalt.

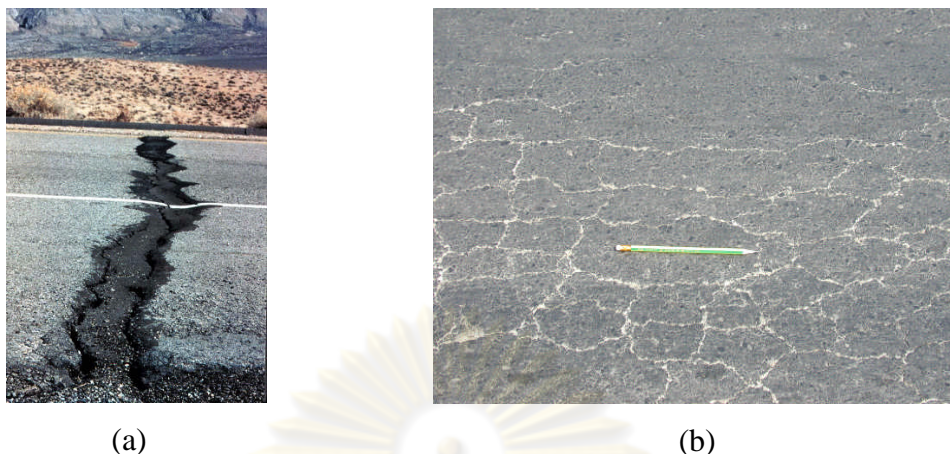


Figure 2.3 (a) Distress of thermal cracking (b) Distress of fatigue cracking

2.3.3 Fatigue cracking or Alligator cracking

When the asphalt pavement supports repeated loads for too long, a creep can occur. This behaviour follows from the horizontal tensile strain below the asphaltic concrete surface and leads to fatigue cracking. Figure 2.4(b) illustrates the characteristic of fatigue cracking. The primary factors resulting in fatigue cracking are: (1) the structure design of pavement (2) the properties of asphalt (3) the asphalt content (4) the air void content in mineral aggregate (VMA) and the characteristics of an aggregate in asphaltic concrete mixture (5) the in place properties of pavement materials (6) temperature and (7) traffic (Finn, 1978).

2.4 Problem and Improvement

The first problem found is the database used for designing material or evaluating materials property. Generally, the flexible pavement design in many tropical countries such as Thailand refers to the standard of America or Europe. These quoted standards were produced from the experimental database of cold climate zone which is totally different from the database collected in the tropical areas. For employing the design standard from elsewhere simply and directly, it may not be suitable for another local area. Consequently, it is essential to transform database, temperatures of cold climate countries, into the herein temperatures which truly exist in the tropical zone.

The second significant one is the assumptions for analysing the asphaltic concrete. This assumption makes use of considering viscoelastic behaviour. Actually, the behaviours of all materials do not express only the elastic behaviour. As the stress-strain relation beyond the first yield shows us, there is the plastic behaviour in a pavement material. For instance, when the material is loaded until it is reached the first yield and then reloaded back to the original condition, the loading path can not be back to the old point. This is called the plastic strain or permanent strain.

Following the problem above, the assumptions for analyzing behaviours of asphaltic concrete are not adequate to describe the behaviour of material. Thus, other knowledge and methods are required to improve the prediction of asphaltic concrete such as the plasticity theory. From previous theory, the constitutive model are produced to explain the thermo-elasto-viscoplastic behaviour of asphaltic concrete and to define the plastic strain and failure strain.

2.5 Critical stress/strain of flexible pavement

The multi-layered system structure of flexible pavement consists of various stiffness of pavement layer. Figure 2.4 exhibits the multi-layered pavement structure of which base layer is granular material. The critical stress/strain occurring in the pavement layer results from the applied wheel load (FHWA, 1987). In the figure, the points 1, 2, 3, and 4 represent the location of critical stress/strain point. In reference to many researches, the pavement material has an ability to resist the stress rather than the strain. Moreover, at the failure of materials the strain is less variable than the stress failure. Therefore, for the design of flexible pavement using analytical method, the strain is employed to be the determiner of failure in each pavement layer. When the strain exists over the limitation of pavement layer, a fatigue cracking and rutting happen according to the manner of strain. The fatigue cracking is influenced by the tensile strain and rutting results from the compressive strain. In flexible pavement design, both of aforementioned are the failure criteria.

The stress and strain are discovered in a pavement layer, when the pavement structure is pressed by a wheel load. The stress and strain existing in the

pavement layer above can be separated into three kinds. The first one is the vertical stresses/strains which press each level of pavement layer and result in the higher density and rutting. The next one is the vertical stresses/strains which affect an unstable structure of pavement especially when the wheel load is very heavy. The last one is the radial stresses/strains which are caused by the deflection beneath the pavement layer of which the category is the asphaltic concrete. These stresses/strains resulting from wheel load cause cracking which occurs in the pavement layers and spreads from the bottom to the surface.

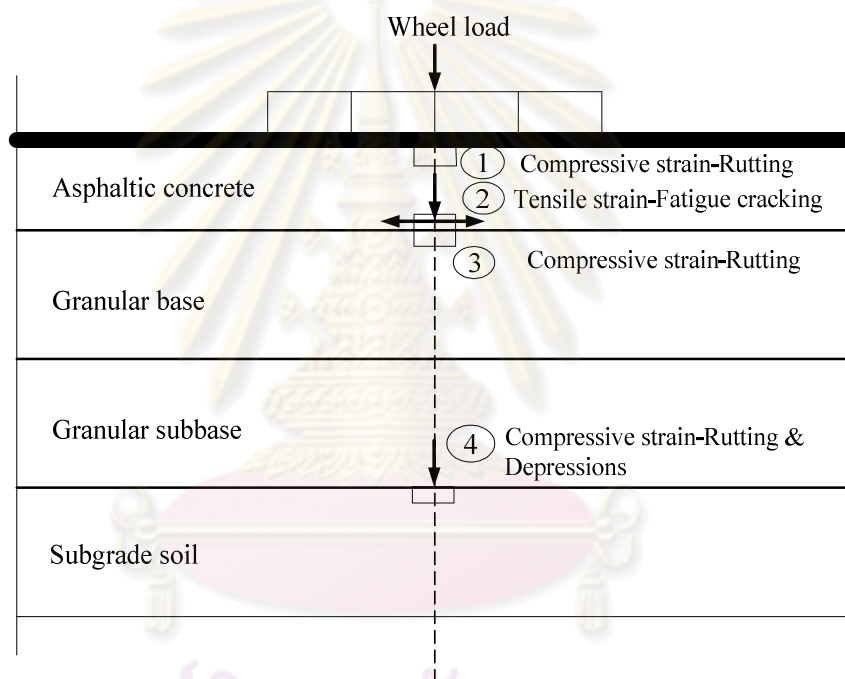


Figure 2.4 Critical stress and strain at each layer of flexible pavement

Number (1) is a vertical compressive strain occurring in a surface layer of asphaltic concrete. It becomes critical when the traffic is extremely congested or very weighty. Taking place of vertical compressive strain in a pavement layer leads to the density of surface and then rutting. In design, the vertical compressive strain in an asphaltic concrete layer is not as the critical strain appointing the failure of pavement owing to the reason that during construction an asphaltic concrete is usually compacted to be very dense.

Number (2) is a radial tensile strain existing below the surface layer and located at the joint between surface and base layer. This strain is influenced by the deflection of the pavement caused by the wheel load. Following from the traffic passed along, the radial tensile strain beneath a surface is continuously accumulated until the asphaltic concrete can not be sustained this traffic load. The situation brings about the cracking below the asphaltic concrete surface. The radial tensile strain happening beneath an asphaltic concrete surface is counted as the critical strain for the design of pavement structure.

Number (3) is a vertical compressive strain taking place in the granular material base layer. Normally, the material used in the construction of base layer must be very firm and well-constructed; therefore, the vertical compressive strain occurring in the base layer above is not as the critical strain which is employed for considering a design of flexible pavement. The vertical compressive strain taking place in the base layer built from the local low-qualified material is the cause of rutting.

Number (4) is a vertical compressive strain happening in a subgrade soil surface of flexible pavement. Since the subgrade soil layer has the lower elastic modulus than the others, the vertical compressive strain taking place in the subgrade soil layer is higher than the others as well. This occurrence leads to the rutting. This strain is also the critical strain used in the flexible pavement design.

2.6 Asphaltic concrete behaviour

At present, the asphaltic concrete behaviour is mostly based on the assumption of viscoelastic and/or elastic material. A strength value of material in the assumption depends on the stress and strain level. In fact, the assumption above is not adequate to reach the material behaviours due to the reason that the behaviours of asphaltic concrete employed in a road construction are not only elastic. Therefore, for approaching material behaviours, the constitutive model is used to appropriately predict the material behaviours. Before referring to the constitutive model theory, the real behaviours of asphaltic concrete are considered and some important aspects of their behaviours are identified in the following section.

The behaviour of asphaltic concrete mixture is mentioned. An asphaltic concrete consists of asphalt cement and aggregate. The behaviour of the asphaltic concrete really depends on the asphalt cement. In different temperature, an asphalt cement can exhibit the viscous and elastic behaviour. Depending on the various temperatures, these can be separated into three ranges: (1) in high temperature (i.e. 100°C), the behaviour of the asphalt cement becomes as the viscous fluid which is concentrated and lubricating like oil. (2) in low temperature (i.e. 0°C), the asphalt cement behaviour acts as the elastic solid which can be changed back to the original condition. (3) in intermediate temperature (i.e. room temperature), in the environment between high temperature and low temperature, both of viscous and elastic behaviour are expressed, which is known as the viscoelastic behaviour.

To define the effects of temperature and strain rate, Kim (2009) presented the qualitative of strain rate versus the temperature which displays the stress-free temperature and the strain rate as illustrated in Figure 2.5 This relation can be used to explain the mode of damage of asphaltic concrete. For instance, an asphaltic concrete specimen will be collapsed with the fracture (tensile) mode at the high strain rate and the low temperature conditions. However, the asphaltic concrete will be failed by the plastic flow at low strain rate and high temperature condition. Another failure possibility is the microcracking at the intermediate strain rate and the low temperature condition.

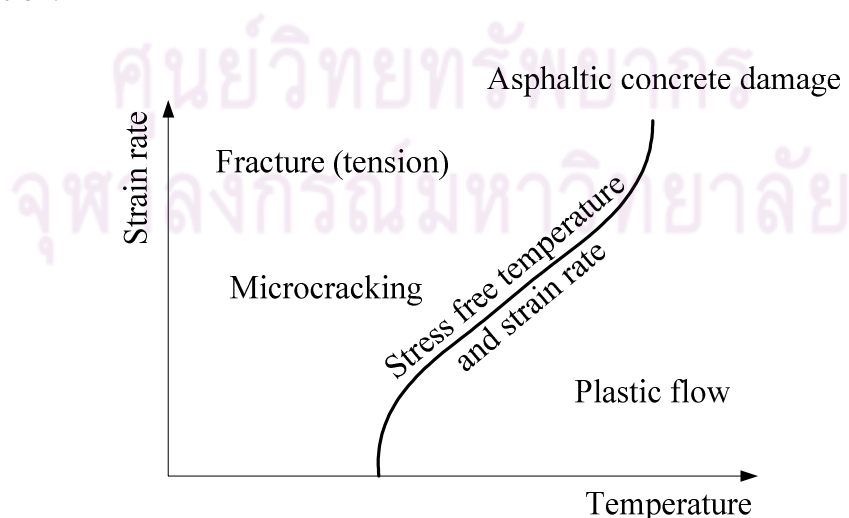


Figure 2.5 Asphaltic concrete affected of temperature and strain rate

2.7 Characteristics of asphaltic concrete

There are two main characteristics of asphaltic concrete which have frequently been considered on the most critical for the analysis and/or the design of flexible pavement. The first one is the fracture characteristic such as resilient modulus (M_r) used to describe the stiffness of asphaltic concrete. The last one is the permanent deformation characteristic or the rutting of asphaltic concrete. Both of these characteristics are employed as the failure criteria in the Asphalt Institute Method.

2.7.1 Resilient modulus

Hveem and Carmany (1948) and Hveem (1955) introduced the concept of resilient behaviour of pavements. Seed *et al.* (1955) at the University of California at Berkeley then followed the progress formed by Hveem, who had developed the repeated load test. After pursuing, the term modulus of resilience was proposed and later changed to be resilient modulus (Seed *et al.*, 1962) as displayed in Figure 2.6.

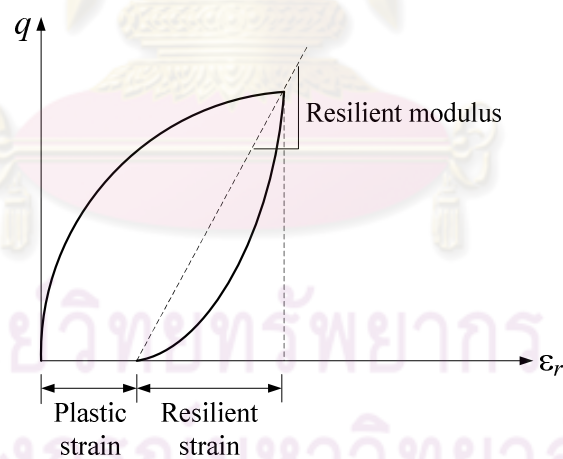


Figure 2.6 Definition of resilient modulus

As figure above the resilient modulus value, which expresses in term of deviator stress (q) and recoverable strain (ϵ_r), can be described by elastic principle as presented in the following equation:

$$M_r = \frac{q}{\epsilon_r} \quad (2.1)$$

For an asphaltic concrete, the resilient modulus is able to investigate from IDT test for a resilient modulus of bituminous mixtures. Therefore, the ASTM D 4123 developed the simple equation which used to calculate the resilient modulus as expressed below:

$$M_r = \frac{P(\nu + 0.2734)}{\delta d} \quad (2.2)$$

where P is dynamic load, ν is Poisson ratio which normally is equal to 0.35 (ASTM D 4123), δ is total recoverable deformation, and d is specimen thickness.

Meor and Teoh (2008) studied the effects of temperature on the resilient modulus of dense asphalt mixes incorporating steel slag fully or partially replacing natural granite aggregates and then subjected to short term oven aging. Two mix types designated as SSDA (asphalt mixture incorporating 100% steel slag as aggregates) and SSGDA (asphalt mixture incorporating 50% steel slag and 50% granite aggregates) were evaluated. The specimens were tested at 10°C, 25°C and 40°C. Some parts of research can be concluded the effect of resilient modulus with temperatures which provided from two asphaltic mixtures as shown in Figure 2.7.

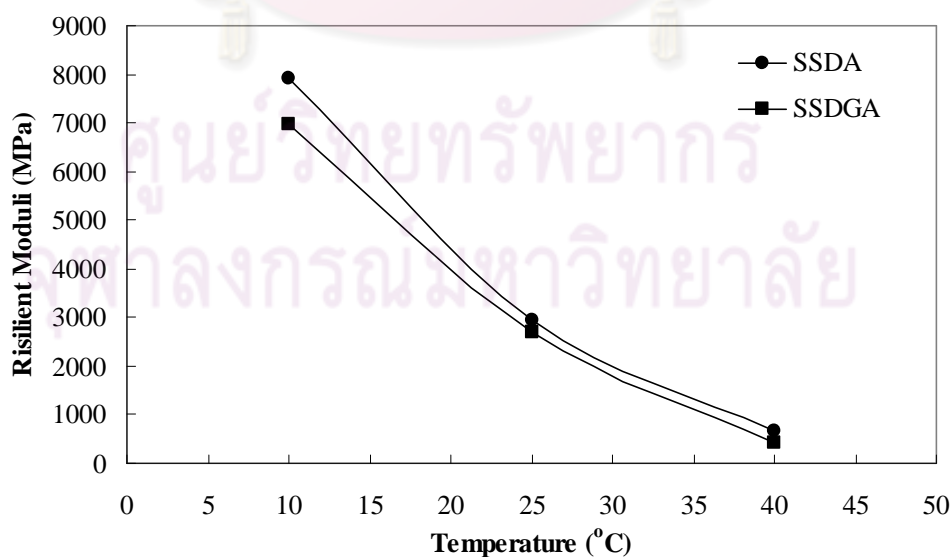


Figure 2.7 Resilient Modulus of short term oven aged SSDA and SSGDA mixes at 6.0% binder content (Meor and Teoh, 2008)

Phromsorn *et al.* (2003) investigated the properties of indirect tensile strength and the resilient modulus of asphaltic concrete in Thailand. The asphaltic concrete samples were thoroughly collected from five regions which are central, north, north-east, east, and south. For the resilient modulus, the samples were tested with four different temperatures which are 15, 25, 35, and 45°C. The result of average of resilient modulus of the asphaltic concrete in Thailand with four different temperatures is displayed in Figure 2.8.

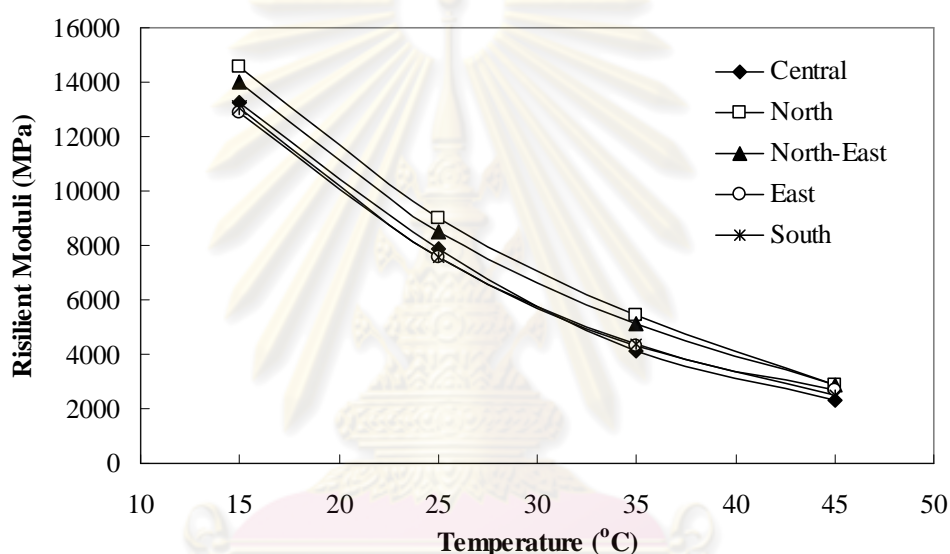


Figure 2.8 Result of the average of resilient modulus: five regions in Thailand (Phromsorn *et al.*, 2003)

2.7.2 Permanent deformation

A permanent deformation or rutting in an asphaltic concrete develops gradually with increasing of load applications, usually appearing as longitudinal direction in the wheel paths accompanied by small upheavals to the sides. The permanent deformation can be described in terms of cumulative permanent strain or plastic strain (ϵ_p) versus the number of loading cycles (N) as illustrated in Figure 2.9(a). The cumulative permanent strain curve can be divided into three zones: primary creep, secondary creep, and creep rupture or tertiary creep. The changing of slope in secondary and tertiary represents the flow number (FN). The classic power-

law model, mathematically expressed by Equation 2.3, is typically used to analyse the test results:

$$\varepsilon_p = aN^b \quad (2.3)$$

where a and b are regression constant defined in Figure 2.9(b)

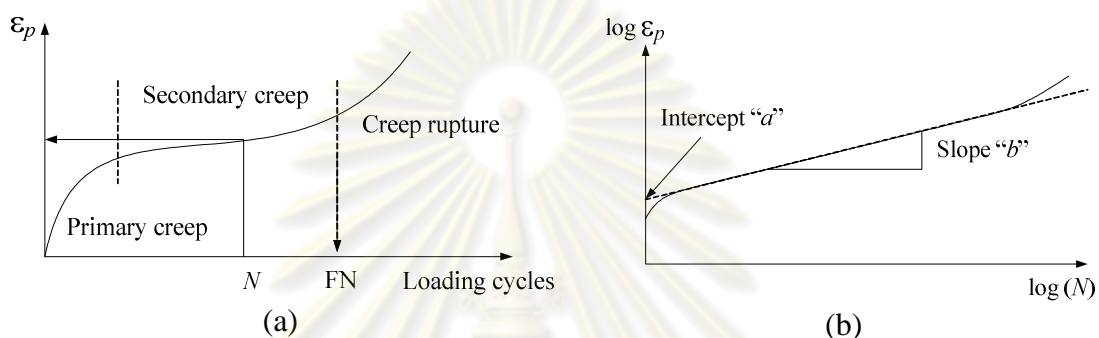


Figure 2.9 (a) Typical relationship between total cumulative permanent strain and loading cycles (b) Regression constants a and b

Jahromi and Khodaii (2008) studied the characteristics and properties of carbon fibre reinforced asphalt mixtures, which might improve the performance of asphaltic concrete. To evaluate the effect of fibre contents on asphaltic mixtures, laboratory investigations were carried out on the samples with fibres and the samples without fibres. Some parts of research can be concluded the correlation between a permanent strain and a stiffness as illustrated in Figure 2.10. A increase in the resilient modulus properties of specimens was followed by a decrease in the permanent deformation.

Thammavong and Lavansiri (2006) studied the feasibility and the suitability of foamed asphalt to stabilize reclaimed asphalt pavement (RAP). For the investigation of permanent deformation, the repeated load deformation test also utilizes the UTM, following the Australian standard test method (AS 2891.12.1-1995). Some parts of research can be concluded the results of permanent deformation test of foamed asphalt mixtures as expressed in Figure 2.11. The 50%RAP and 0%RAP foamed asphalt mixtures show superior to 100%RAP foamed asphalt

mixtures that whether they experience lower accumulated strain than 100% RAP samples.

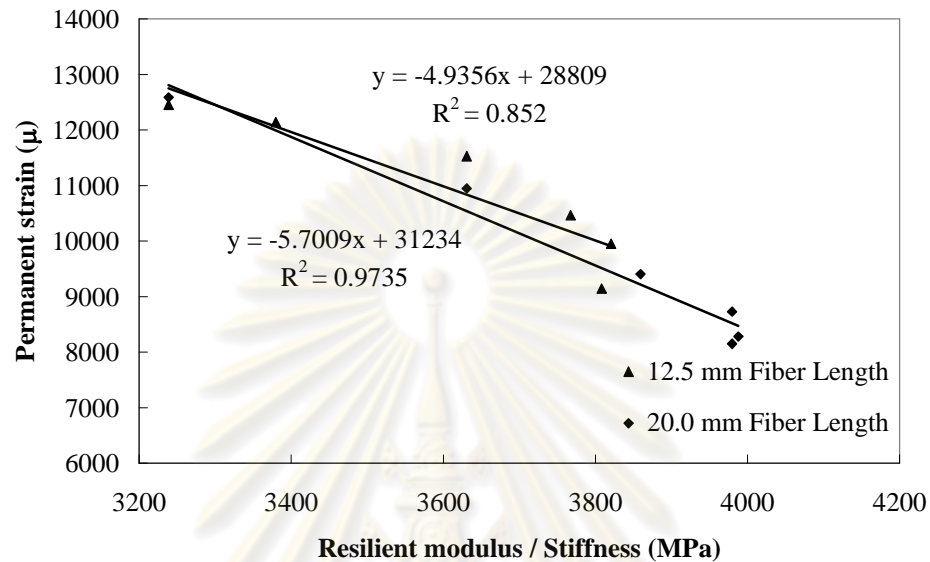


Figure 2.10 Relation of permanent strain at 6500 cycles and stiffness (Jahromi and Khodaii, 2008)

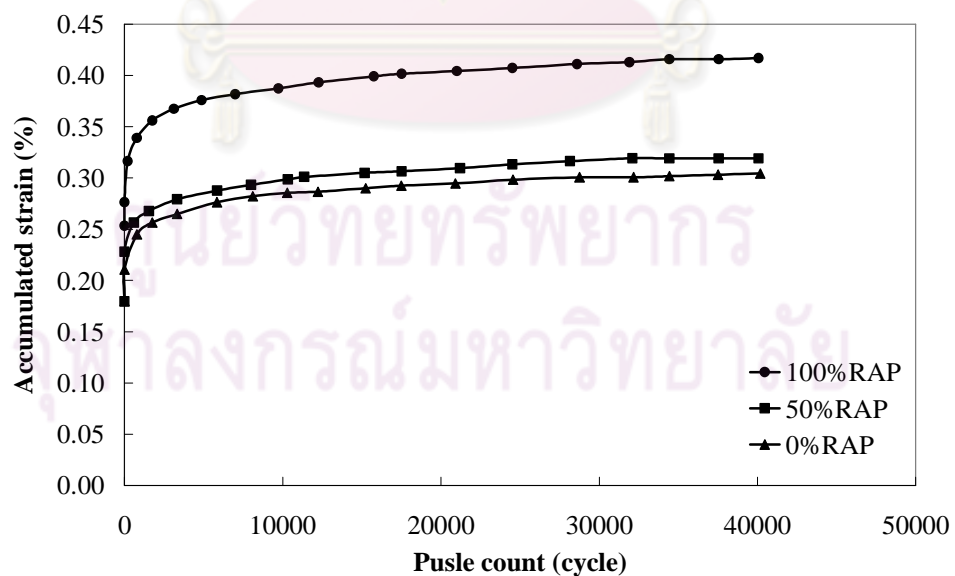


Figure 2.11 Result of the accumulated strain of loading pulses (Thammavong and Lavansiri, 2003)

2.8 Constitutive model for asphaltic concrete

The knowledge of structure mechanics and continuum mechanics contribute to the numerical method. This method based on the finite element and the finite difference method has been most widely used. These methods attempt to satisfy the realistic constitutive model. In the view of complexities in the material behaviour, the constitutive model is developed for decreasing the weakness in the prediction of material behaviour. The constitutive model theory which can approach the material behaviour is mentioned in this section.

2.8.1 Viscoelastic model

The elastic property of solid and viscous behaviour of liquid is controlled by the viscoelastic material. The theory of viscoelasticity is naturally applied to the analysis of layered system because the behaviour of HMA of which viscoelastic material depends on the time of loading. The behaviour of linear viscoelastic can be described by mechanics model. These models are established with two basic elements which are a linear spring with spring constant (E) and a dashpot (pistons moving in a viscous fluid) with coefficient of viscosity (μ).

The basic model consists of an elastic model and a viscous model. Firstly, the elastic model, which is appropriate with an elastic material, is characterized by a linear spring as illustrated in Figure 2.12(a), and obeys Hook's law. Secondly, the viscous model, which is appropriate with a viscous material, is characterized by a dashpot as illustrated in Figure 2.12(b), and obeys Newton's law. For the viscous model, a stress is depending on the time rate of strain (i.e. $\sigma = \mu \frac{\partial \varepsilon}{\partial t}$). The equations of

both elastic model and viscous model are expressed by

$$\text{Elastic model:} \quad \sigma = E\varepsilon \quad (2.4)$$

$$\text{Viscous model:} \quad \varepsilon = \frac{\sigma t}{\mu} \quad (2.5)$$

where σ is stress, ε is strain, and t is time.

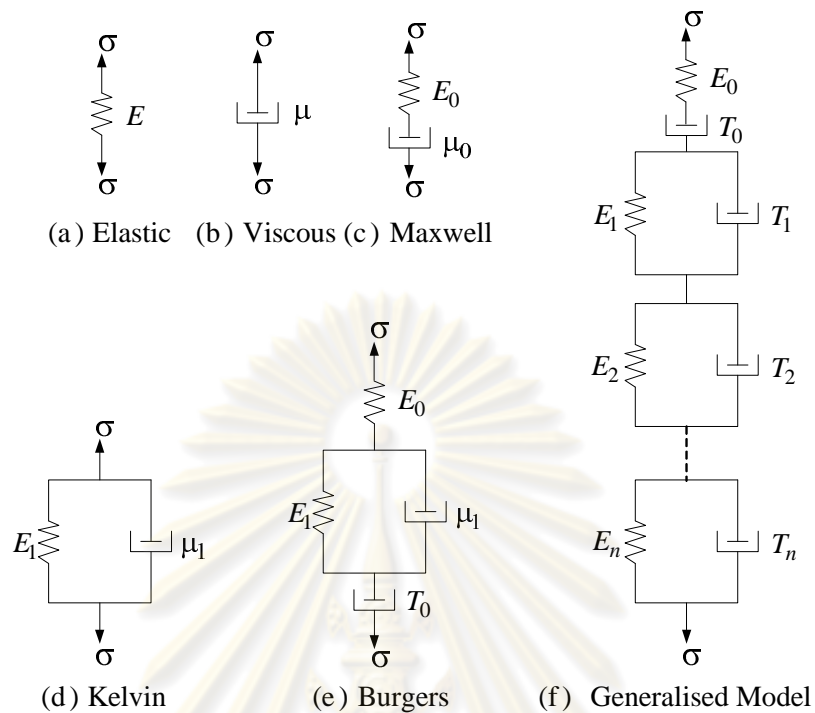


Figure 2.12 Mechanical models for viscoelastic materials

The Maxwell model is a combination of elastic and viscous model in series as shown in Figure 2.12(c). This model corresponds to a viscoelastic fluid. Under constant stress, the total strain is the sum of strain of both an elastic model and a viscous model. This equation can be written as follows:

$$\varepsilon = \frac{\sigma}{E_0} + \frac{\sigma t}{\mu_0} = \frac{\sigma}{E_0} \left(1 + \frac{t}{T_0} \right) \quad (2.6)$$

where $T_0 = \frac{\mu_0}{E_0}$ is relaxation time: it characterizes the rate of decay of the force. The subscript 0 is used to indicate a Maxwell model.

The Kelvin model is quite different from Maxwell model. This model is a combination of elastic and viscous model in parallel as indicated in Figure 2.12(d). This model is capable of predicting viscoelastic solid. Both of elastic and viscous models have the same strain which is shown in equation below, but the total stress is the sum of two stresses (i.e. $\sigma = E_1 \varepsilon + \mu_1 \frac{\partial \varepsilon}{\partial t}$).

$$\varepsilon = \frac{\sigma}{E_1} \left[1 - \exp\left(-\frac{t}{T_1}\right) \right] \quad (2.7)$$

where $T_1 = \frac{\mu_1}{E_1}$ is retardation time it characterizes the rate of decay of the displacement. The subscript 1 is used to indicate a Kelvin model. If σ_0 is applied instantaneously to the model, the linear spring will be activated. In addition, if this strain is kept constant, the stress will gradually relax and, after a long period of time, will become to zero (i.e. $\sigma = \sigma_0 \exp\left(-\frac{t}{T_0}\right)$).

The Burgers model is a combination of Maxwell and Kelvin models in series as illustrated in Figure 2.12(e). Under constant stress, the strain equation can be written as follows:

$$\varepsilon = \frac{\sigma}{E_0} \left(1 + \frac{t}{T_0} \right) + \frac{\sigma}{E_1} \left[1 - \exp\left(-\frac{t}{T_1}\right) \right] \quad (2.8)$$

For the Burgers model, the total strain consists of an instantaneous elastic strain ($\frac{\sigma}{E_0}$), a viscous strain ($\frac{\sigma t}{E_0 T_0}$), and a retarded strain ($\frac{\sigma}{E_1} \left[1 - \exp\left(-\frac{t}{T_1}\right) \right]$). Although a

Burgers model well represents the behaviour of viscoelastic material, a single Kelvin model is usually not sufficient to define the long period of time.

The generalized model can be used to characterize any viscoelastic material as shown in Figure 2.12(f). Under constant stress, the strain of this model can be written as:

$$\varepsilon = \frac{\sigma}{E_0} \left(1 + \frac{t}{T_0} \right) + \sum_{i=1}^n \frac{\sigma}{E_i} \left[1 - \exp\left(-\frac{t}{T_i}\right) \right] \quad (2.9)$$

where n represents the number of Kelvin models. The generalized model can explain the effect of load duration. Under the single load application, the instantaneous and

the retarded elastic strain predominates, and the viscous strain is negligible. However, under a large number of load repetitions, the accumulation of viscous strains is the cause of permanent deformation.

2.8.2 Viscoelastic damage model

Park *et al.* (1996) initially developed a simple constitutive model for the uniaxial stress-strain behaviour of asphaltic concrete with time-dependent damage growth, called a viscoelastic damage model. For this model, the constitutive model is defined by referring from the pseudo strain energy density function (W^R) and internal state evolution law. The following equations constitute the viscoelastic model used in the characterization of asphaltic concrete. The pseudo strain energy density function can be defined as:

$$W^R = \frac{1}{2} C(S) (\varepsilon^R)^2 \quad (2.10)$$

where $C(S)$ is material damage function of single damage parameter (S) and ε^R is pseudo strain. The ε^R , which bases on an elastic-viscoelastic correspondence principle, can be written as:

$$\varepsilon^R = \frac{1}{E_R} \int_0^t E(t-t_R) \frac{d\varepsilon}{dt_R} dt_R \quad (2.11)$$

where E_R is reference modulus (i.e. initial modulus), $E(t)$ is relaxation modulus, t_R is reduced time, and t is time. To implement numerically the viscoelastic damage model, a series function is used to represent the relaxation modulus, $E(t)$ (Park and Kim, 2001):

$$E(t) = E_\infty + \sum_{i=1}^N \frac{E_i}{\left(1 + \frac{t}{\rho_i}\right)^m} \quad (2.12)$$

where E_∞ is long-time equilibrium modulus, E_i is elastic modulus associated with a relaxation time, ρ_i is relaxation time, and m is material constant for the transition of modulus. In Substituting Equation 2.12 into Equation 2.11 and integrating for a process at constant strain rate, the pseudo strain is expressed as:

$$\varepsilon^R = \frac{\dot{\varepsilon}}{E_R} \left\{ E_\infty t + \sum_{i=1}^N E_i \rho_i \left[\frac{\left(1 + \frac{t}{\rho_i}\right)^{1-m} - 1}{1-m} \right] \right\} \quad (2.13)$$

where $\dot{\varepsilon}$ is constant strain rate and time. t can be computed from $t = \varepsilon/\dot{\varepsilon}$. The relation between a stress and a strain is defined in term of pseudo strain as:

$$\sigma = \frac{\partial W^R}{\partial \varepsilon^R} = C(S) \varepsilon^R \quad (2.14)$$

The model also uses an internal state evolution law for damage to micro-crack growth:

$$\dot{S} = \left(-\frac{\partial W^R}{\partial S} \right)^\alpha \quad (2.15)$$

where α is material-dependent constant for damage function. For the prediction of temperature effect, Schapery (1999) and Schwartz *et al.* (2002) introduced the features into the model to describe the effect of temperature, using time-temperature superposition as explained in the next topic.

2.8.3 Elasto-visco-plastic model

The characteristic of asphaltic concrete does not show only the completely elastic behaviour as described in previous topic. The theory of the elasto-visco-plastic (EVP) is generally applied to the stress-strain analysis of pavement engineering. EVP theory can be described by the mechanical model as shown in Figure 2.13. This model

composes of three basic elements which are a linear spring with spring constant (E), a slip friction with coefficient of friction (k), and a dashpot (pistons moving in a viscous fluid) with the coefficient of viscosity (μ).

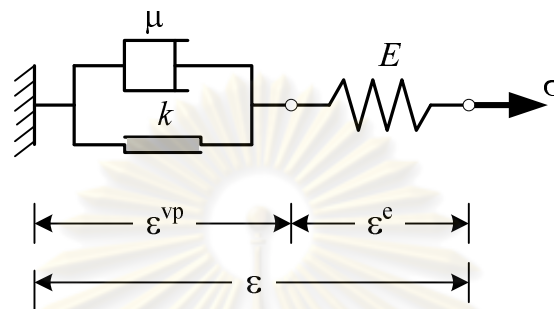


Figure 2.13 Elasto-visco-plastic model

2.8.4 Elasto-visco-plastic model (Schapery continuum model)

Schapery (1999) was to develop the viscoplastic constitutive model for an uniaxial loading. The axial viscoplastic strain is assumed by strain hardening model:

$$\epsilon_{vp} = \left(\frac{p+1}{A} \right)^{\frac{1}{p+1}} \left(\int_0^t g(\sigma) dt \right)^{\frac{1}{p+1}} \quad (2.16)$$

where ϵ_{vp} is total viscoplastic strain, $g(\sigma)$ is uniaxial stress loading function, and A and p are material constants. As for the constant stress creep condition $g(\sigma)$ is independent of time and $g(\sigma)$ is assumed a power law as $B\sigma^q$. For this case, the presentation of viscoplastic strain become as in equation below.

$$\epsilon_{vp} = \left(\frac{p+1}{D} \right)^{\frac{1}{p+1}} (\sigma^q)^{\frac{1}{p+1}} t^{\frac{1}{p+1}} \quad (2.17)$$

where $D = A/B$. B and q are material properties. For asphaltic concrete material, the viscoplastic parameter p , q , and D were calculated by using the uniform load and uniform time creep and recovery test.

2.9 Time-temperature superposition

The properties of viscous material e.g. asphaltic concrete can be assumed to be a function of time and temperature. In general, it is difficult to describe the mechanic behaviour of asphaltic concrete under previous two functions. Fortunately, the asphalt binders are the simple of thermorheological material, which means an effect of time can be replaced by an effect of temperature, and vice versa. The asphaltic concrete property as a function of time (or frequency) such as the complex modulus (E^*) or shear dynamic modulus (G^*) at varies temperatures can be shifted along the horizontal log time (or log frequency) axis to form a single characteristic of master curve. The E^* and G^* can be estimated following as the dynamic modulus test (AASHTO TP 62) and the shear dynamic modulus test (AASHTO TP 7). For example in Figure 2.14, the modulus at any temperature can be modelled with a single curve at a reference temperature named as a master curve. All curves are shifted by means of the temperature shift parameter ($a_T(T)$) which is defined:

$$a_T(T) = \frac{t}{t_R} \quad (2.18)$$

where t is time (before shifting), and t_R is reduced time or time at reference temperature (after shifting) (see Figure 2.14).

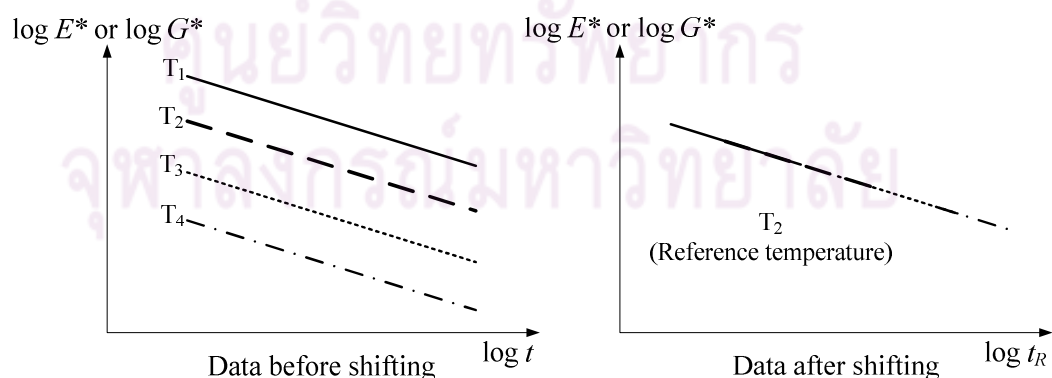


Figure 2.14 Data shifting to construct master curve

Schapery (1999) developed the Schapery continuum damage model which explains the conceptual of visco-plasticity with growing damage. This model consists

of the visco-elastic correspondence principles, the microstructure damage, and strain hardening visco-plastic. Schapery continuum damage model is the separation of total strain ε_t into its components:

$$\varepsilon_t = \varepsilon_{ve} + \varepsilon_d + \varepsilon_{vp} \quad (2.19)$$

where ε_{ve} is linear visco-elastic strain, ε_d is strain due to microstructure damage, and ε_{vp} is visco-plastic strain. For calculation the temperature shift parameter corresponding the total strain ε_t , Schapery (1999) concluded the components of ε_t , as Equation 2.19, may be interchanged using the time-temperature superposition.

$$a_{T_{ve}}(T) = a_{T_d}(T) = a_{T_{vp}}(T) \quad (2.20)$$

where $a_{T_{ve}}(T)$, $a_{T_d}(T)$ and $a_{T_{vp}}(T)$ are temperature shift parameter for visco-elastic, microstructure damage, and visco-plastic behaviour, respectively.

Schwartz *et al.* (2002) presented the time-temperature superposition with growing damage, which it was verified by the uniaxial compression constant strain rate tests at large-strain values. According to the uniaxial compression test results, the master curves (stress vs. reduced time) and corresponding time-temperature shift functions curve are obtained. The procedure producing both of previous curves is called cross-plot method. Note that since the strain value is fixed, this plot is similar to a modulus versus a log time curve.

The procedure of cross-plot is schematically illustrated in Figure 2.15 and can be explained as follows. Firstly, a given magnitude of strain reference is selected. For this strain at a given temperature, the magnitude of stress and time are determined for each strain rate. Secondly, these values are constructed the relation of log stress and log time for the given strain magnitude. Finally, a log stress and a log time curve for each temperature are shifted to produce the master curve, and the temperature shift function is constructed by the same procedure as the dynamic modulus test and the shear dynamic modulus test.

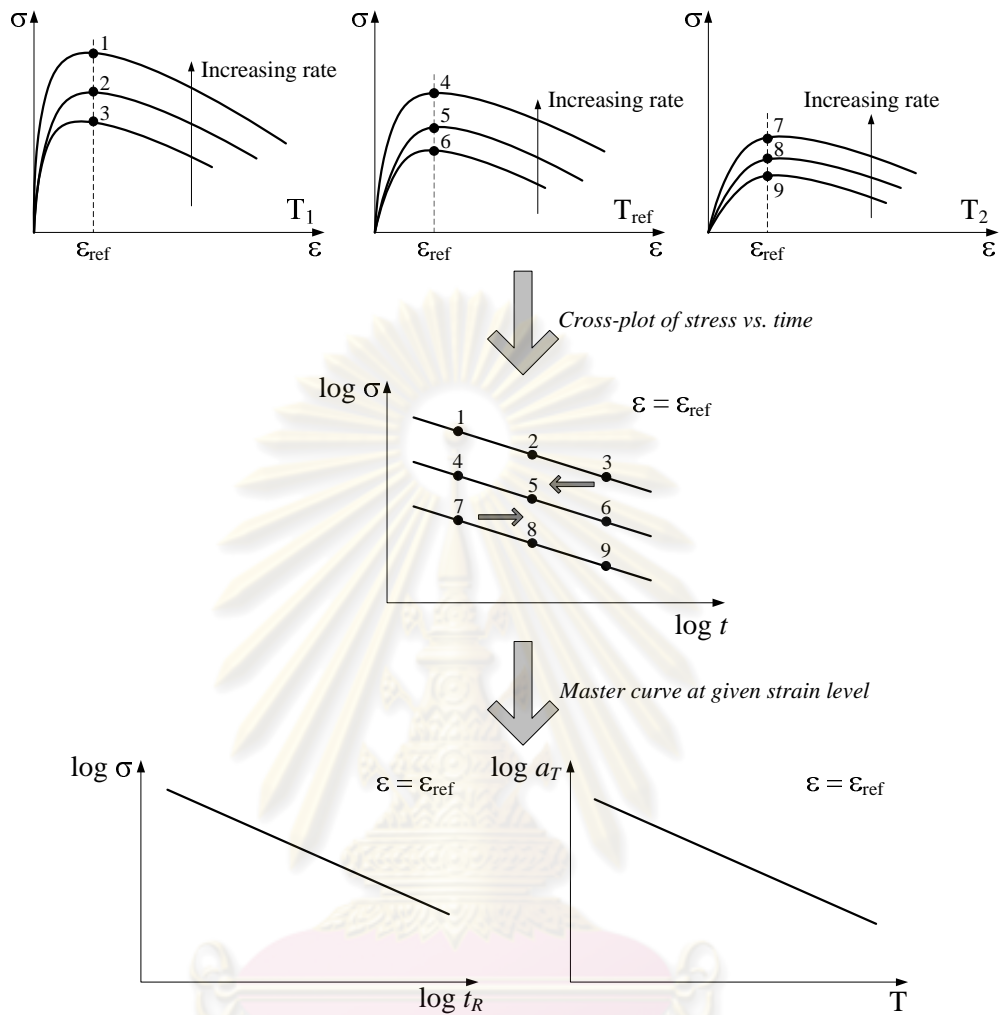


Figure 2.15 Schematic of time-temperature superposition principle by using cross plot

2.10 Rate process theory

A rate process theory is the theory used for explaining the strength behaviour of material and the particle rank of material. For instance, the particle rank of soil is defined by mean of an activated energy (E_a) and frequency (f) which force the movement of soil particle as shown in Figure 2.16

Mitchell and Soga (2005) concluded that the movement of soil particle varies according to the frequency of activated energy ($\dot{\epsilon} \propto f$). As for this condition the strain rate equation can be written following as:

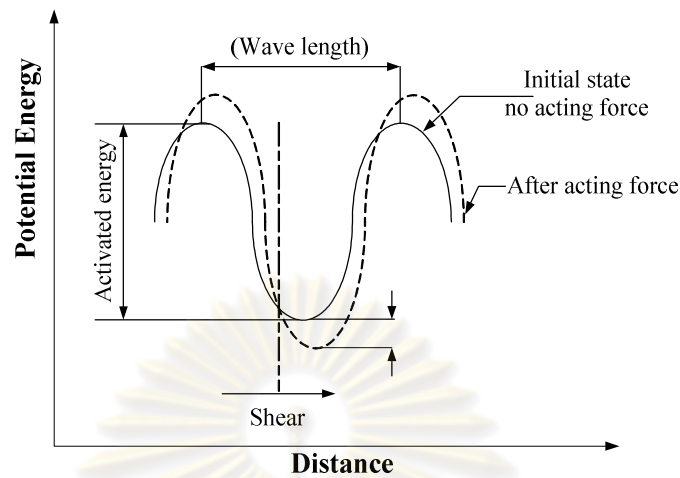


Figure 2.16 Imitation of the activated energy of soil when it is forced by shear

$$\dot{\epsilon} = 2X \frac{k\theta}{h} \exp\left(-\frac{E_a}{R\theta}\right) \sinh\left(\frac{\tau\lambda}{2k\theta}\right) \quad (2.21)$$

where X is various constant, k is Boltzmann's constant (1.38×10^{-23} J/K), h is Planck's constant (6.624×10^{-32} J/s), E_a is activated energy, R is universal gas constant (8.3114 J/(K.mol)), and θ is absolute temperature. In case of solid with stable temperature

$\frac{\tau\lambda}{2k\theta} > 1$. Accordingly, the strain rate can be written as $\dot{\epsilon} \propto \sinh\left(\frac{\tau\lambda}{2k\theta}\right)$ or

$\dot{\epsilon} = r \sinh\left(\frac{\tau}{\mu r}\right)$ in which r represents the constant using the same numerative unit as the strain rate.

2.11 Hyperplasticity approach

For the plasticity theory, there has been an emphasis on the use of thermodynamic principle to develop a new approach to a plasticity modelling called hyperplasticity. There are two types of hyperplasticity approach which based on the law of thermodynamics. Firstly, the hyperplasticity theory for rate-independent material is proposed by Houlsby and Puzrin (2006). For this theory, the entire constitutive model is identified by two scalar potential functions. These functions are

an energy function and a yield function (y). This section uses here the example of Gibb free energy (g):

$$\text{Energy function:} \quad g = g(\sigma_{ij}, \alpha_{ij}) \quad (2.22)$$

$$\text{Yield function:} \quad y = y^g(\sigma_{ij}, \alpha_{ij}, \chi_{ij}) = 0 \quad (2.23)$$

where σ_{ij} is stress tensor, α_{ij} is internal variable (or plastic strain) tensor, and χ_{ij} is generalized stress.

In the formulation described by Houlsby and Puzrin (2000), the following derivative relationships are obtained:

$$\chi_{ij} = -\frac{\partial g}{\partial \alpha_{ij}}, \quad \varepsilon_{ij} = -\frac{\partial g}{\partial \sigma_{ij}}, \quad \text{and} \quad \dot{\alpha}_{ij} = \lambda \frac{\partial y^g}{\partial \chi_{ij}} \quad (2.24)$$

where $\dot{\alpha}_{ij}$ is plastic strain rate, ε_{ij} is strain tensor, and λ is arbitrary non-negative multiplier.

Secondly, the hyperplasticity theory for rate-dependent material is developed by Houlsby and Puzrin (2006). This model is also identified two potential functions. The energy function does not change from rate-independent model, yet the yield function is replaced by flow potential (w). Many rate-dependent materials are considered the thermally activated processes. Therefore, for more understanding, the rate process theory (Mitchell and Soga, 2005) may be used in the sophisticated geotechnical problem. Its equation can be written as follow:

$$w = \mu r^2 \int_0^1 \left(\cosh \left(\frac{\langle |\dot{\chi}| - k(\hat{\alpha})\eta \rangle}{\mu r} \right) - 1 \right) d\eta \quad (2.25)$$

where k is strength parameter, μ is viscosity coefficient, and r is constant with the dimensions of strain rate. The Macaulay brackets is $\langle \cdot \rangle$; $\langle x \rangle = 0$, $x < 0$; and $\langle x \rangle = x$, $x \geq 0$.

For the realistic modelling which gives a smooth transition between an elastic and an elastic-plastic behaviour, an extension of single yield surface to continuous hyperplasticity is considered by Houlsby and Puzrin (2006). This approach employs an infinite number of yield surface expressed in term of an internal coordinate (η). However, a finite number N of a surface must be practically employed instead of an infinite number of yield surface as defined in equation below.

$$\text{Energy function: } g(\sigma_{ij}, \alpha_{ij}^{(1)}, \dots, \alpha_{ij}^{(N)}) \quad (2.26)$$

$$\text{Yield function: } y^g(\sigma_{ij}, \alpha_{ij}^{(1)}, \dots, \alpha_{ij}^{(N)}, \chi_{ij}^{(1)}, \dots, \chi_{ij}^{(N)}) = 0 \quad (2.27)$$

The kinematic hardening mechanism is selected as a key stage in developing a model. The hardening term is expressed in the energy function. For this case, the presentations of Gibbs free energy function become as below equation.

$$g = -\frac{\sigma^2}{2E_0} - \sigma \int_0^1 \hat{\alpha} d\eta + \int_0^1 \frac{\hat{H} \hat{\alpha}^2}{2} d\eta \quad (2.28)$$

where σ is stress, E_0 is initial stiffness, η is “internal coordinate” which effectively specifies size of the yield surface, and $\hat{\alpha} = \hat{\alpha}(\eta)$ is internal parameter that plays the role of the plastic strain. The “kernel function” $\hat{H} = \hat{H}(\eta)$, which defines the basic shape of the stress-strain curve is defined for this specific model as:

$$\hat{H}(\eta) = \frac{E_0}{2(a-1)} (1-\eta)^3 \quad (2.29)$$

where a is shape parameter controlling the rate of change of tangent stiffness (see detail Likitlersuang *et al.*, 2007). Strain hardening or softening can be introduced by allowing k to be dependent on $\hat{\alpha}$. Here we adopt an exponentially decaying function which allows more consistent modelling of the response at large strain:

$$k(\hat{\alpha}) = k_0 \exp(-\alpha/\alpha_0) \quad (2.30)$$

where α is cumulative total plastic strain, k_0 is initial strength value, and α_0 is reference strain which controls the rate of reduction of strength.

In 2007 Likitlersuang and Houlsby developed the rate-dependent hyperplasticity model for predicting the behaviour of Bangkok Clay. The Gibbs free energy functional and the flow potential are defined as Equation 2.28 and 2.25 respectively. The incremental stress-strain response is then given by:

$$d\varepsilon = \frac{d\sigma}{E_0} + \left[\int_0^1 r \sinh \left(\frac{\langle |\sigma - \hat{H}\hat{\alpha}| - k(\hat{\alpha})\eta \rangle}{\mu r} \right) S(\sigma - \hat{H}\hat{\alpha}) d\eta \right] dt \quad (2.32)$$

where $S(x)$ represents extended signum function $S(x) = -1, x < 0$; $-1 \leq S(x) \leq 1, x = 0$; $S(x) = 1, x > 0$. To predict the behaviour of stress and strain of rate-dependent material, 6 parameters ($E_0, k_0, \mu, r, \alpha_0, a$) are used.

2.12 Summary

From these three parts of literature review, the typical of flexible pavement structure, the failure criteria, the critical stress/strain of flexible pavement, the asphaltic concrete behaviour, and the asphaltic concrete characteristic are discussed in details by the investigation of the conventional engineering knowledge. Moreover, the asphaltic concrete behaviour is approached by the study of viscoelastic model and elasto-visco-plastic model. The effect of time-temperature of asphaltic concrete can be then comprehended by studying the principle of time-temperature superposition with growing damage (Schwartz *et al.*, 2002). We can also define the strength behaviour of material and the particle rank of material by the rate process theory depending on the relation of potential-distance relation and strain rate equation (Mitchell and Soga, 2005). Lastly, the hyperplasticity theory (Houlsby and Puzrin, 2006) and development of hyperplasticity model (Likitlersuang and Houlsby, 2007) are concluded.

CHAPTER 3

Experimental programme

3.1 Introduction

This chapter consists of description of experimental programme and its result. Firstly, the material, the specimen preparation, testing apparatus, and testing procedure are briefly described. The salient features of test procedure are furthermore explained. Next, the illustration of testing results is presented. The stress-strain relation under the static indirect tensile test (S-IDT) and the static unconfined compression test (S-UC) are shown. The resilient modulus at the different temperatures studied from the cyclic indirect tensile test (C-IDT) is determined. The flow number (FN) at various temperatures by cyclic unconfined compression test (C-UC) is also concluded here.

3.2 Material properties

Materials employed in this study are designed according to Marshall Method. This is because it is still a standard design in Thailand and other developing countries. The penetration grade of AC 60/70 is selected as asphalt binder. The limestone with nominal max size of 12.5 mm is used in this study. All materials based on the standards for highway construction (DH.-S) and the standards for materials (DH.-SP) of Department of Highway, Thailand.

The engineering properties of AC 60/70 are the specific gravity of 1.02 and the asphalt lost by absorption of 0.24%. For the aggregate, the properties are the bulk specific gravity of 2.70 and the LA abrasion of 25%. The gradation for mixing is shown in Figure 3.1. All of these materials are practically used for the road construction in Thailand. These selected materials are designed with 5.5% by weight of AC 60/70.

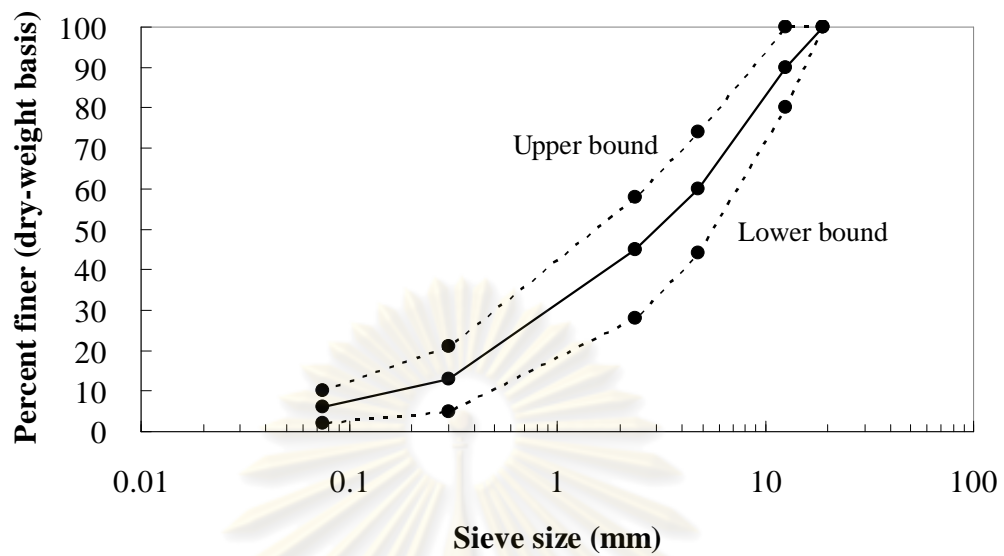


Figure 3.1 Gradation of aggregate

3.3 Specimen preparations

The asphaltic concrete mixtures are compacted by Superpave Gyratory Compactor (SGC) as shown in Figure 3.2. The SGC is operated by computer. The mould of SGC is rotated through a 1.25 ± 0.02 degree pivot angle. While the mould is being rotated at 30 rev/min, a 600 ± 18 kPa static load is placed on the specimen through the use of ram. The specimen dimension is 100 mm diameter with 65 mm height for the indirect tensile tests; on the other hand, the specimen of 100 mm diameter with 150 mm height is prepared for unconfined compression tests. After compaction using SGC the density of 2400-2450 kg/m³ (based on Marshall mixed design) and the air void content of 3-5% were achieved.

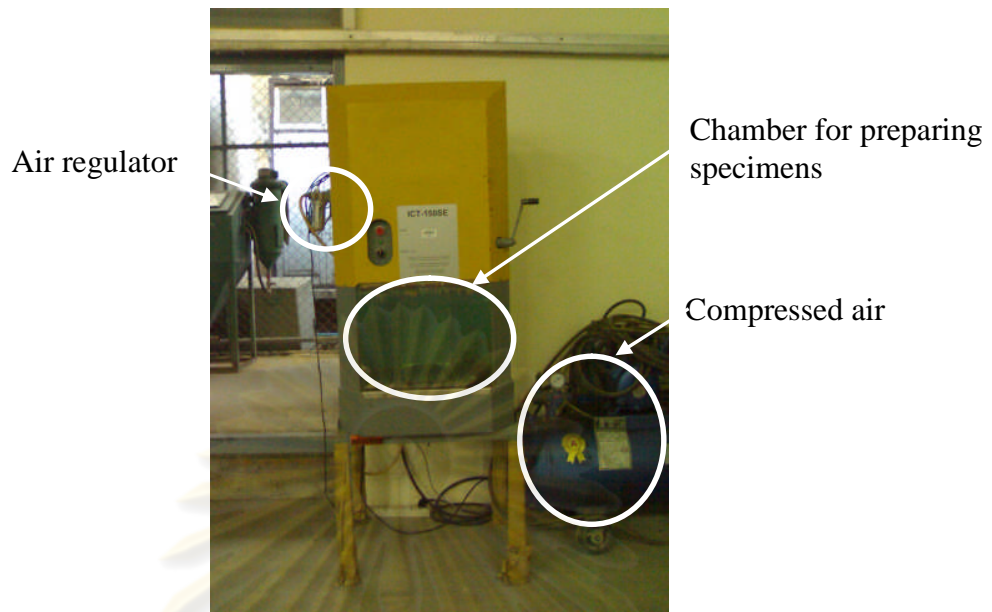


Figure 3.2 Superpave gyratory compactor

3.4 Test apparatuses

The main apparatuses used are composed of the Instron UTM-1.2MN for the static load condition and the Controls UTM-14kN for the cyclic load condition. Since the Controls UTM-14kN is unable to provide enough capacity of loading for the static test, the Instron UTM-1.2MN is chosen for the static condition. Firstly, the Instron UTM-1.2MN is employed for studying the properties of asphaltic concrete as presented in Figure 3.3(a). Instron UTM-1.2MN can be used for both a static scheme and a cyclic scheme. This machine is however used only for the static scheme in this occasion, only a works ability of static scheme is presented in this part. Instron UTM-1.2MN is able to control the loading rates in both a stress and a strain condition. The loading are provided by hydraulic actuator which is controlled by electronic pneumatic servo-valve. The maximum capacity of Instron UTM-1.2MN is 1.2MN. IST Systems FastTrack and Labtronic 8800 Test Control Systems is used to control the Instron UTM-1.2MN. These controlling systems are connected to the computer system. The software called Merlin is employed to communicate between the operator and the machine via the controlling systems. The limitation of Instron UTM-1.2MN is an open-air system which cannot control the temperature during test. To manage the desired temperature, the specimens are cured using the temperature chamber. While

transferring the specimens to the Instron UTM-1.2MN, the foam box is employed to control the temperature of specimens.

Secondly, the Controls UTM-14kN is used for studying the temperature properties of asphaltic concrete as shown in Figure 3.3(b). The effectivenesses of Controls UTM-14kN are a load manner and a loading wave shape. Several loading wave shapes such as a haversine wave and a square wave are provided by pneumatic actuator of the machine. Moreover, the Controls UTM-14kN gives the maximum load at 14 kN with 0 to 70 Hz. There are four paths of the machine: (1) Reaction load frame, it is designed for 100 mm diameter specimen in both an indirect tensile and an axial load. Pneumatic actuator is controlled by electronic pneumatic servo-valve. (2) Temperature chamber, a specimen can be set in the selected temperature from 0°C to 60°C by employing this chamber. (3) Control and Data Acquisition System (CDAS) is employed to control an operation, and it is connected to the computer system, LVDTs, and the load system to deal with the data. (4) Software is used to communicate between the operator and the machine via CDAS.



(a)



(b)

Figure 3.3 (a) Instron UTM-1.2MN (b) Controls UTM-14kN

3.5 Experimental procedures

In this section the procedures of all tests are explained. The test modes are composed of indirect tensile (IDT) and unconfined compression (UC). All of these tests base on static and cyclic conditions. They are performed under different factors such as strain rate and temperature that are interpreted as follows:

3.5.1 Static and cyclic indirect tensile tests

In the static study the specifications of static test are based on the Static Indirect Tensile Test (S-IDT) or ASTM D 4867. The temperature at 25°C and the rate of loading at 0.0083 s⁻¹ are recommended for the static condition referring to ASTM D 4867. Resulting from the purpose in studying the effect of rate of loading and temperature to the asphaltic concrete behaviour, the values of both rate of loading and temperature are varied. Four different loading rates of 0.0250, 0.0083, 0.0025, and 0.0008 s⁻¹ are applied to investigate the effect of loading rate on the micro-cracking development until reaching the failure. Following the S-IDT test, the temperatures selected are 10°C, 25°C, 40°C, and 55°C. These temperature ranges practically occur on the pavement layer in Thailand. The specimen size of 100 mm diameter and 65 mm height is used for this test. The radial strains are measured by two strain gauges (gauge length 20 mm). The S-IDT test setup utilised in this research is shown in Figure 3.4(a). All of specimens are tested using UTM-1.2MN and data collecting system as shown in Figure 3.4(b). The UTM-1.2MN is however unable to control the selected temperatures during testing; consequently, the temperature chamber (Figure 3.3b) is used for setting the required temperatures and the foam box is also employed for managing the temperatures when transferring to the specimens. The programme of S-IDT is shown in Table 3.1.

In the cyclic condition the specifications of testing is also based on ASTM standard, which consists of the Indirect Tension Test for Resilient Modulus of Bituminous Mixtures (C-IDT) or ASTM D 4123. Following this standards, the indirect tensile strength value (ITS) at 25°C is used for the prediction of resilient modulus (M_r) at all temperatures. The C-IDT test is nevertheless applied to be suitable

for the asphaltic concrete in the conditions of real field. For this research, the ITS values at each temperature are used separately. For instance, the ITS value at 10°C is the amplitude for determining the resilient modulus at 10°C.

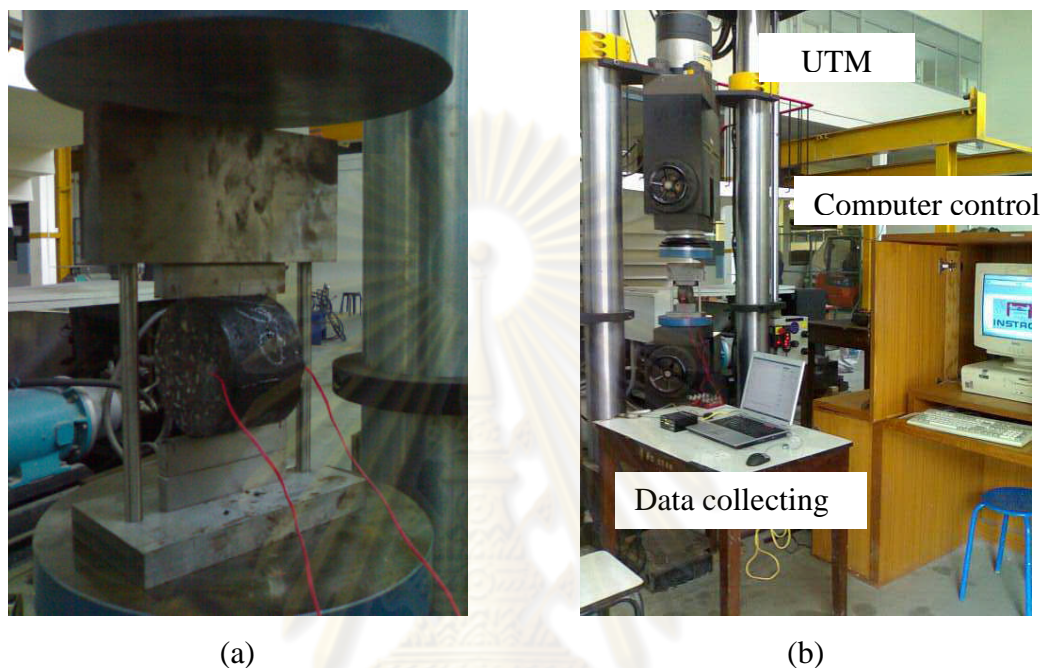


Figure 3.4 (a) Schematic of S-IDT test setup (b) Instruments for S-IDT test

For the apparatuses employed in C-IDT test, Figure 3.3(b) illustrates the Controls UTM-14kN, and Figure 3.5 shows the test utilised. To measure the horizontal deformation, the LVDT (Linear Variable Differential Transducer) is then installed. After that a specimen is loaded in the haversine function across its diametric plane. As mentioned above, the temperatures at 10°C, 25°C, 40°C, and 55°C are also selected for C-IDT test. The peak loading forces of S-IDT test used for each temperature are 2.48, 0.97, 0.35, and 0.14 kN. These values are equivalent to 10% of ITS at any particular temperature for each test. The specimens are continuously loaded by 1 Hz frequency with 155 cycles which first 150 cycles are for preload condition and last 5 cycles are for measuring the resilient modulus. The format of this load duration is 1 by 9 as illustrated in Figure 3.6. The seating stress or 10% of maximum stress is applied to remain the contacting between the actuator and the specimen during every loading cycle. The programme used for the C-IDT test is shown in Table 3.1.



Figure 3.5 Schematic of C-IDT test setup

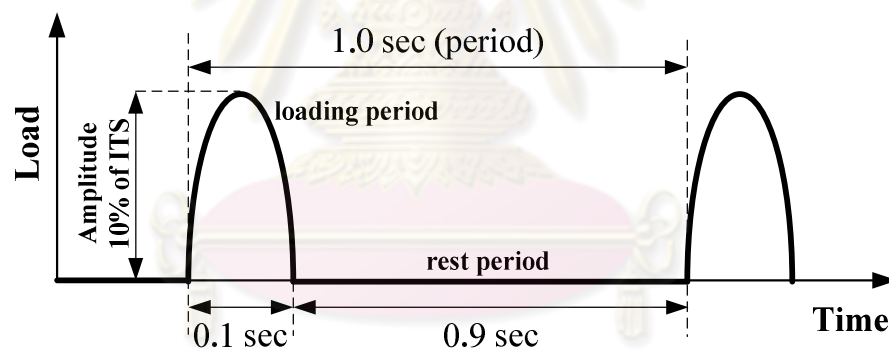


Figure 3.6 Shape and condition of loading

Table 3.1 Testing programme for the IDT test

| Type | Condition | Strain rate (per sec) | Temperature (°C) | | | |
|-----------------------|-----------|--|------------------|----|----|----|
| | | | 10 | 25 | 40 | 55 |
| Indirect tensile test | Static | 0.0250 | × | × | × | × |
| | | 0.0083 | × | × | × | × |
| | | 0.0025 | × | × | × | × |
| | | 0.0008 | × | × | × | × |
| | Cyclic | 1 Hz Load frequencies and 1:9 Load duration | × | × | × | × |

3.5.2 Static and cyclic unconfined compression test

For the static unconfined compression test (S-UC), the standard of S-IDT test is applied to the specification of this condition. The specimen dimension of this static condition is 100 mm diameter and 150 mm height. According to the main studying in the influence of rate of loading and temperature, both of these values are varied. Following this object, four different strain rates which are 0.0006, 0.0017, 0.0056, and 0.0167 s^{-1} is studied to investigate the effect of loading rate on the micro-cracking development until attaining failure. The temperatures selected are 10°C , 25°C , 40°C , and 55°C . In the static condition, the S-UC specimen is loaded along the specimen height. The vertical strains are afterwards measured by two strain gauges and the internal displacement gauge of Instron UTM-1.2MN. The S-UC test setup utilised in this research is shown in Figure 3.7(a). All specimens are tested using Instron UTM-1.2MN as same as the S-IDT test is run as expressed in Figure 3.4(b). For managing the selected temperature of specimen, the solution is same as the way of S-IDT test. Table 3.2 expresses the programme for S-UC.

For the cyclic condition, the specifications of testing are based on NCHRP report 465. This report consists of the Test Method for Repeated Load Testing of Asphalt Concrete Mixture in Uniaxial Compression. Similarly to C-IDT, the C-UC test is tested using Controls UTM-14kN as illustrated in Figure 3.3(b). The setup utilised in this research is shown in Figure 3.7(b). According to the stress level of passenger car, each specimen is loaded with this level at 207 kPa. A specimen 100 mm diameter by 150 mm height is prepared before it is loaded in the haversine function. LVDT which is used for collecting the vertical deformation is then installed to estimate the permanent deformation. The temperatures selected for C-UC test are also 10°C , 25°C , 40°C , and 55°C . The specimens are continuously loaded by 1 Hz frequency with 40,000 cycles or until they are failed. The format of this load duration is 1 by 9 as illustrated in Figure 3.6. The seating stress or 10% of maximum stress is applied during load duration.

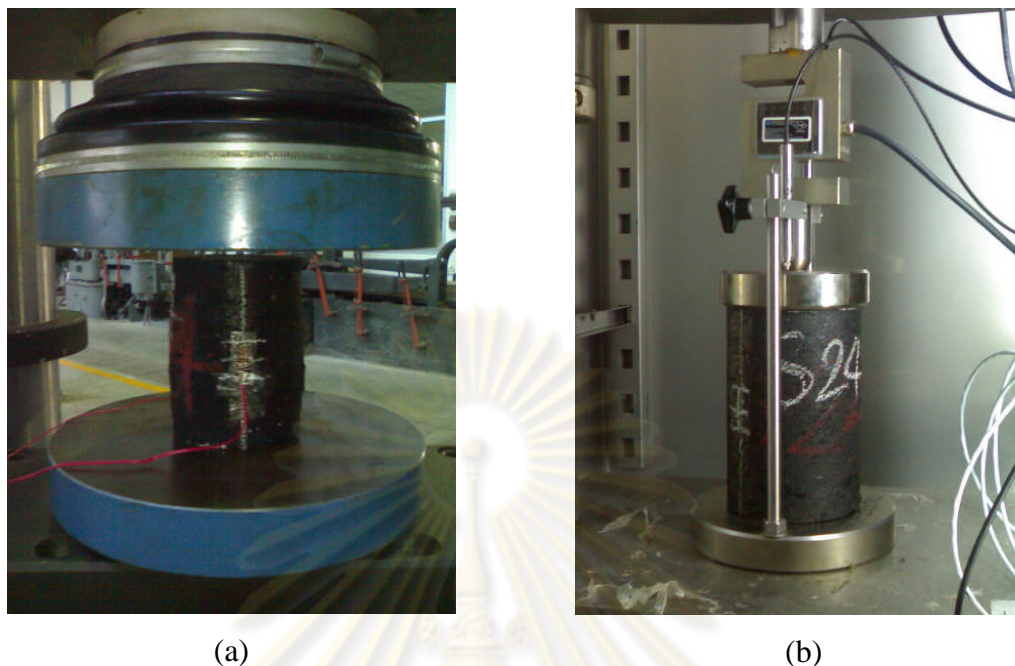


Figure 3.7 (a) Schematic of S-UC test setup (b) Schematic of C-UC test setup

Table 3.2 Testing programme for the UC test

| Type | Condition | Strain rate (per sec) | Temperature ($^{\circ}\text{C}$) | | | |
|--------------------------------|-----------|--|------------------------------------|----|----|----|
| | | | 10 | 25 | 40 | 55 |
| Unconfined compression test | Static | 0.0006 | × | × | × | × |
| | | 0.0017 | × | × | × | × |
| | | 0.0056 | × | × | × | × |
| | | 0.0167 | × | × | × | × |
| | Cyclic | 1 Hz Load frequencies and 1:9 Load duration | × | × | × | × |

3.6 Experimental results

This section describes the results of the series of performance tests i.e. S-IDT, S-UC, C-IDT, and C-UC. An analysis on the influence of temperature and/or strain rate is conducted. The experimental results can be summarised following as:

3.6.1 Static indirect tensile test (S-IDT)

The mechanical responses of the S-IDT tests varied temperature from 10°C , 25°C , 40°C , and 55°C are shown in Figures 3.8 to 3.11 respectively. At the

lowest temperature 10°C in Figure 3.8, the asphaltic concrete shows the highest peak stress and completely tensile behaviour. It can be observed the strength suddenly drops (softening) after peak due to the fact that at low temperature the asphaltic concrete behaves as a brittle material especially at the quickest test (0.0250 s⁻¹). The failure mechanism exhibits almost pure tensile mode as shown in Figure 3.12.

At standard temperature (25°C) the S-IDT behaviour can be competently expressed similarly at 10°C, but for the stress-strain curve of lowest strain rate (0.0008 s⁻¹), it displays both a tensile and a compressive modes. This can be investigated from Figure 3.9 that the initial stiffness is very steep, but the stress-strain relation trends to rebound after reaching peak region. This is because the boundary of tension zone at the diametric plane is smaller than the compression zones near the top and the bottom cap. That means the compression behaviour might dominate. Moreover, the stress-strain behaviours of specimens at 40°C (Figure 3.10) are similar to those at 25°C. It can be even observed more effect of compression zones around the top and the bottom cap especially at the slowest test (0.0008 s⁻¹). At the highest temperature (55°C) the stress-strain behaviour can be measured only the quickest test (0.0250 s⁻¹); nevertheless, its behaviour is not in purely tensile mode. There is moreover no the tensile behaviour observed at the other strain rates (see Figure 3.11).

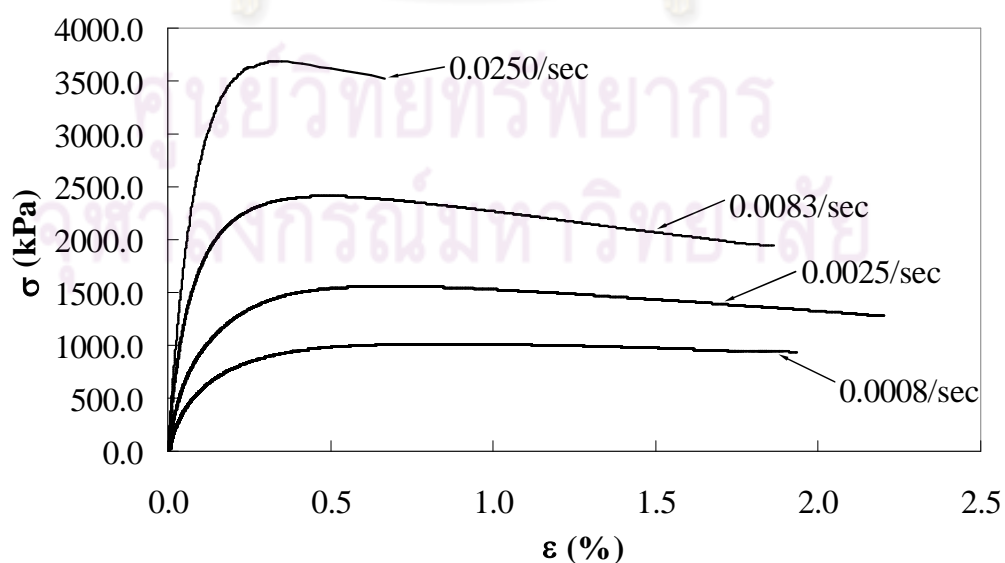


Figure 3.8 Stress-strain behaviour of S-IDT tests with different strain rates at 10°C

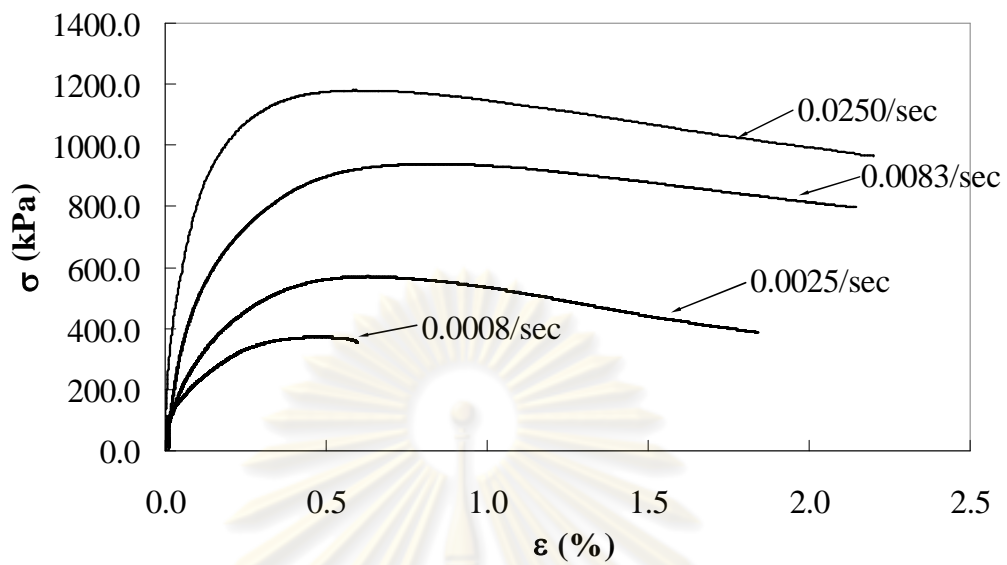


Figure 3.9 Stress-strain behaviour of S-IDT tests with different strain rates at 25°C

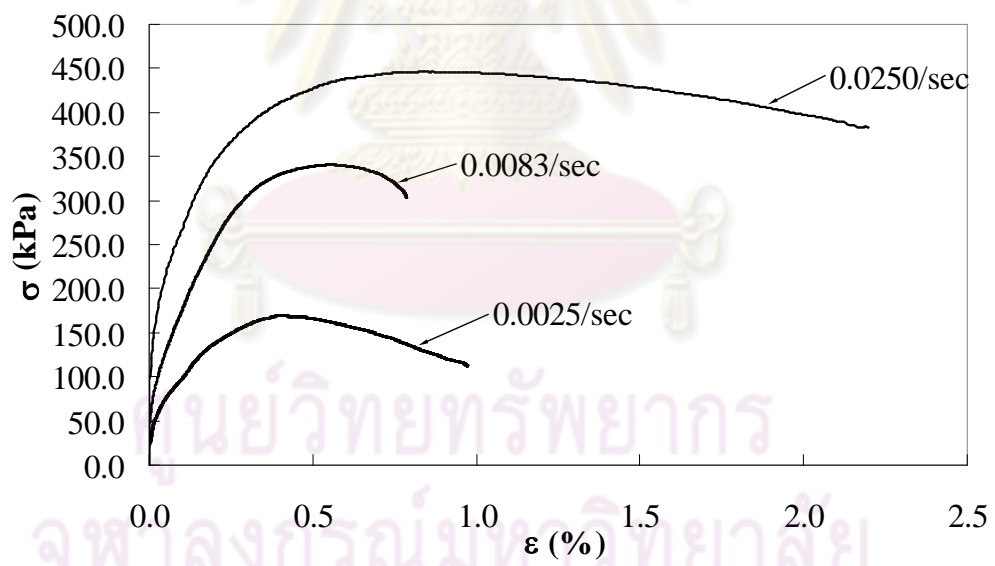


Figure 3.10 Stress-strain behaviour of S-IDT tests with different strain rates at 40°C

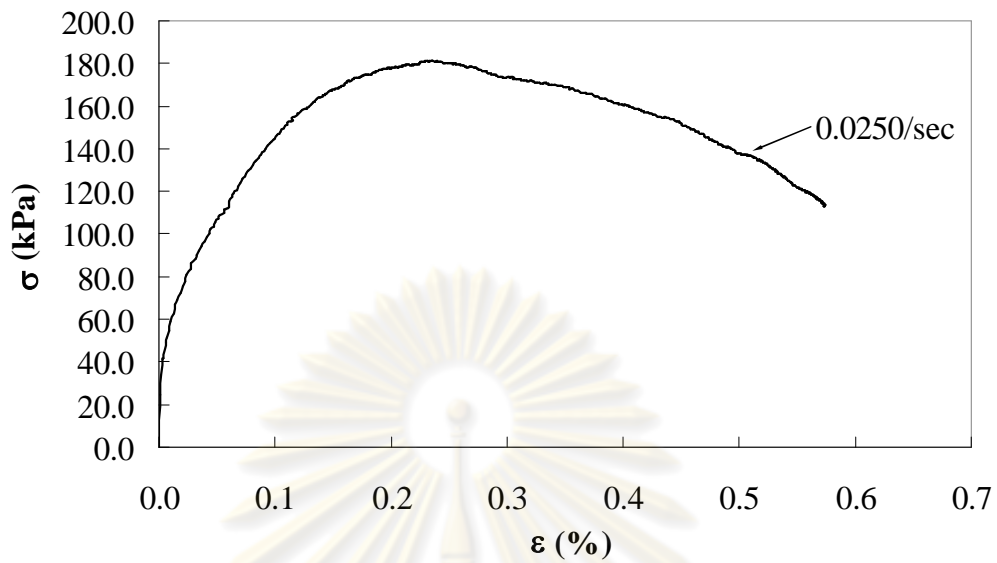
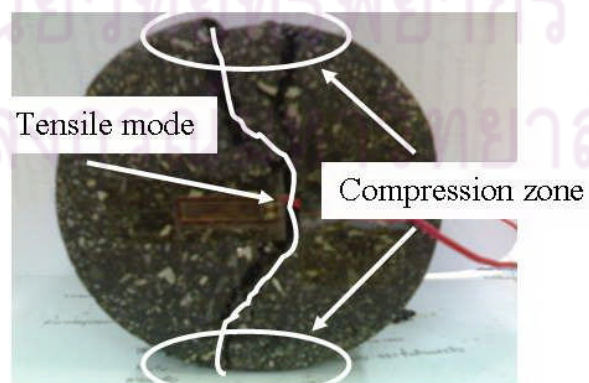


Figure 3.11 Stress-strain behaviour of S-IDT test at 55°C



(a)



(b)

Figure 3.12 Example of failure mechanism of asphaltic concrete under S-IDT test at (a) 10°C and strain rate of 0.0083/sec (b) 55°C and strain rate of 0.0008/sec

3.6.2 Static unconfined compression test (S-UC)

The experimental results and analyses of S-UC test are presented. Figure 3.13 to 3.16 summarise the measured stress and strain responses of the S-UC tests for all four temperatures. At 10°C (Figure 3.13) the maximum stress typically occurred at the strain value of approximately 1.5%. The magnitude of maximum stress increased with increasing of strain rate; however, the strain rate hardly influenced the strain at peak. The overall characters of data from 25°C, 40°C, and 55°C are similar to those finding from 10°C. Nevertheless, there are the evident anomalies in the data of 40°C and 55°C at the rate of 0.0056 s⁻¹. The curves are slightly flatter and the maximum stress values are smaller than what we expected. In the S-UC mode, all of specimens tested are perfectly failed in the compression mode. The typically failure mode was observed as shown in Figure 3.17.

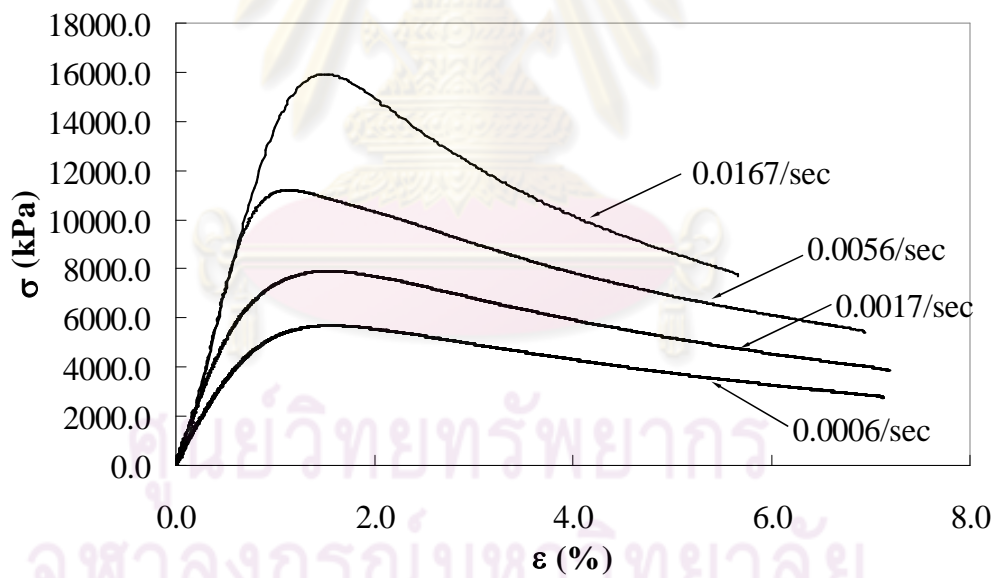


Figure 3.13 Stress-strain behaviour of S-UC tests with different strain rates at 10°C

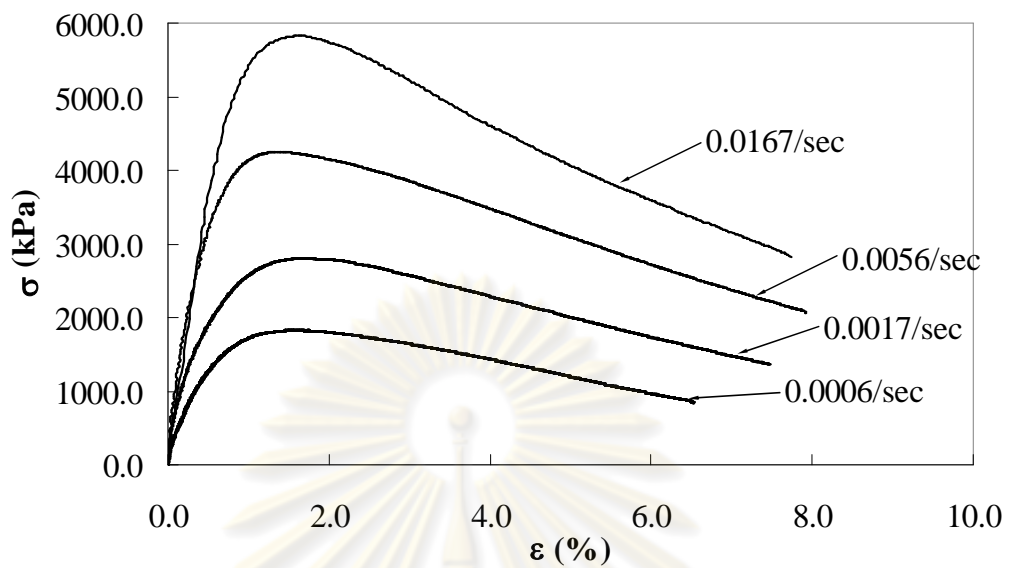


Figure 3.14 Stress-strain behaviour of S-UC tests with different strain rates at 25°C

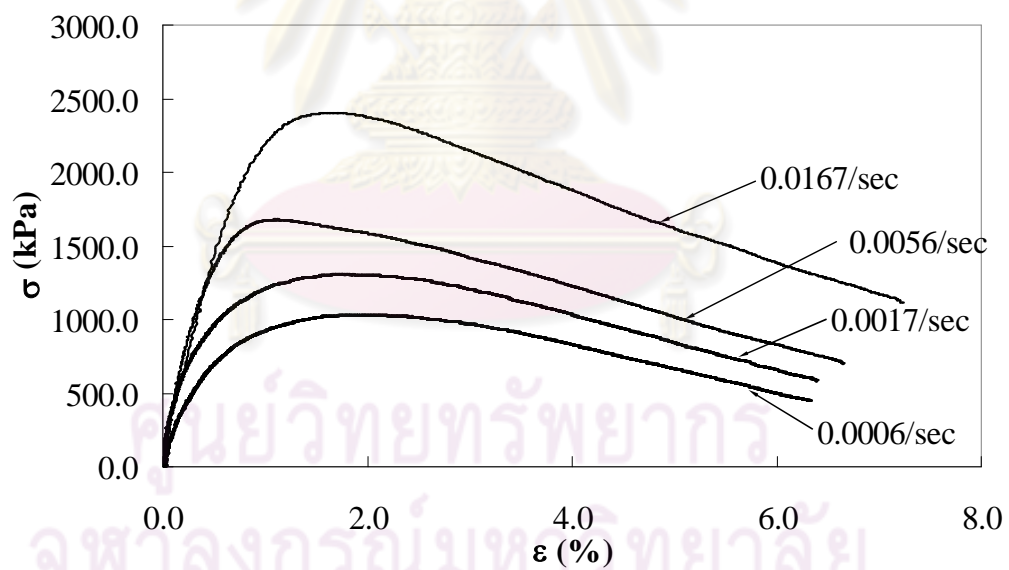


Figure 3.15 Stress-strain behaviour of S-UC tests with different strain rates at 40°C

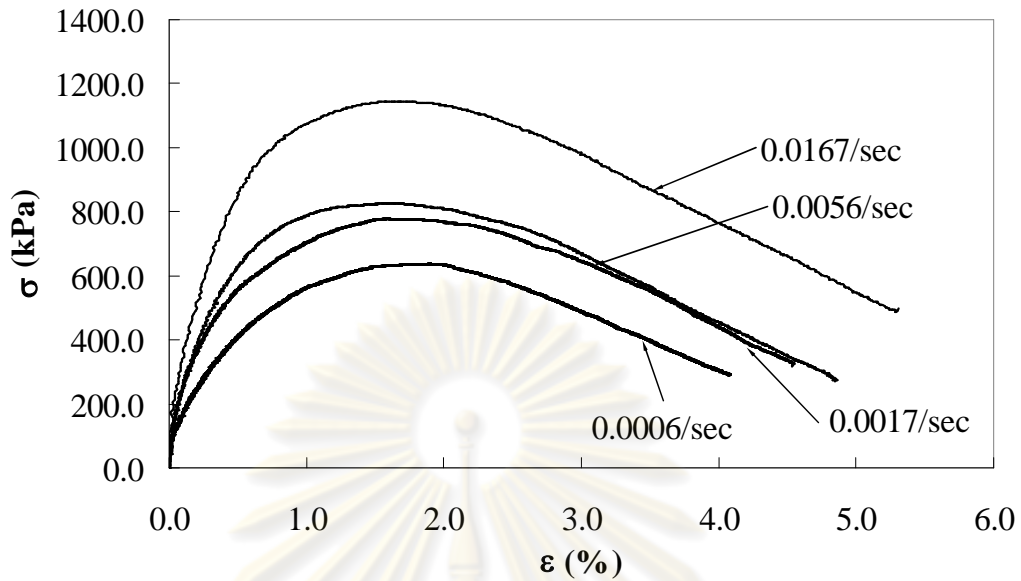


Figure 3.16 Stress-strain behaviour of UC tests with different strain rates at 55°C



Figure 3.17 Typical failure mechanism of asphaltic concrete under S-UC test

3.6.3 Cyclic indirect tensile test (C-IDT)

Following the outcome of C-IDT test, the resilient modulus under the changes of temperature which are at 10°C (283K), 25°C (298K), 40°C (313K), and 55°C (328K) are 14.47, 5.39, 0.66, and 0.26 GPa respectively. This result shows that the resilient modulus decrease when the temperature increase. Additionally, it can be

found that the increase in the value of resilient modulus form into an exponential function as presented in Equation 3.1 and Figure 3.18.

$$M_r = 7.00 \times 10^{12} \exp(-0.095\theta) \text{ GPa}; R^2 = 0.974 \quad (3.1)$$

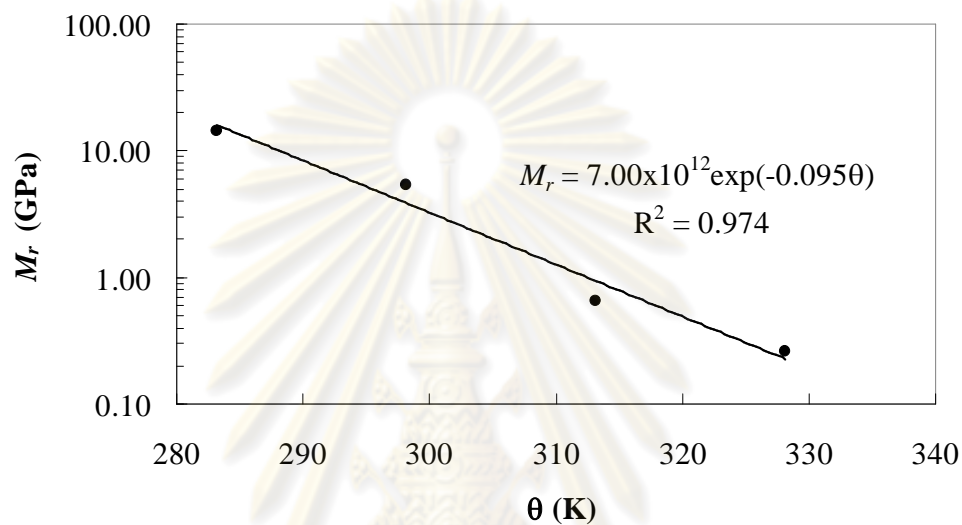


Figure 3.18 Variation of resilient modulus with temperatures

3.6.4 Cyclic unconfined compression test (C-UC)

It is noticeable that the asphaltic concrete displays the perfectly elastic behaviour at 10°C. This means that the asphaltic concrete which is at 10°C does not exhibit the permanent deformation behaviour. In the asphaltic concrete the permanent deformation can be observed at 25°C (Figure 3.19). The total strain which happens in the zone of primary creep and the ends in the zone of secondary creep is 0.45% approximately. The specimen does not fail in the testing limit of 40,000 cycles (Figure 3.19). The permanent deformation under the preferred four temperatures is displayed in Figure 3.19 to 3.21 for 25°C, 40°C, and 55°C respectively.

The permanent deformation can be investigated when the relation between the strain and the number of cycle is at 40°C (Figure 3.20). The asphaltic concrete specimen is failed at the 12,000 cycle. The relation between the strain and the number of cycle at the highest selected temperature (55°C) is quite same as when it is at 40°C.

The FN is however less than FN of 40°C. The FN of 55°C is approximately 3,000 as shown in Figure 3.21

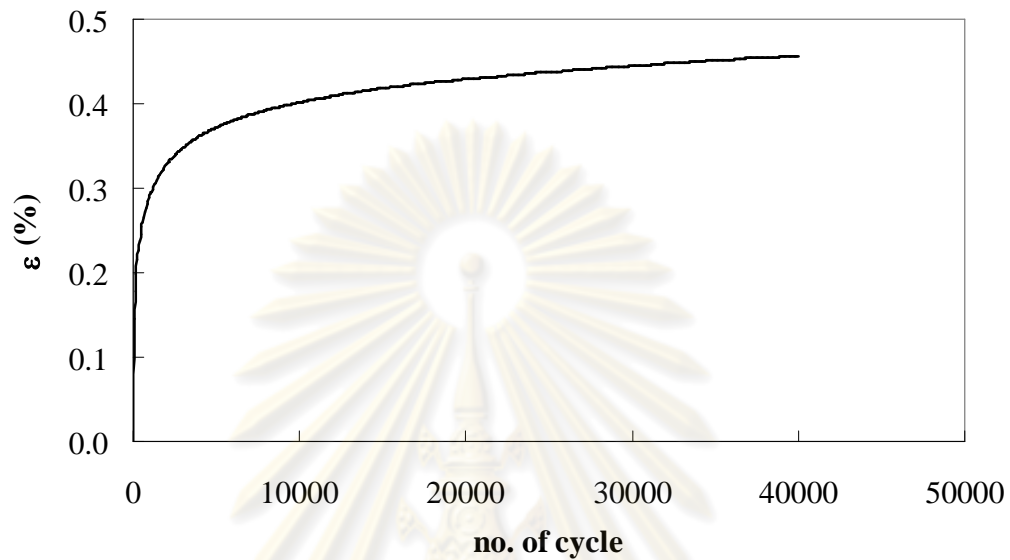


Figure 3.19 Relation of Strain and number of cycle for prediction the FN at 25°C

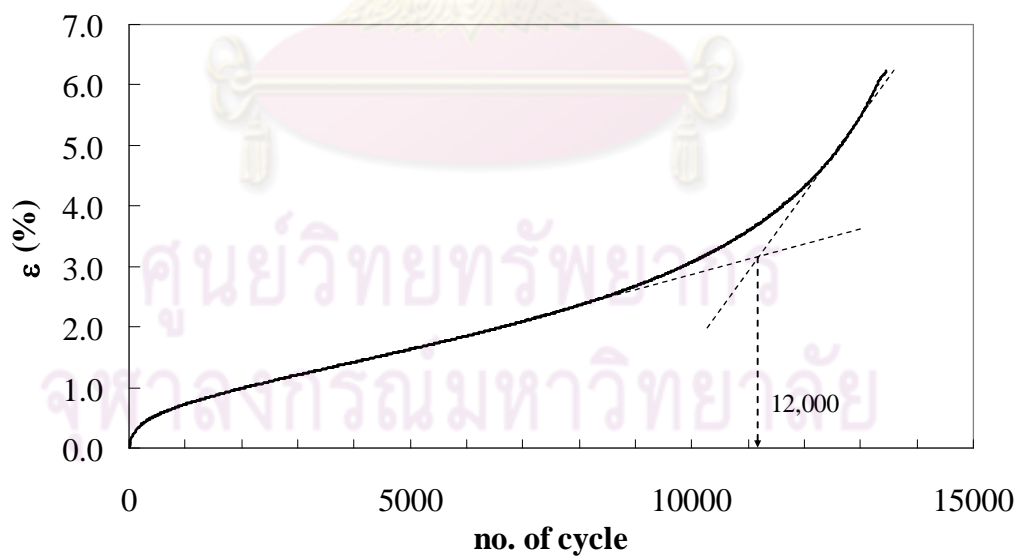


Figure 3.20 Relation of strain and number of cycle for prediction the FN at 40°C

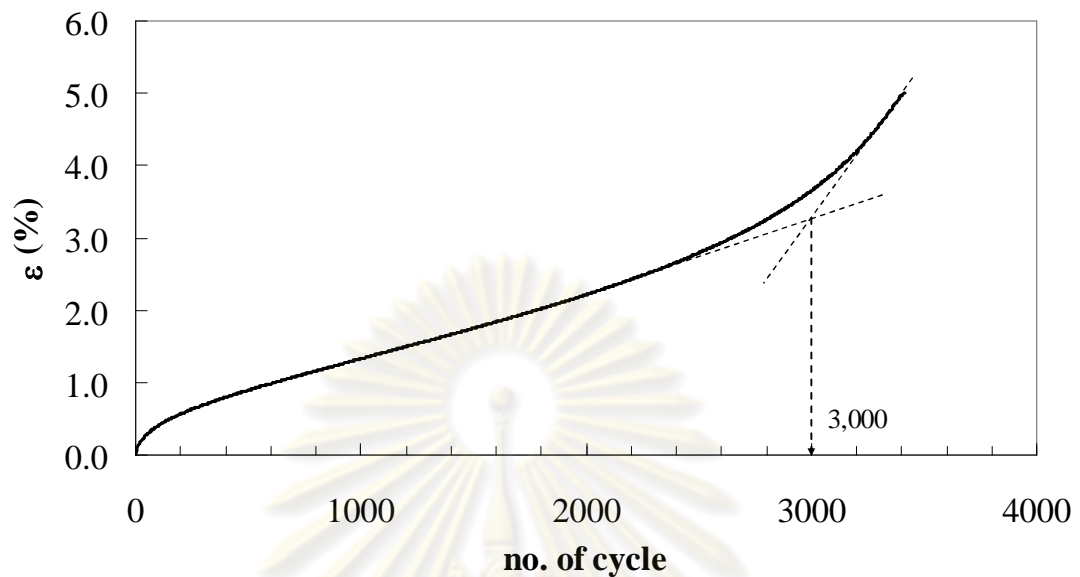


Figure 3.21 Relation of strain and number of cycle for prediction the FN at 55°C

3.7 Summary

In this chapter the asphaltic concrete behaviour can be evaluated by four the experimental tests. The material properties, testing apparatus, specimen preparation, and testing procedure are explained. The S-IDT and S-UC test show that the changing of both strain rate and temperature influence stress-strain relation. The C-IDT and C-UC are proved that the temperature affects to the resilient modulus and the resistance of permanent deformation properties.

ศูนย์วิทยทรัพยากร
จุฬาลงกรณ์มหาวิทยาลัย

CHAPTER 4

Analysis of experimental result

4.1 Introduction

This chapter refers to the result of experimental test in Chapter 3. The analyses of those experiments are described here. The stress-strain-strength characteristics of asphaltic concrete which are maximum stress, strain at peak, and the secant Young's modulus at 50% of maximum stress of static indirect tensile test (S-IDT) and static unconfined compression test (S-UC) are also concluded. The relation of resilient modulus and temperature tested by cyclic indirect tensile test (C-IDT) is then produced. An analysis on the influence of Poisson's ratio on the C-IDT test is conducted. The simple power-law equation for estimating the permanent deformation is summarised. The constant parameters for defining the simple power-law equation are also presented in a form of empirical formulas. From the S-IDT and S-UC, the time-temperature shift function is produced using cross plot method.

4.2 Static indirect tensile test (S-IDT)

As an experimental result, the maximum stress (σ_{\max}), the strain at peak ($\varepsilon_{\text{peak}}$), and the secant Young's modulus at 50% of maximum stress (E^{50}) of S-IDT test are measured as presented in the Table 4.1. Figure 4.1 to 4.2 show the variation of E^{50} and σ_{\max} with temperature of the S-IDT test. It can be concluded that both E^{50} and σ_{\max} roughly increase following the increase of strain rate and temperature. However, the data of strain at peak of S-IDT tests are even scattering and cannot be concluded as shown in Figure 4.3. The range of $\varepsilon_{\text{peak}}$ from S-IDT tests is 0.23- 0.91% (average 0.5%). Comparing with concrete which has the tensile strain before failure around 0.8-1.0%, the tensile strain at peak of asphaltic concrete closes to the typical value of concrete.

Table 4.1 Summarise of stress-strain-strength values from S-IDT tests

| Temperature (T, °C) | Strain rate ($\dot{\epsilon}$, s ⁻¹) | Secant Young's modulus at 50% of maximum stress (E^{50} , MPa) | Maximum stress (σ_{max} , kPa) | Strain at peak (ϵ_{peak} , %) |
|---------------------|--|---|--|---|
| 10 | 0.0008 | 646.49 | 1015.80 | 0.91 |
| | 0.0025 | 1126.86 | 1558.38 | 0.67 |
| | 0.0083 | 2492.28 | 2411.35 | 0.48 |
| | 0.0250 | 3560.99 | 3688.94 | 0.32 |
| 25 | 0.0008 | 294.80 | 372.10 | 0.49 |
| | 0.0025 | 305.78 | 570.27 | 0.63 |
| | 0.0083 | 525.04 | 938.89 | 0.81 |
| | 0.0250 | 1117.31 | 1180.08 | 0.59 |
| 40 | 0.0008 | N/A | N/A | N/A |
| | 0.0025 | 168.96 | 168.96 | 0.55 |
| | 0.0083 | 180.38 | 340.67 | 0.55 |
| | 0.0250 | 393.07 | 446.27 | 0.85 |
| 55 | 0.0008 | N/A | N/A | N/A |
| | 0.0025 | N/A | N/A | N/A |
| | 0.0083 | N/A | N/A | N/A |
| | 0.0250 | 280.24 | 181.29 | 0.23 |

N/A = Not Available (Test cannot be performed.)

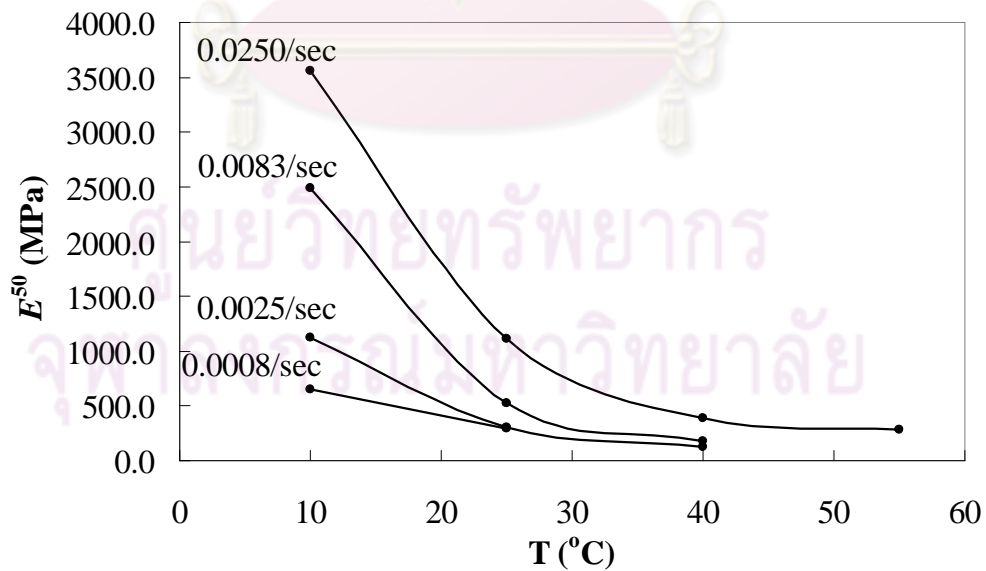


Figure 4.1 Variation of E^{50} with temperature of S-IDT tests

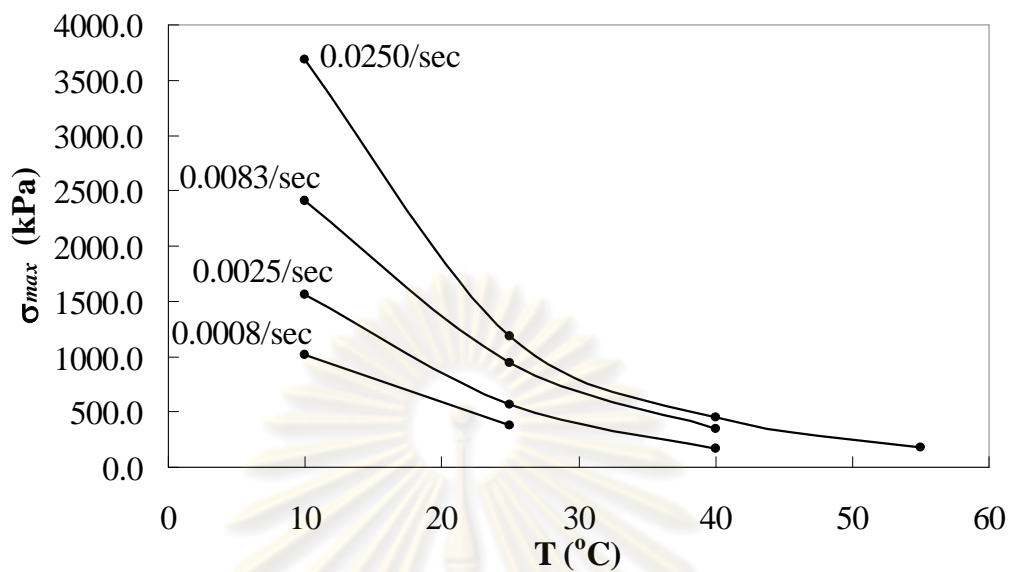


Figure 4.2 Variation of σ_{max} with temperature of S-IDT tests

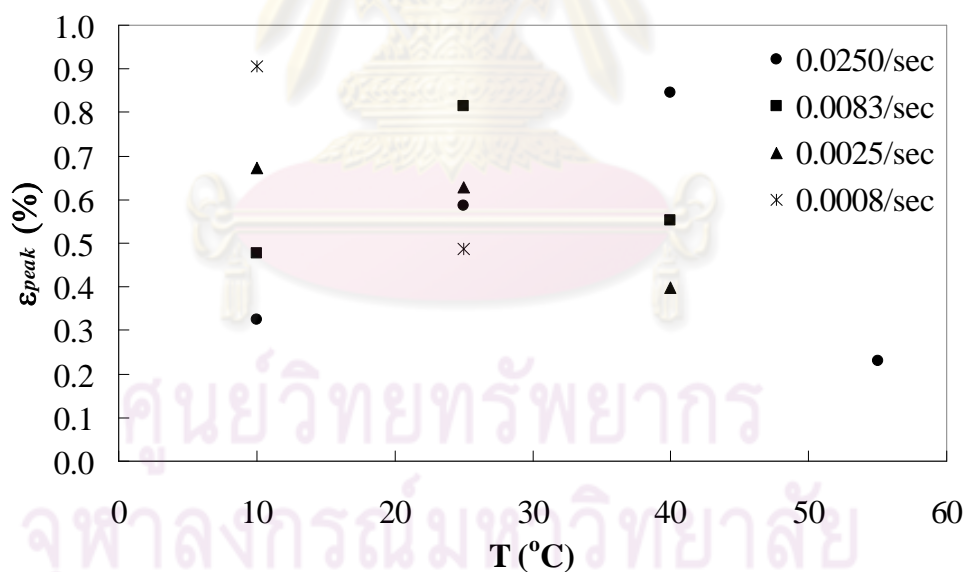


Figure 4.3 Variation of ϵ_{peak} with temperature of S-IDT tests

4.3 Static unconfined compression test (S-UC)

As an experimental result, the σ_{max} , ϵ_{peak} , and the E^{50} of S-UC test is measured as summarised in Table 4.2. Figure 4.4 to 4.5 show the variation of E^{50} and σ_{max} with the temperature of the S-UC test. It can be concluded that both E^{50} and

σ_{\max} roughly increase following the increase of strain rate and temperature. However, there are the evident anomalies of E^{50} under the S-UC condition at the strain rate of 0.0167 and 0.0056 s^{-1} data and at the temperature of 25°C and 40°C (see Figure 4.4). This is because it is difficult to control the first touch between the specimen and the loading plate perfectly. Resulting from those, there is a slightly effect at the beginning stress-strain curve of highest strain rate. The range of strain at peak of S-UC tests is scattering around 1.10-1.90% (average 1.50%) and can be zoned by upper and lower bound as shown in Figure 4.6. This value is smaller than what is typically found in a concrete (the compressive strain at failure of concrete is around 3%).

Table 4.2 Summarise of stress-strain-strength values from S-UC tests

| Temperature (T, °C) | Strain rate ($\dot{\epsilon}$, s^{-1}) | Secant Young's modulus at 50% of maximum stress (E^{50} , MPa) | Maximum stress (σ_{\max} , kPa) | Strain at peak (ϵ_{peak} , %) |
|---------------------|---|---|---|---|
| 10 | 0.0006 | 742.84 | 5685.64 | 1.58 |
| | 0.0017 | 1107.29 | 7894.84 | 1.53 |
| | 0.0056 | 1409.99 | 11202.93 | 1.13 |
| | 0.0167 | 1419.54 | 15910.43 | 1.52 |
| 25 | 0.0006 | 325.71 | 1827.37 | 1.57 |
| | 0.0017 | 508.35 | 2807.38 | 1.68 |
| | 0.0056 | 864.86 | 4251.71 | 1.36 |
| | 0.0167 | 741.44 | 5824.72 | 1.64 |
| 40 | 0.0006 | 172.29 | 1032.94 | 1.83 |
| | 0.0017 | 300.72 | 1307.77 | 1.67 |
| | 0.0056 | 365.01 | 1678.48 | 1.10 |
| | 0.0167 | 303.62 | 2405.62 | 1.66 |
| 55 | 0.0006 | 102.31 | 636.89 | 1.90 |
| | 0.0017 | 166.60 | 778.01 | 1.58 |
| | 0.0056 | 179.99 | 827.23 | 1.64 |
| | 0.0167 | 240.33 | 1145.52 | 1.64 |

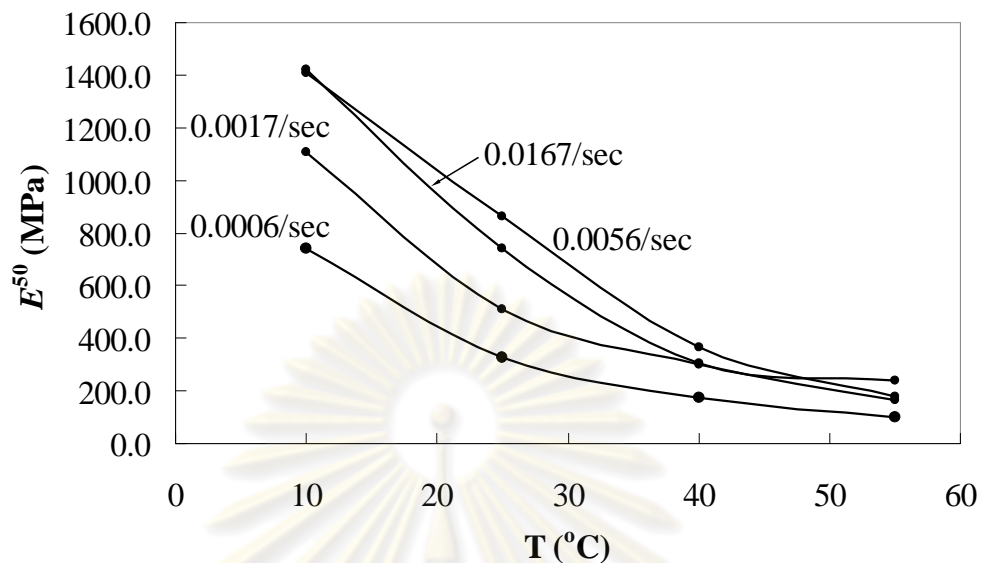


Figure 4.4 Variation of E^{50} with temperature of S-UC tests

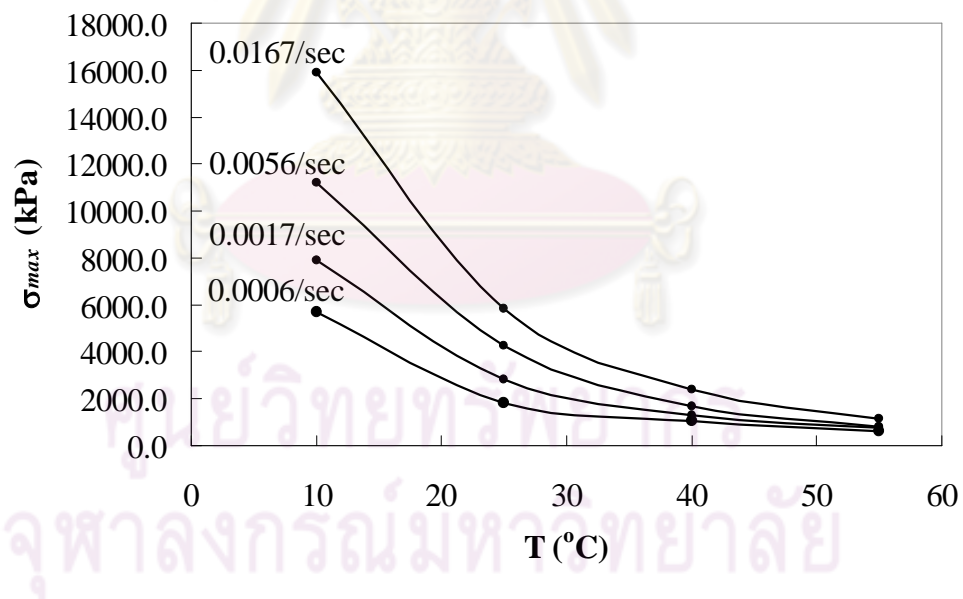


Figure 4.5 Variation of σ_{max} with temperature of S-UC tests

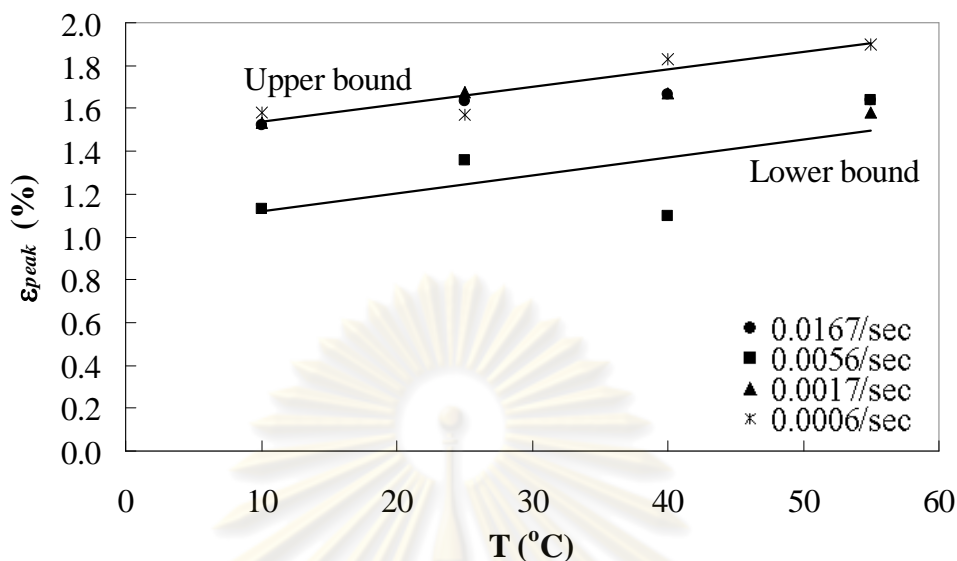


Figure 4.6 Variation of ε_{peak} with temperature of S-UC tests

4.4 Cyclic indirect tensile test (C-IDT)

Following the result of C-IDT test as explained in Section 3.6.3, the equation employed to estimate the resilient modulus (M_r) at different temperature can be determined in Equation 2.2. The Equation 4.1 shows the relationship of M_r with absolute temperature (θ) in Kelvin. The physical meaning of Equation 4.1 can be shown that where θ is 0 K or -273°C approximately, the resilient modulus value is 7.00×10^{12} GPa.

$$M_r = 7.00 \times 10^{12} \exp(-0.095\theta) \text{ GPa}; R^2 = 0.974 \quad (4.1)$$

According to Equation 4.1, an estimated resilient modulus is based on the Poisson's ratio of 0.35. Relying on ASTM D 4123, the Poisson's ratio of 0.35 is recommended for calculating M_r , but it may not fit to the actual experiment finding. The study of resilient modulus directly measured from the stress-strain curve and the changing values of Poisson's ratio from 0.20, 0.35 and to 0.50. The data scatter around the range of $\nu = 0.2 - 0.5$ as shown in Figure 4.7. For this analysis, each Poisson's ratio value is considered by relying on the least square method to find more suitable one instead of the recommend value of 0.35. As for this study the direct

measurement is hypothesised as it is possible to be the most proper. We can provide the suitable value of Poisson's ratio by means of least square parameter $((x_1 - x_2)^2)$ where x_1 is measured value and x_2 is calculation value. When the Poisson's ratio are 0.20, 0.35, and 0.50, the least square parameter are 48.04, 10.85, and 1.39 respectively.

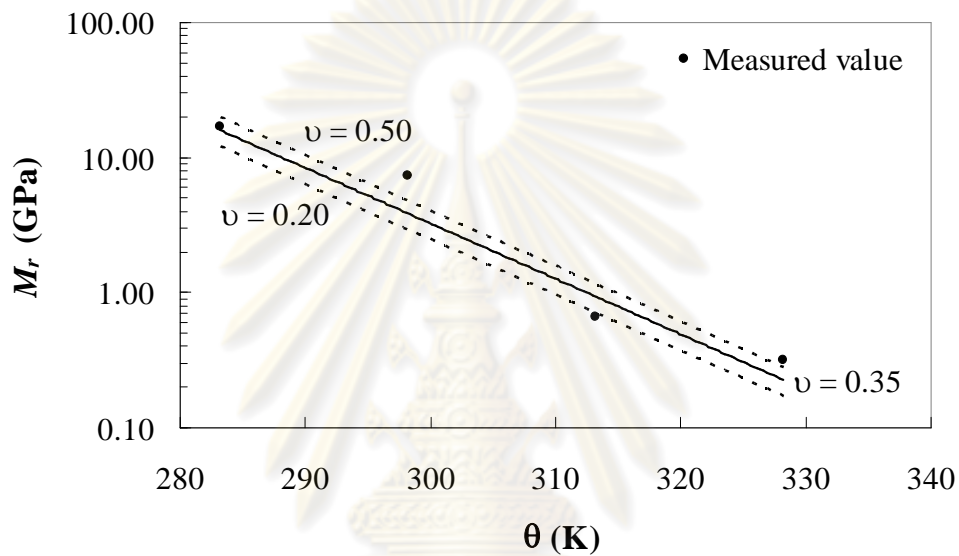


Figure 4.7 Parametric study for C-IDT test

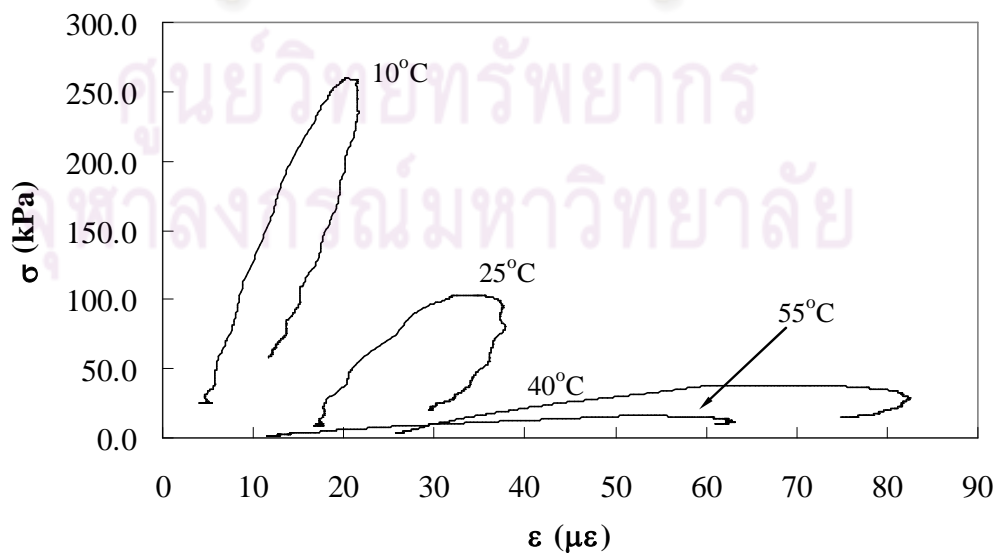


Figure 4.8 Relation of stress-strain at last cycle under C-IDT test

An investigation of stress-strain relation in the final cycle expresses that the permanent strain in the asphaltic concrete exists more obviously when the temperature is higher. This can be observed during unloading that the asphaltic concrete does not show purely recoverable behaviour.

4.5 Cyclic unconfined compression test (C-UC)

The simple power-law equation for estimating the permanent deformation can be written in form of a function of number of cycle as presented in Equation 2.3. The constants a and b are the regression constant which defined from the relation of strain and number of cycle in log-log plot as illustrated in Figure 2.9(b). The previous equation and constants can be produced by C-UC test as presented in Section 3.6.4. Figure 4.9 to 4.11 display the relation of strain and number of cycle for producing the classic power-law model at 25°C, 40°C, and 55°C.

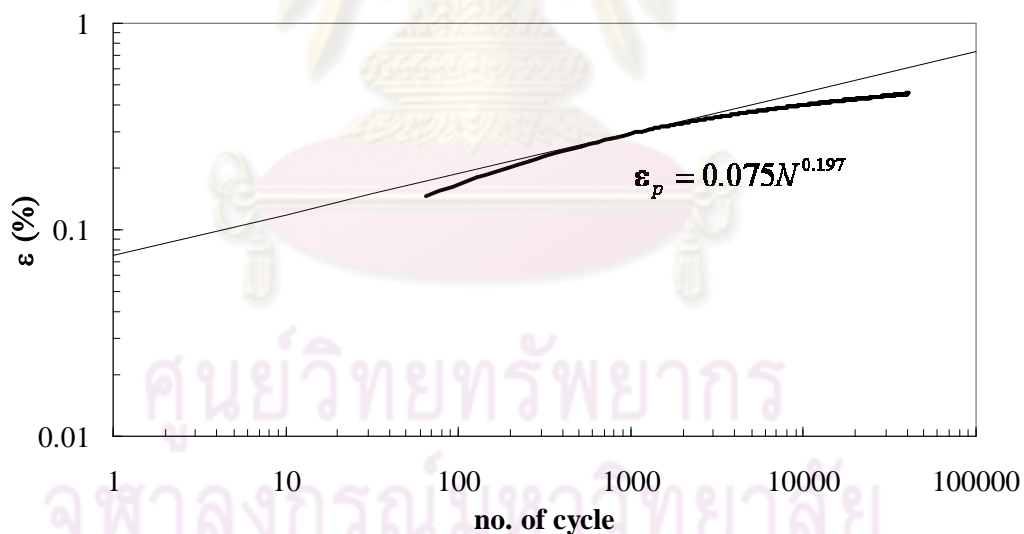


Figure 4.9 Relation of strain and number of cycle for producing the classic power-law model at 25°C

The relation of the constant a and b increase and decrease as it run in form of the exponential function. This relation is illustrated in semi-log plot as shown in Figure 4.12 and 4.13. These graphs can be employed to estimate the constants a and b at the various temperatures by the linear regression analysis as presented in Equation

4.2 and 4.3. These equations show the relationship of constant a and b with absolute temperature in Kelvin. Equation 4.2 and 4.3 are able to be defined in physical meaning as when θ is 0 K or -273°C approximately, the constant a and b value are 93.6 and 1.0×10^{-5} .

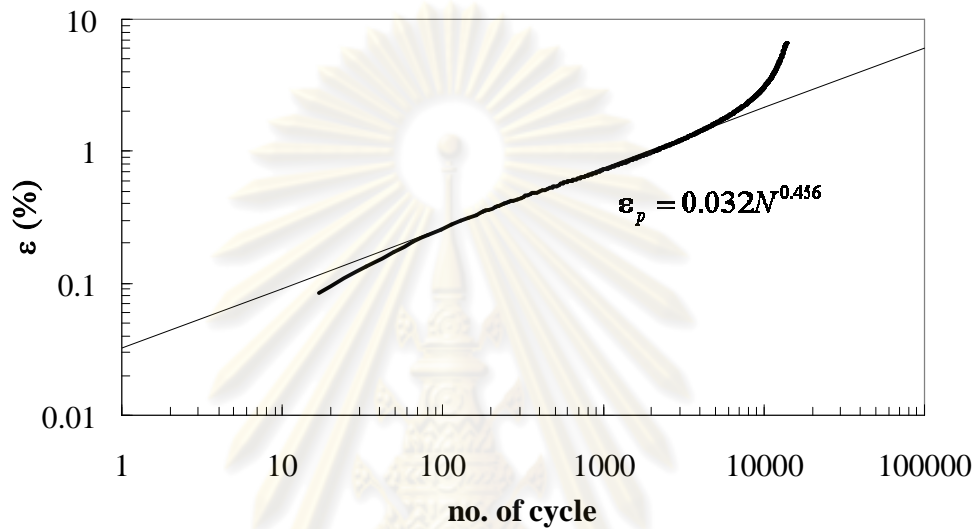


Figure 4.10 Relation of strain and number of cycle for producing the classic power-law model at 40°C

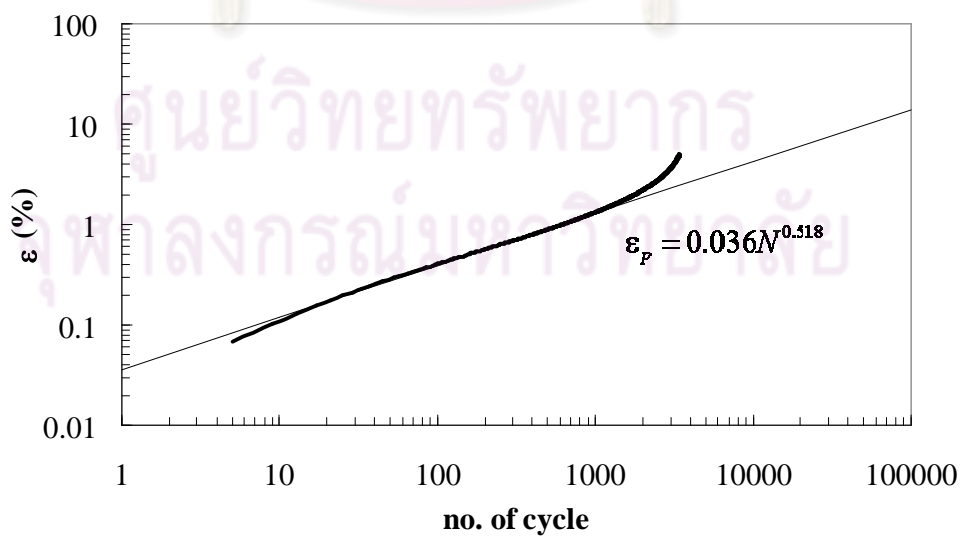


Figure 4.11 Relation of strain and number of cycle for produce the classic power-law model at 55°C

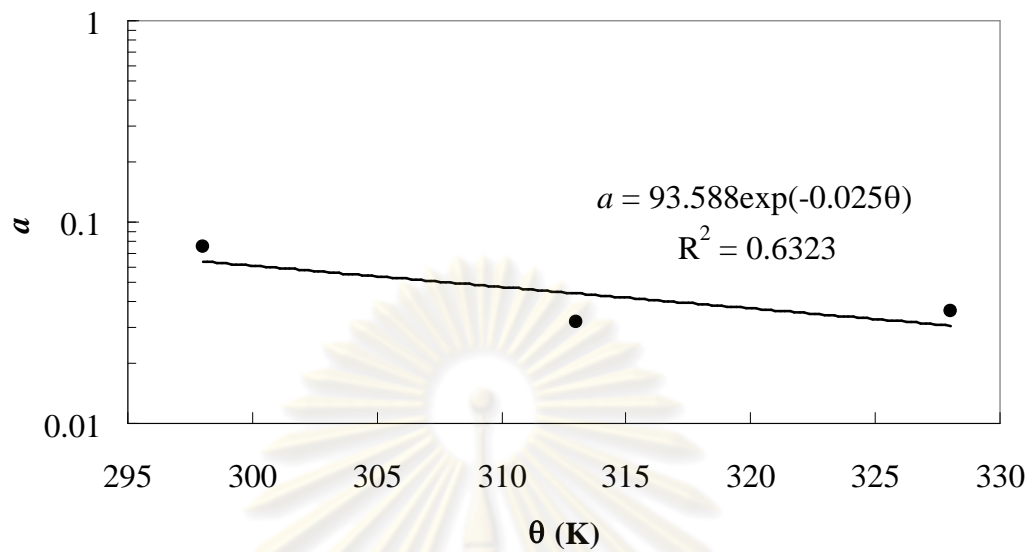


Figure 4.12 Variation of a parameter with temperature

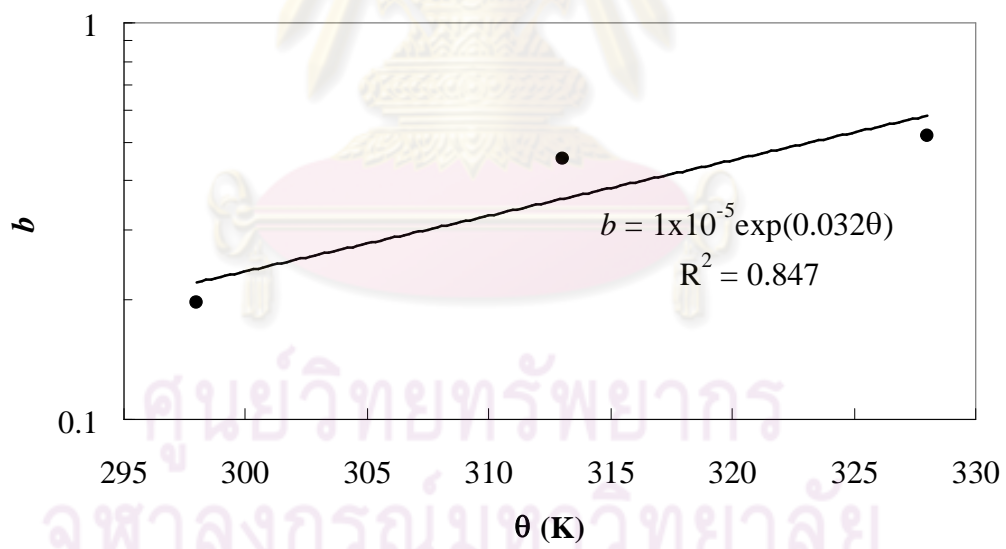


Figure 4.13 Variation of b parameter with temperature

$$a = 93.60 \exp(-0.025\theta); R^2 = 0.632 \quad (4.2)$$

$$b = 1.00 \times 10^{-5} \exp(0.032\theta); R^2 = 0.847 \quad (4.3)$$

4.6 Time-temperature superposition

From the results of the series of S-IDT and S-UC tests varied temperatures and rates of strain, the time-temperature superposition of asphaltic concrete can be analysed based on the framework of Schwartz *et al.* (2002) as described in Section 2.9. However, the analysis is extended to both S-IDT and S-UC tests. The reference strain of S-IDT and S-UC tests are selected at 0.5% and 1.5% since they are represented the average strain at peak of tension and compression tests respectively. The relation between the stress at a reference strain (σ_{ref}) and a reduce time (t_R) of both S-IDT and S-UC tests can be approximated by linear relationship as shown in Figure 4.14. The relationship between a temperature shift parameter (a_T) and temperature (T) can be concluded:

$$\log a_T = -0.0913T + 2.2353 \quad (4.4)$$

where T is temperature in °C. The regression analysis illustrated that the Equation 4.4 has $R^2 = 0.9978$ as shown in Figure 4.15.

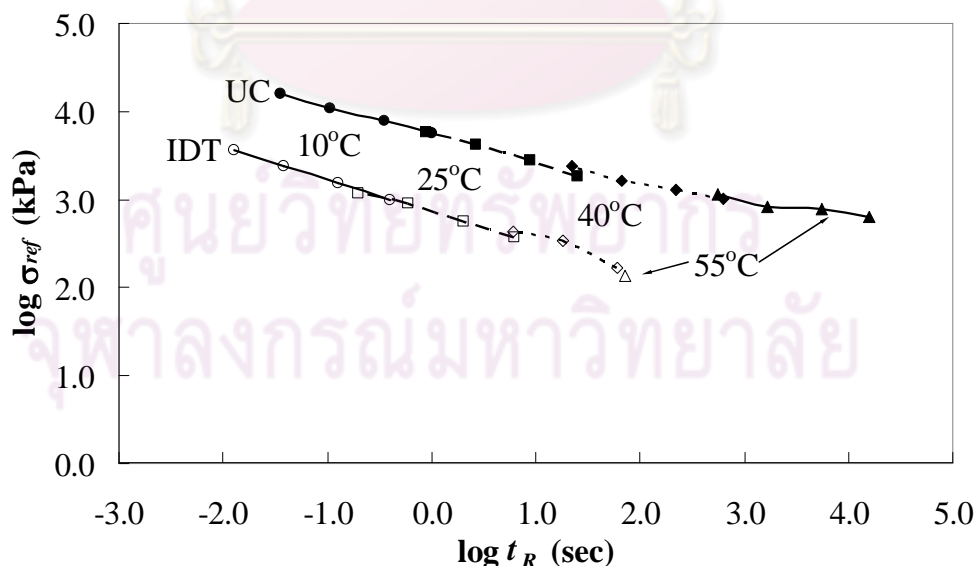


Figure 4.14 Stress-reduce time master curve from S-IDT and S-UC tests

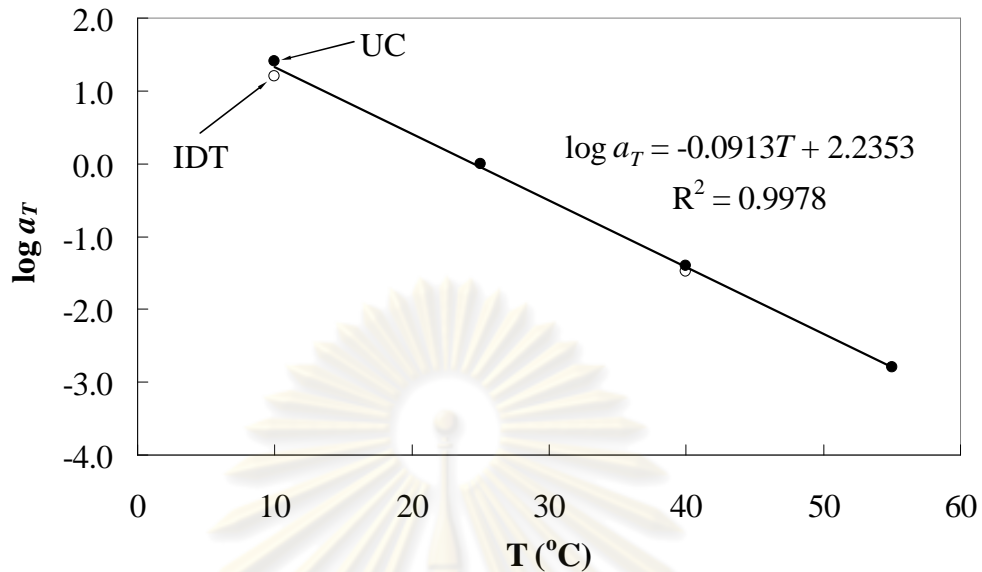


Figure 4.15 Time-temperature shift function from S-UC and S-IDT tests

4.7 Summary

We can conclude from S-IDT and S-UC test that the stress-strain-strength characteristic of asphaltic concrete relied on the changing of strain rate and temperature. From the result of C-IDT test, the empirical equation of resilient modulus and temperature can be used for the database of pavement design. The study of elastic parameter demonstrates that the most proper value of Poisson's ratio is 0.50. In C-UC test the permanent deformation can be predicted by the simple power-law equations by mean of using a and b as constant parameters. From S-IDT and S-UC we can produce the time-temperature shift function based on the framework of Schwartz *et al.* (2002). The analysis of time-temperature superposition shows that it is truly useful for estimating a compressive strength value at the various temperatures and the strain rates. For example, to determine the compressive strength when its temperature is at 40°C and its strain rates is 0.0056 s⁻¹, $a_T(40^\circ\text{C})$ is firstly determined. The $a_T(40^\circ\text{C})$ value of 0.04 can be then used to find out a strain rate by using this equation, $\dot{\epsilon}_{new} = a(T) \times \dot{\epsilon}_{old}$ ($\epsilon = \epsilon_{ref}$). The calculated strain rate is 0.000224s⁻¹. It is concluded that the compressive strength at the strain rate 0.0056s⁻¹ and the temperature 40°C can be replaced by the result at the standard temperature 25°C and the strain rate 0.000224s⁻¹.

CHAPTER 5

Development of constitutive model for asphaltic concrete

5.1 Introduction

This chapter presents a development of constitutive model for the shear response of asphaltic concrete, taking into account of strain rate and temperature effects. This constitutive model is expanded from Likitlersuang and Houlsby (2007). The viscous behaviour of model corresponds to the results of Rate Process Theory, and it is used to define the strain-rate and time dependent behaviour. After developing the model, a series of unconfined compression test reported by Schwartz *et al.* (2002) and Schapery continuum model are verified with the new model.

5.2 Constitutive equations

In this research the constitutive model for predicting the shear response behaviour of asphaltic concrete under the various selected temperatures and the strain rates are modified from the rate-dependent hyperplasticity model which is proposed by Likitlersuang and Houlsby (2007). The important parameters are considered as functions of temperature. The particular form of the flow potential (Equation 2.25) is chosen so that it results in viscous behaviour corresponding to rate process theory (for a useful information of this theory see Mitchell and Soga, 2005). An important feature of the rate process theory is that it also suggests how the parameters should vary with temperature. The viscous component of the stress σ_{visc} in the model is related to the plastic strain rate $\dot{\alpha}$ through an expression of the form:

$$\dot{\alpha} = r \sinh\left(\frac{\sigma_{\text{visc}}}{\mu r}\right) \quad (5.1)$$

where μ is viscosity coefficient and r is constant with the dimensions of strain rate. However, and very importantly, rate process theory (see Mitchell and Soga, 2005) leads to an expression of the form:

$$\dot{\varepsilon} = A\theta \exp\left(\frac{-B}{\theta}\right) \sinh\left(\frac{\sigma_{visc}}{C\theta}\right) \quad (5.2)$$

where A , B , and C are constants. The meaning of these constants is $\mu r = C\theta$, $r = A\theta \exp(-B/\theta)$, and $\mu = (C/A)\exp(B/A)$. Rate process theory does not allow the form of variation of E_0 and k_0 to be determined, but as μ represents measure of viscous strength and k_0 is a measure of cohesive strength it is reasonable to model them with the same overall functional form. For simplicity, E_0 is modelled in form of variation with temperature. Consequently, E_0 is $E_1 \exp(\theta_E/\theta)$, and k_0 is $k_1 \exp(\theta_k/\theta)$. For modifying the rate-dependent hyperplasticity model (Likitlersuang and Houlsby, 2007) using the rate process theory, the Gibb free energy function is defined as:

$$g = -\frac{\sigma^2}{2E_1 \exp(\theta_E/\theta)} - \sigma \int_0^1 \hat{\alpha} d\eta + \int_0^1 \frac{E_1 \exp(\theta_E/\theta)}{2(a-1)} (1-\eta)^3 \frac{\hat{\alpha}^2}{2} d\eta \quad (5.3)$$

where E_1 is reference Young's modulus, θ_E is reference temperature of E term, and θ is absolute temperature. The flow potential is specified as:

$$w = CA\theta^2 \exp\left(-\frac{B}{\theta}\right) \int_0^1 \left(\cosh \left(\frac{\left\langle \left\langle \sigma - \frac{E_1 \exp(\theta_E/\theta)}{2(a-1)} (1-\eta)^3 \hat{\alpha} \right| - k_1 \exp(\theta_k/\theta) \exp(-\alpha/\alpha_0) \eta \right\rangle \right\rangle}{C\theta} \right) - 1 d\eta \quad (5.4)$$

where k_1 is reference strength parameter, and θ_k is reference temperature of k term. According to these both equations, the stress-strain relation can be expressed as:

$$d\varepsilon = \frac{d\sigma}{E_1 \exp(\theta_E/\theta)} + \frac{\sigma \theta_E d\theta}{\theta^2 E_1 \exp(\theta_E/\theta)} + \left[A\theta \exp\left(-\frac{B}{\theta}\right) \int_0^1 \sinh \left(\frac{\left\langle \left\langle \sigma - \frac{E_0}{2(a-1)} (1-\eta)^3 \hat{\alpha} \right| - k_1 \exp(\theta_k/\theta) \exp(-\alpha/\alpha_0) \eta \right\rangle \right\rangle}{C\theta} \right) S(\sigma - \hat{H}\hat{\alpha}) d\eta \right] dt \quad (5.5)$$

To predict the behaviour of stress and strain of asphaltic concrete under different temperatures and strain rates, the rate-dependent hyperplasticity model used 9 parameters ($E_1, \theta_E, k_1, \theta_k, \alpha_0, a, A, B, C$).

5.3 Model calibration and effect of temperature

The two models are calibrated against each of the sets of data from Schwartz *et al.* (2002), in which they report tests on a 12.5 mm dense graded Superpave mixture from the Maryland State Highway Administration (MSHA) at temperatures 5°C, 25°C, 40°C, and 60°C. The first model is Schapery continuum model which reported by Park *et al.*, (1996) and Schapery (1999) as reported in Chapter 2. The model calibration here is limited to only the viscoelastic damage model. This is because the viscoplastic model requires data from creep and recovery tests and use of the nonlinear least-squares optimization technique. Besides, there is no the report of creep and recovery results in Schwartz *et al.* (2002).

The viscoelastic behaviour requires the relaxation modulus, $E(t)$, which is defined by the series function in Equation 2.12. The viscoelastic parameters in Equation 2.12 are usually evaluated by curve fitting of the master relaxation modulus curve as shown in Figure 5.1. The microstructural damage, modelled by the material damage function $C(S)$, could be simply fitted with an exponential function. The exponential damage function at 5°C, 25°C, 40°C, and 60°C is presented in Figure 5.2 to 5.5. The temperature shift function $a_T(T)$ for the time-temperature superposition can be fitted by an exponential function as presented in Schwartz *et al.* (2002).

For predicting the constitutive behaviour, the relation between a stress and a strain is defined in term of pseudo strain as expressed in Equation 2.14. The pseudo strain can be estimated using the power-law series in Equation 2.13. The six parameters ($E_\infty, E_i, \rho_i, E_R, \alpha$ and m) and two material functions ($C(S)$ and $a_T(T)$) are presented in Tables 5.1 and 5.2 respectively.

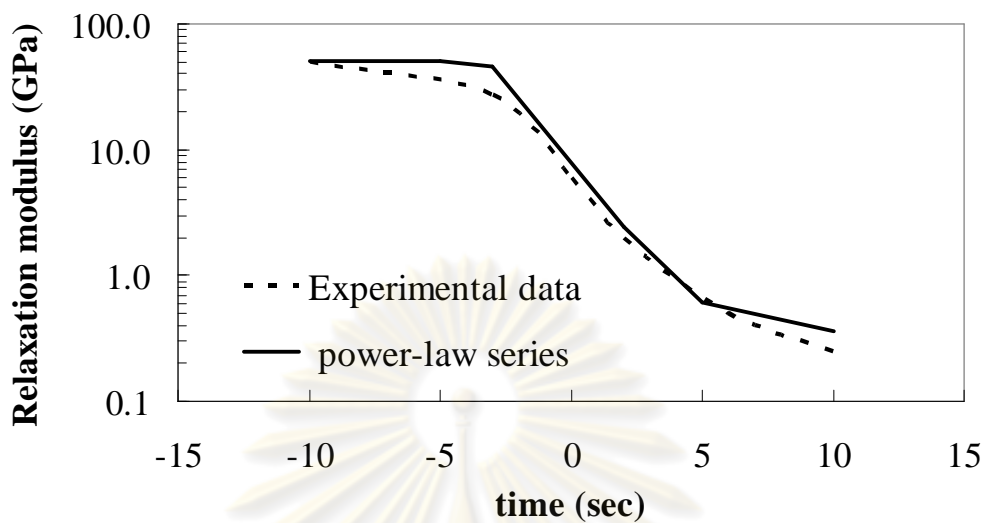


Figure 5.1 Curve fitting of series function of relaxation modulus

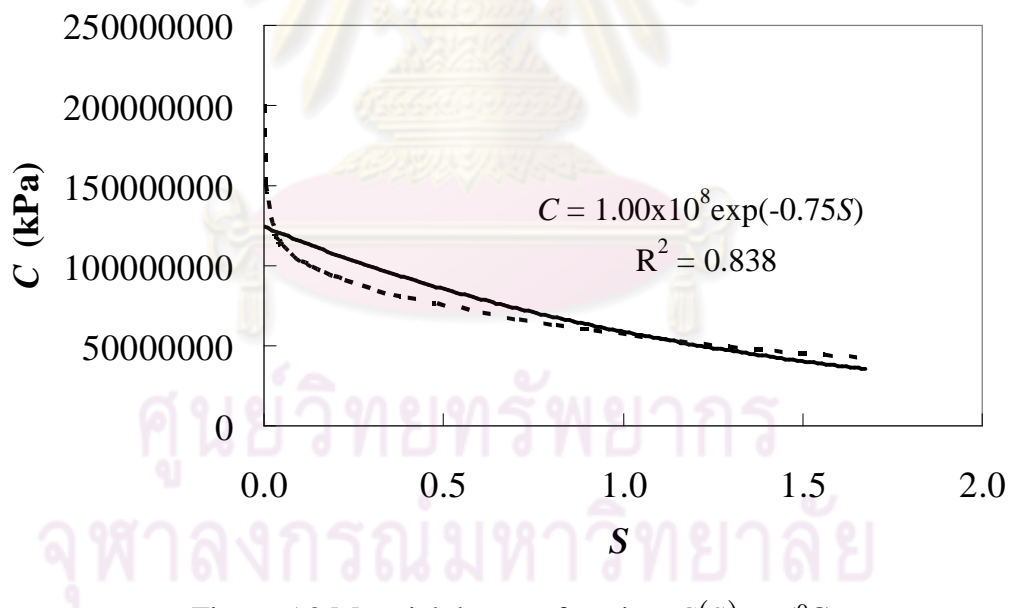


Figure 5.2 Material damage function $C(S)$ at 5°C

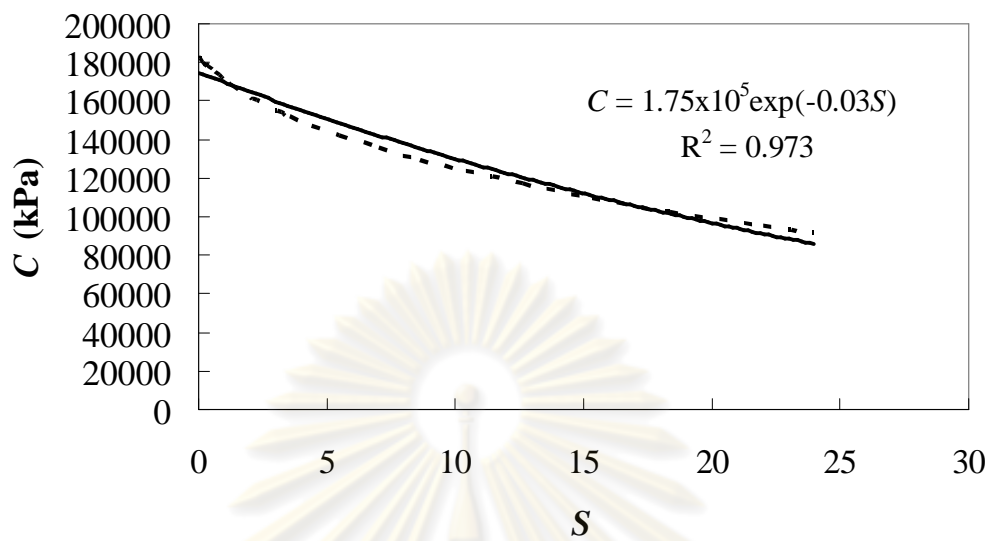


Figure 5.3 Material damage function $C(S)$ at 25°C

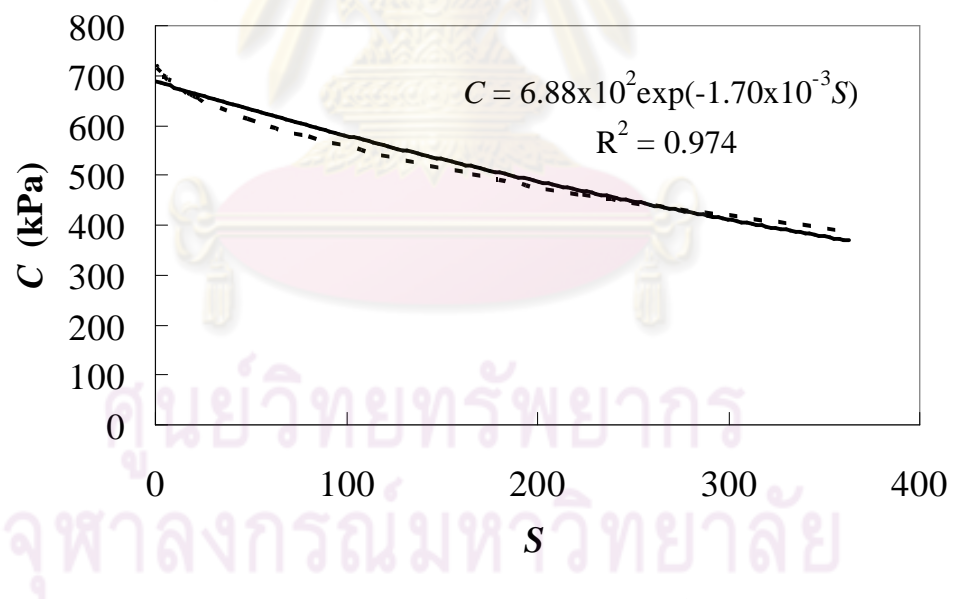


Figure 5.4 Material damage function $C(S)$ at 40°C

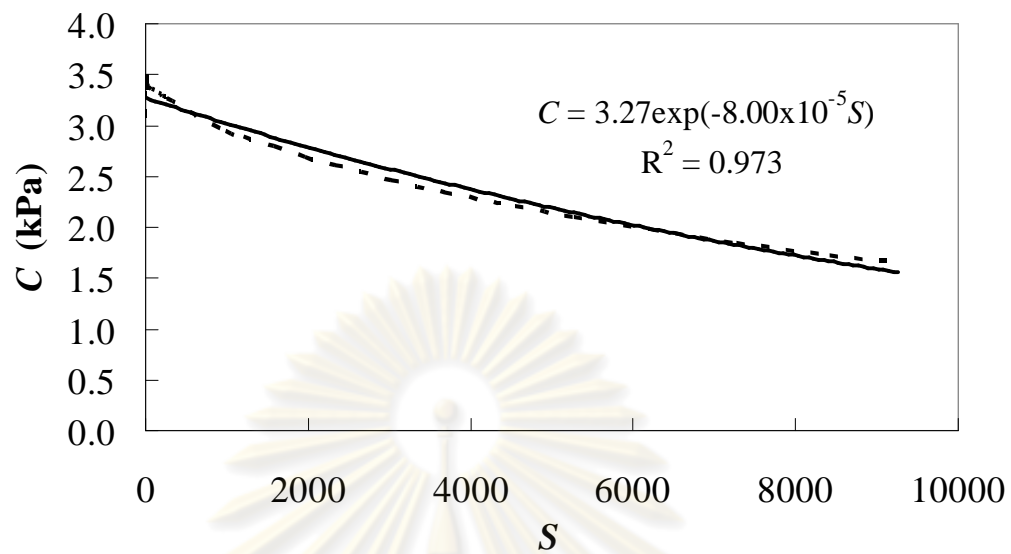


Figure 5.5 Material damage function $C(S)$ at 60°C

Table 5.1 Fitted parameter values of the viscoelastic damage model at different temperatures

| Parameters | Temperature ($^{\circ}\text{C}$) | | | |
|--------------------|------------------------------------|--------------------|--------------------|--------------------|
| | 5 | 25 | 40 | 60 |
| E_{∞} (MPa) | 3.50×10^2 | | | |
| E_i (MPa) | 5.00×10^4 | | | |
| ρ_i (s) | 2.50×10^{-3} | | | |
| E_R (MPa) | 8.22×10^3 | 1.91×10^3 | 5.58×10^2 | 2.28×10^2 |
| α (-) | 4.76 | 1.67 | 2.41 | 2.87 |
| m (-) | 0.50 | 0.40 | 0.35 | 0.36 |

Table 5.2 Curve fitted function parameters of the viscoelastic damage model at different temperatures

| Function | Temperature ($^{\circ}\text{C}$) | Expression |
|---------------|------------------------------------|--|
| $C(S)$ | 5 | $C(S) = 1.00 \times 10^8 \exp(-0.75S)$ |
| | 25 | $C(S) = 1.75 \times 10^5 \exp(-0.03S)$ |
| | 40 | $C(S) = 6.88 \times 10^2 \exp(-1.70 \times 10^{-3} S)$ |
| | 60 | $C(S) = 3.27 \exp(-8.00 \times 10^{-5} S)$ |
| $a_T(\theta)$ | | $a_T = \exp(-1.1116\theta + 2.6775)^*$ |

* from Schwartz *et al.* (2002)

For the second model (rate-dependent hyperplasticity model) in Equation 5.5, the appropriate parameter values were also determined for each temperature as shown in Table 5.3. The process of fitting involved some optimization of parameter values, but the values do not represent rigorous least square optimal values. In some cases (*e.g.* at high temperature) it was found that the results were insensitive to the values of certain parameters, and in these cases little importance was attached to the values of those parameters. It was found that all the data could be fitted with adequate accuracy with $\alpha_0 = 0.02$ and the shaping parameter $a = 3$.

To study the new constitutive model, we start to determine the temperature parameters (A , B , and C) based on Equation 5.2. For calculating these parameters, the values of μ and μr are plotted in Figures 5.6 and 5.7 respectively and fitted with functions of the appropriate form, with $A = 2.65 \times 10^{15} \text{ K}^{-1} \text{ s}^{-1}$, $B = 1.28 \times 10^4 \text{ K}$, and $C = 5.64 \times 10^{-3} \text{ MPaK}^{-1}$. The only one of these constants that can be interpreted in a straightforward physical manner is B , which is equal to $\Delta F/R$, where R is the gas constant ($8.3144 \text{ JK}^{-1} \text{ mol}^{-1}$) and ΔF is the activation energy for the thermally activated rate process. The estimated value of the activation energy is therefore 106 kJ/mol, which compares well with values reported by Mitchell and Soga (2005) of 226 kJ/mol for concrete and 113 kJ/mol for soil asphalt.

The derived values of the constants at each temperature are shown in Table 5.4. Additionally, Figures 5.8 and 5.9 show plot of E_0 and k_0 (on a logarithmic scale) against $1/\theta$ and demonstrate that the data can satisfactorily be fitted by the above expressions with $E_1 = 1.08 \times 10^{-8} \text{ GPa}$, $\theta_E = 5.45 \times 10^3 \text{ K}$, $k_1 = 5.73 \times 10^{-4} \text{ MPa}$, and $\theta_k = 2.71 \times 10^3 \text{ K}$.

Table 5.3 Fitted parameter values of the rate-dependent hyperplasticity model at different temperatures ($\alpha_0 = 0.02$ and $a = 3.0$)

| Temperature (°C) | Absolute temperature θ (K) | E_0 (GPa) | k_0 (MPa) | μ (MPa s) | r (s ⁻¹) | μr (MPa) |
|------------------|-----------------------------------|-------------|-------------|---------------|------------------------|---------------|
| 5 | 278 | 2.93 | 11.00 | 264 | 0.00574 | 1.52 |
| 25 | 298 | 1.29 | 4.15 | 8.95 | 0.19 | 1.66 |
| 40 | 313 | 0.39 | 3.51 | 0.71 | 2.44 | 1.74 |
| 60 | 333 | 0.12 | 2.07 | 0.16 | 12.5* | 1.97 |

* Quality of fit to data not significantly affected by this value

Table 5.4 Derived parameter values of the rate-dependent hyperplasticity model as functions of temperature ($\alpha_0 = 0.02$, $a = 3.0$)

| Temperature (°C) | Absolute temperature θ (K) | $E_0 = E_1 \exp\left(\frac{\theta_\epsilon}{\theta}\right)$ (GPa) | $k_0 = k_1 \exp\left(\frac{\theta_k}{\theta}\right)$ (MPa) | $\mu = \frac{C}{A} \exp\left(\frac{B}{\theta}\right)$ (MPa s) | $r = A\theta \exp\left(\frac{-B}{\theta}\right)$ (s ⁻¹) | $\mu r = C\theta$ (MPa) |
|------------------|-----------------------------------|---|--|---|---|-------------------------|
| 5 | 278 | 3.54 | 9.88 | 213.00 | 0.00737 | 1.57 |
| 25 | 298 | 0.95 | 5.13 | 9.67 | 0.17 | 1.68 |
| 40 | 313 | 0.39 | 3.32 | 1.23 | 1.43 | 1.77 |
| 60 | 333 | 0.14 | 1.97 | 0.11 | 17.70 | 1.89 |

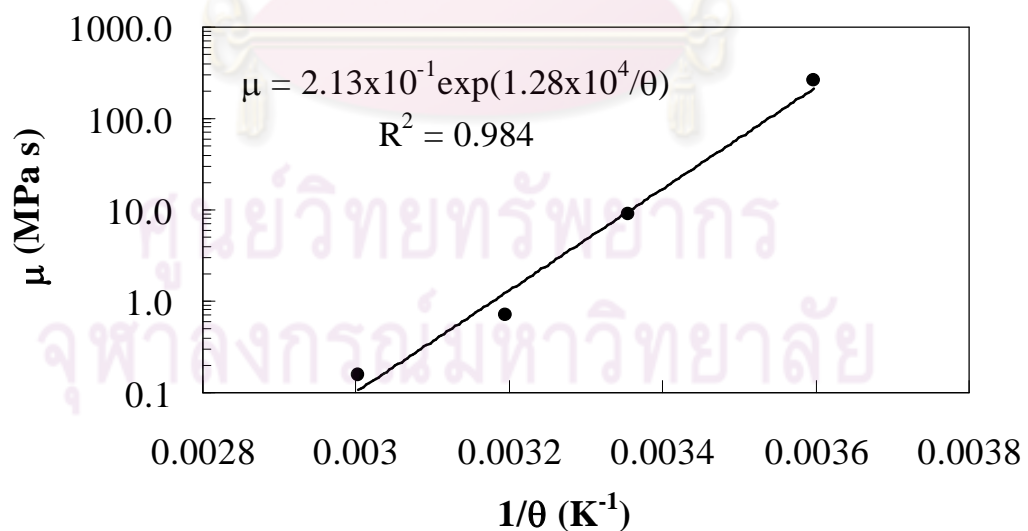


Figure 5.6 Variation of μ with temperature

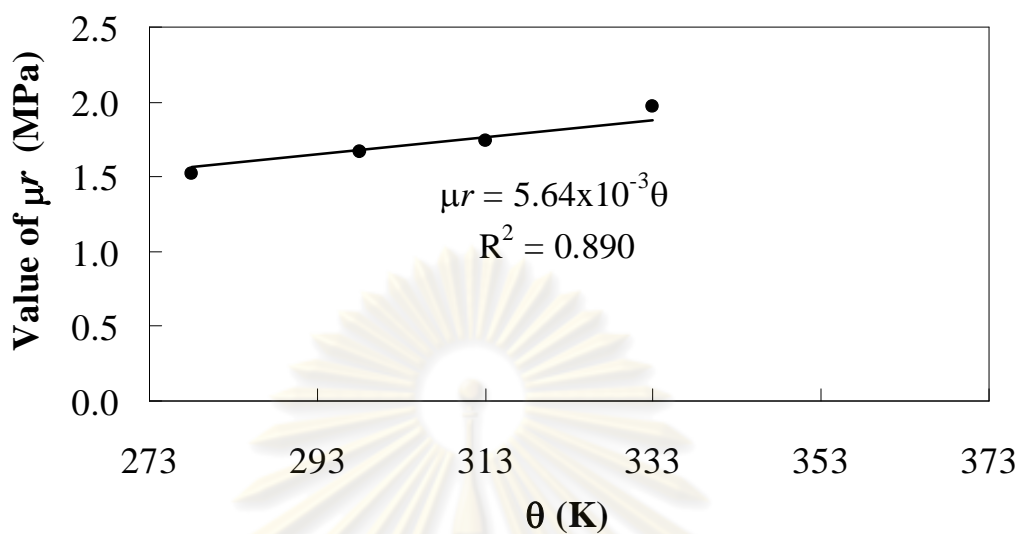


Figure 5.7 Variation of μr with temperature

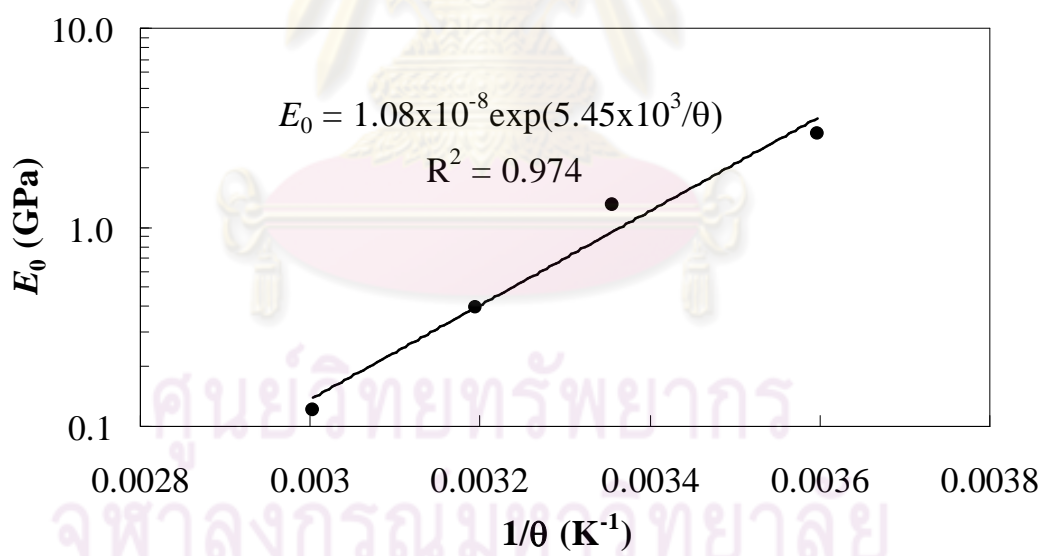


Figure 5.8 Variation of E_0 with temperature

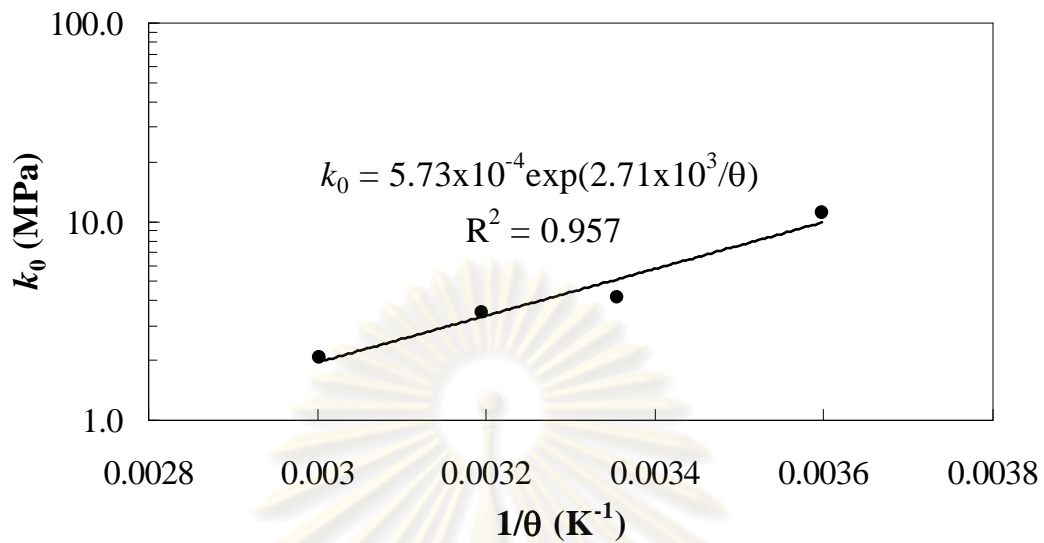


Figure 5.9 Variation of k_0 with temperature

The four sets of unconfined compression tests (each at a different temperature) reported by Schwartz *et al.* (2002) involved nominal strain rates of 0.0005, 0.0015, 0.0045 and 0.0135 s^{-1} . Figures 5.10 to 5.13 show all the stress-strain curves at 5°C, 25°C, 40°C, and 60°C respectively, including test data from Schwartz *et al.*, 2002 (dotted line), the viscoelastic damage model predictions (light color) and the rate-dependent hyperplasticity model predictions (dark color). In Figure 5.10 (at the lowest temperature), there is only one complete stress-strain curve available at 0.0005 s^{-1} strain rate. Both the viscoelastic damage and rate-dependent hyperplasticity models provide a good fit to the experimental data in the intermediate range of temperatures 25°C and 40°C as presented in Figures 5.11 and 5.12. However, the viscoelastic damage model exhibits rather more softening behavior than the experiments, especially for the fastest test (the strain rate of 0.0135 s^{-1}) and for the highest temperature (40°C). For the highest temperature, in Figure 5.13, the rate-dependent hyperplasticity model predicts rather less viscous behavior as compared to the experiments (the four dark lines are closer together than dotted lines in Figure 5.13).

The agreement between the tests and the hyperplasticity theory is generally good, especially the prediction of peak strength as shown in Figure 5.14(a). The fitting of strain to peak strength is not quite as good as illustrated in Figure

5.14(b). Overall the fit of the rate-dependent hyperplasticity model is as least as good as that of the viscoelastic damage model, but the new model is slightly simpler in structure. The new model has the particular advantage that the entire specification of the model is captured within two scalar functions (the Gibbs free energy and the flow potential).

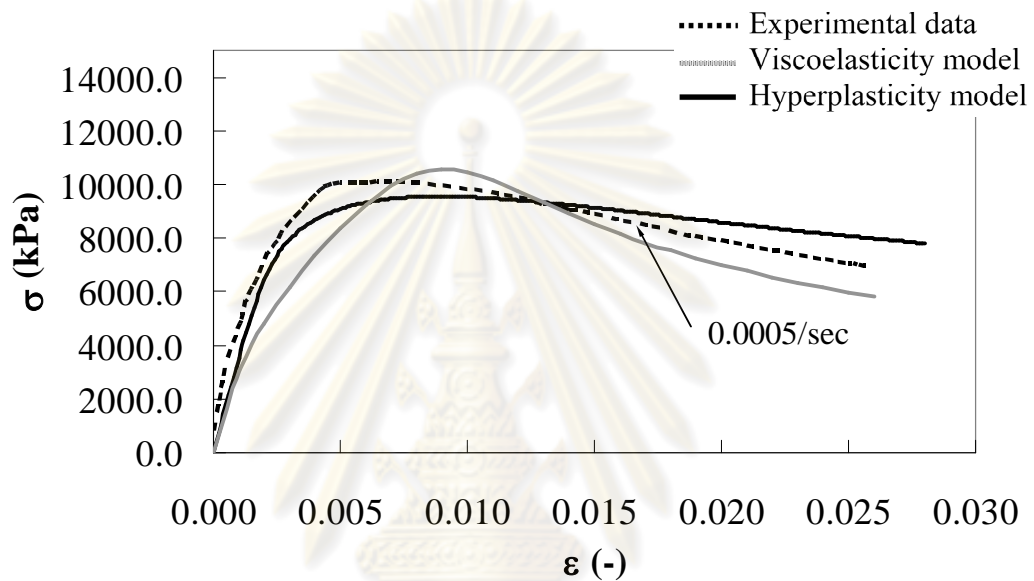


Figure 5.10 Stress-strain curve of asphaltic concrete at 5°C for different strain rates

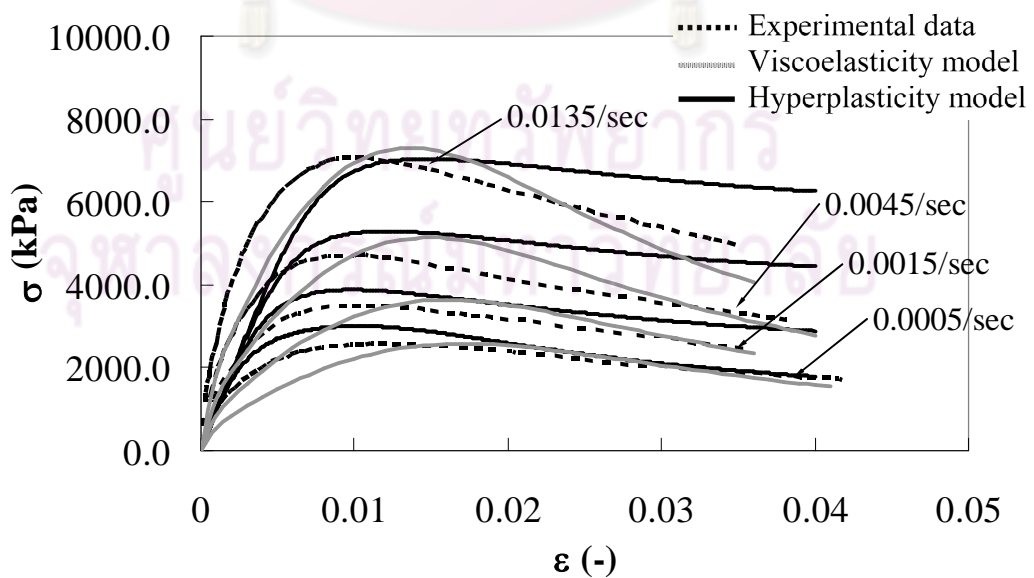


Figure 5.11 Stress-strain curve of asphaltic concrete at 25°C for different strain rates

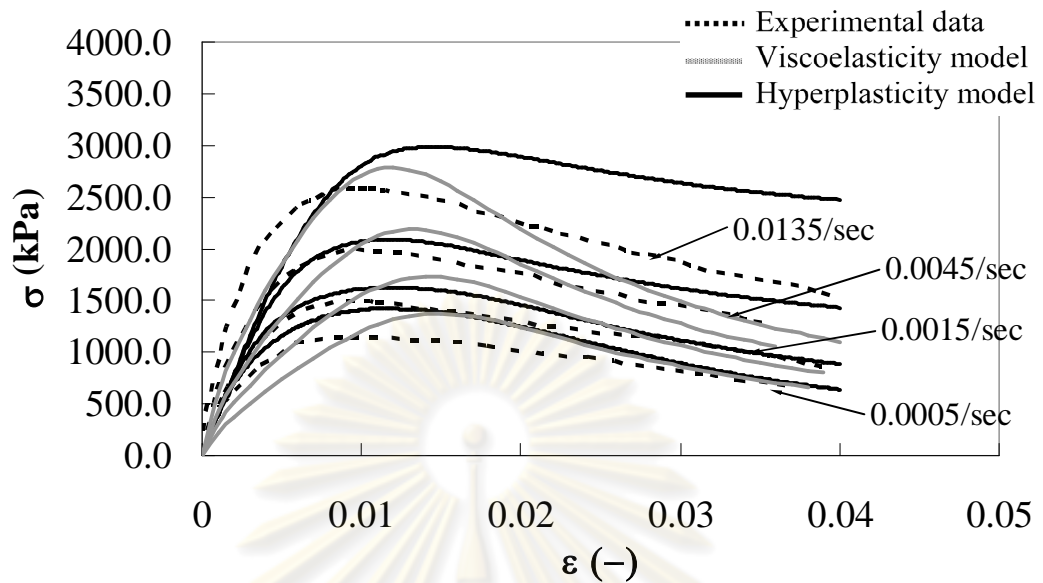


Figure 5.12 Stress-strain curve of asphaltic concrete at 40°C for different strain rates

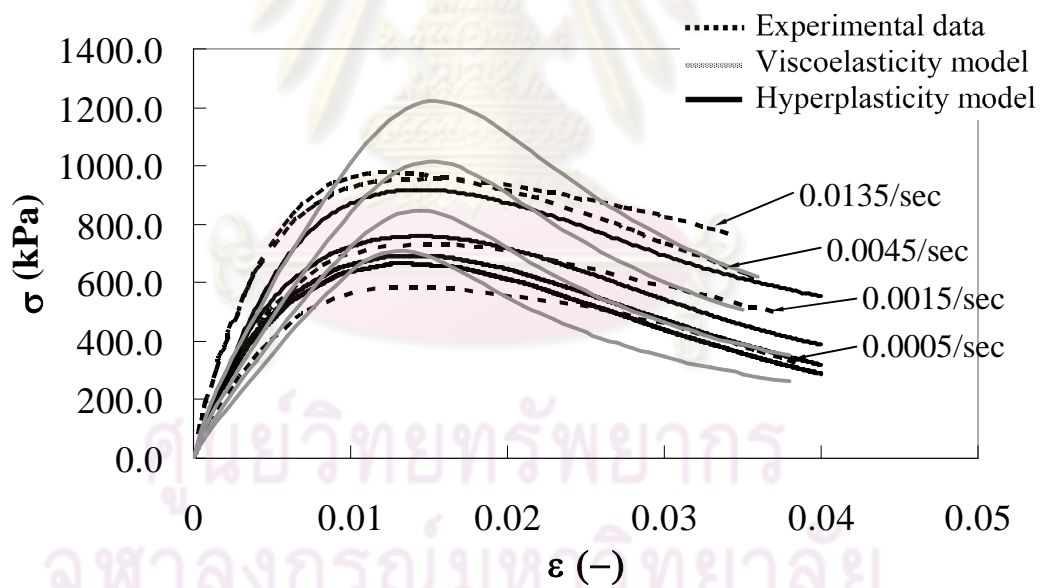
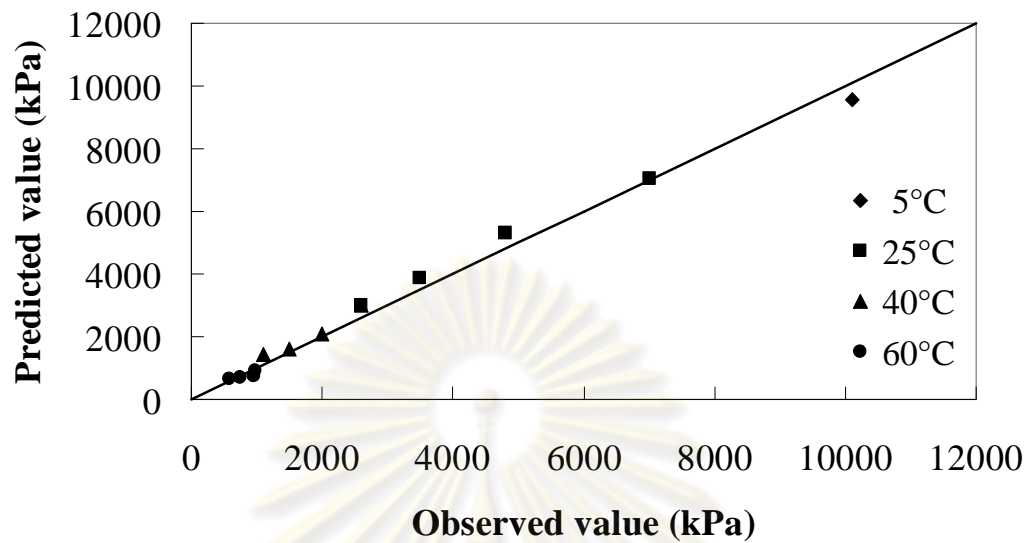
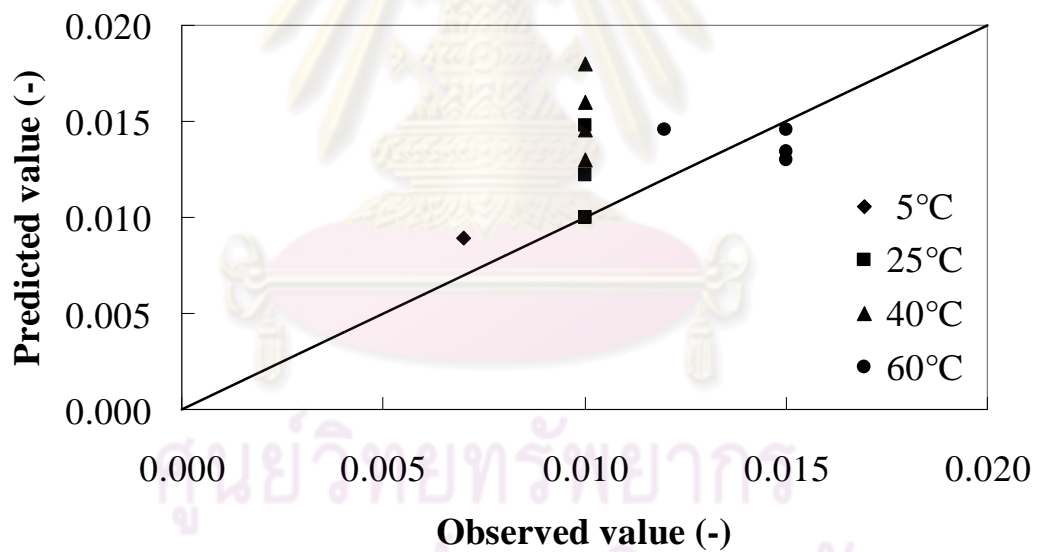


Figure 5.13 Stress-strain curve of asphaltic concrete at 60°C for different strain rates



(a)



(b)

Figure 5.14 Comparisons of experimentally observed and theoretically predicted value (a) peak strength; (b) strain at peak strength

5.4 Summary

The constitutive model created from the rate-dependent hyperplasticity (Likitlersuang and Houlsby, 2007) and the rate process theory (Mitchell and Soga, 2005) is performed to predict the stress-strain-temperature-time response of asphaltic

concrete. This constitutive model is then compared with the well-known model of Park *et al.*, (1996) and Schapery (1999). The constitutive model has been calibrated against a series of unconfined compression test reported by Schwartz *et al.* (2002) and viscoelastic damage model, and is shown to fit a suite of shear tests at different temperatures and a wide range of strain rates. However, the stress at the peak point of this model is little higher than the same point of experimental testing.

The prediction of viscoelastic damage model shows that the stress-strain curve of this model is quite equal to the curve of experimental test. This model relies on the assumption of internal state evolution law (damage law) which expresses in term of damage parameter; therefore, the stress-strain curve after post peak suddenly drops. In practical the rate-dependent hyperplasticity model is based on only law of thermodynamic to create two potential equations, and the stress-strain relation can be defined by these potential equations. Thus, it is easy to apply this model to the numerical method.

For viscoelastic damage model, it is depended on many theories such as law of thermodynamic, time-temperature superposition principle, and internal state evolution law. Consequently, many parameters and function parameters are necessarily to be the accessories in prediction of the constitutive behaviour. The viscoelastic damage model is furthermore founded on curve fitting analysis. Table 5.5 shows all required tests for parameter evaluation of both viscoelastic damage and rate-dependent hyperplasticity models. This example only presents the models feature based on compressive behaviour. It can be concluded that the viscoelastic damage model requires creep and recovery tests by SuperPave Performance Tester (SPT) apart from unconfined compression tests. However, it is also needed some numerical techniques such as curve fitting and finite different method to define the model parametric function. On the other hand, the rate-dependent hyperplasticity model requires unconfined compression tests varied strain rates and temperatures. The parameter determination involves simple optimisation technique.

Table 5.5 List of experimental programme for model parameter determination based on unconfined compression test

| Model | Parameters | Experimental program | Testing equipment |
|--------------------------------------|--|---|-------------------|
| Viscoelastic damage model | E_{∞}, E_i, ρ_i | Creep and recovery tests (at least three different temperatures) | UTM* |
| | $E_R, \alpha, m, C(S)$ | Static unconfined compression test (at least three different strain rates) | UTM |
| | $a_T(\theta)$ | Creep and recovery tests or Unconfined frequency sweep test (at least three different temperatures) | UTM or SPT* |
| Rate-dependent hyperplasticity model | $E_I, \theta_E, k_1, \theta_k, A, B, C, \alpha_0, a$ | Static unconfined compression test (at least three different strain rates and three different temperatures) | UTM |

* UTM = Universal Testing Machine and SPT = SuperPave Performance Tester

CHAPTER 6

Numerical prediction

6.1 Introduction

This chapter focuses on the prediction of rate-dependent hyperplasticity model reported in Chapter 5 against the stress-strain curve. This is because the viscoelastic damage model needs more result of advanced experimental testing than the result of this research. The stress-strain relations are obtained from the experimental tests in Chapter 3. For prediction of this model, the series of static indirect tensile test (S-IDT), static unconfined compression test (S-UC), and cyclic indirect tensile test (C-IDT) at different strain rate and/or temperature are used.

6.2 Numerical implementation

The constitutive model is developed in this chapter for the asphaltic concrete material based on hyperplasticity approach. In order to validate a model with static and a cyclic test, a model for the asphaltic concrete at the different strain rates and the temperatures is introduced in the Chapter 5. An original model was explained in the form of functional. To implement this model into computational code, it is necessary to modify the continuous form to be discrete form or that means the integration sign is replaced by summation. In practice, the infinite numbers of surfaces have to be replaced by the finite number N of surfaces. Each surface i is labelled ($1 \leq i \leq N$), and the factor i/N plays the same role as an internal coordinate η . In the following equations the model is presented in terms of the finite number of yield surfaces, as it requires less sophisticated mathematics and leads more directly implementation. Note that the integrals have to be replaced by the summations. The Gibb free energy function is defined as:

$$g = -\frac{\sigma^2}{2E_1 \exp(\theta_E/\theta)} - \frac{\sigma}{N} \sum_{i=1}^N \alpha_i + \sum_{i=1}^N \frac{E_1 \exp(\theta_E/\theta)}{2N(a-1)} \left(1 - \frac{i}{N}\right)^3 \frac{\alpha_i^2}{2} \quad (6.1)$$

The flow potential is specified as:

$$w = CA\theta^2 \exp\left(-\frac{B}{\theta}\right) \left[\frac{1}{N} \times \sum_{i=1}^N \cosh\left(\frac{|\sigma - H_i \alpha_i| - k_1 \exp(\theta_k / \theta) \exp(-\alpha_i / \alpha_0) \left(\frac{i}{N}\right)}{C\theta}\right) - 1 \right] \quad (6.2)$$

After differentiation (see more detail Likitlersuang *et al.*, 2009) the rate-dependent hyperplasticity model can be written as:

$$\Delta \varepsilon = \frac{\Delta \sigma}{E_1 \exp(\theta_E / \theta)} + \frac{\sigma \theta_E \Delta \theta}{\theta^2 E_1 \exp(\theta_E / \theta)} + \left[A\theta \exp\left(-\frac{B}{\theta}\right) \frac{1}{N} \times \sum_{i=1}^N \sinh\left(\frac{|\sigma - H_i \alpha_i| - k_1 \exp(\theta_k / \theta) \exp(-\alpha_i / \alpha_0) \left(\frac{i}{N}\right)}{C\theta}\right) \right] S(\sigma - H_i \alpha_i) \Delta t \quad (6.3)$$

$$\text{where } H_i = \frac{E_1 \exp(\theta_E / \theta)}{2(a-1)} \left(1 - \frac{i}{N}\right)^3$$

The prediction of model parameters for asphaltic concrete is together studied for static and cyclic conditions, but the input parameters of each mode are separate. As we have known that their conditions of loading are completely different; for example, the test under static condition displays a large strain, and the test under cyclic condition shows small strain.

A flow chart illustrated in Figure 6.1 is employed for the prediction of static test and cyclic test. To predict the constitutive model, the potential equations which are an energy function and a flow potential function are firstly defined. In case of static condition the 9 parameters are specify to be the initial parameters, and the rate-dependent constant (2 constants) are then determined by the condition of testing. For the cyclic condition, the amplitude of stress (10% of ITS) is set up according to the standard cyclic loading, and the time step (Δt) is set up to be constant at 0.05 sec for the loading condition and the unloading condition, and at 0.9 for the rest condition. After that the increment of strain ($\Delta \varepsilon$) of Equation 6.3 is calculated. This computed strain is then calculated to estimate the increment of stress ($\Delta \sigma$). Following this calculation, stress (σ), and strain (ε) are updated. Finally, all previous processes are continuously repeated until the completed stress-strain relation is achieved. Note that

the loading condition used for prediction the model can be roughly approximated by triangular shape as presented in Figure 6.2.

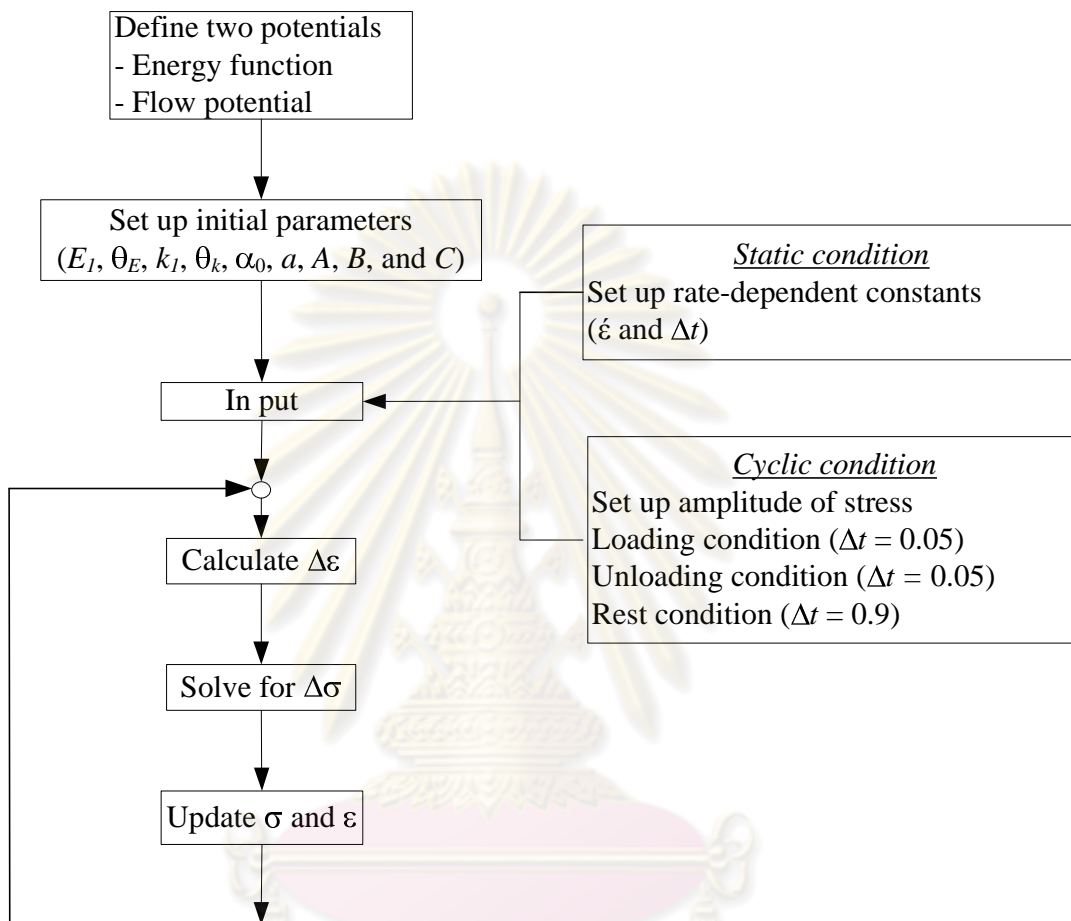


Figure 6.1 Calculation flow chart for rate-dependent hyperplasticity model

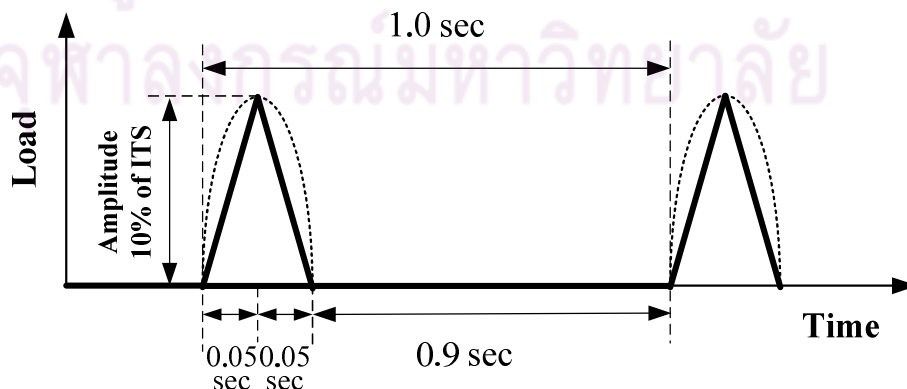


Figure 6.2 Shape and condition of loading in the calculation

6.3 Model prediction of static condition

The rate-dependent hyperplasticity model presented in Section 6.2 is predicted against the sets of S-IDT test and S-UC test from AC 60/70 mixed material. The temperature conditions of both tests are varied at 10°C, 25°C, 40°C, and 55°C. The loading rates are applied to the IDT test at 0.0008, 0.0025, 0.0083, and 0.0250 s⁻¹ and to the UC test at 0.0006, 0.0017, 0.0056, and 0.0167 s⁻¹.

The parameters which are best fitted for the rate-dependent hyperplasticity model by least square method are expressed in Table 6.1. According to these parameters, the comparisons between the rate-dependent hyperplasticity model and the testing results under the changing of temperature are shown in Figure 6.3 to 6.6 for S-IDT test and 6.7 to 6.10 for S-UC test respectively.

Table 6.1 Summarised parameters of the rate-dependent hyperplasticity model for S-IDT and S-UC tests

| Parameters | unit | S-IDT test | S-UC test |
|------------|-----------------------------------|-----------------------|-----------------------|
| E_I | GPa | 3.10×10^{-3} | 2.00×10^{-5} |
| θ_E | K | 2.32×10^3 | 3.91×10^3 |
| k_1 | MPa | 7.00×10^{-7} | 6.00×10^{-6} |
| θ_k | K | 4.20×10^3 | 4.07×10^3 |
| A | s ⁻¹ . K ⁻¹ | 9.00×10^{15} | 9.00×10^{18} |
| B | K | 1.39×10^4 | 1.55×10^4 |
| C | MPa. K ⁻¹ | 9.00×10^{-4} | 2.70×10^{-3} |
| α_0 | - | 1.00×10^{-2} | 3.50×10^{-2} |
| a | - | 4.0 | |

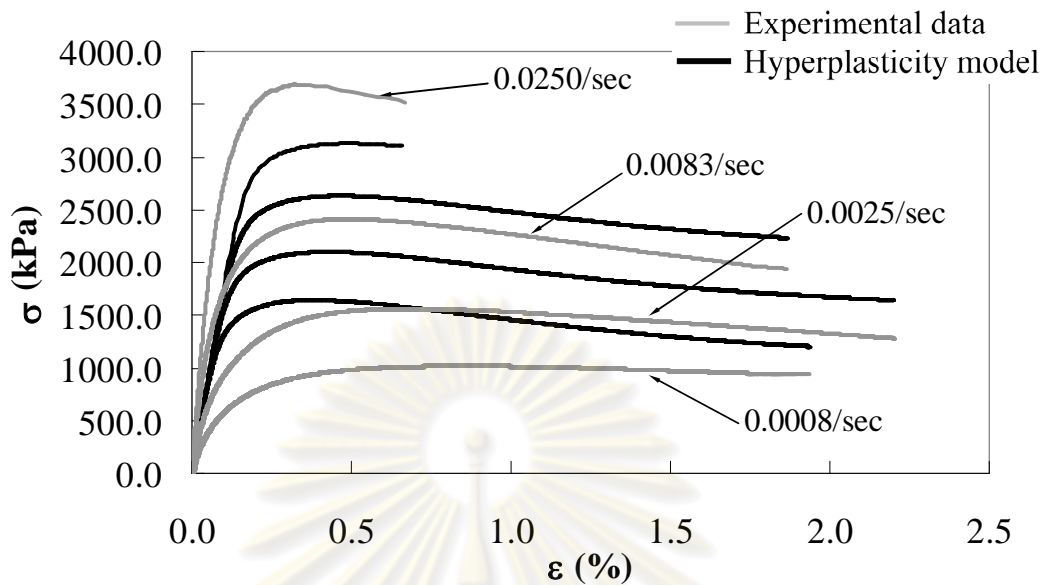


Figure 6.3 Stress-strain curves of asphaltic concrete under S-IDT test at 10°C

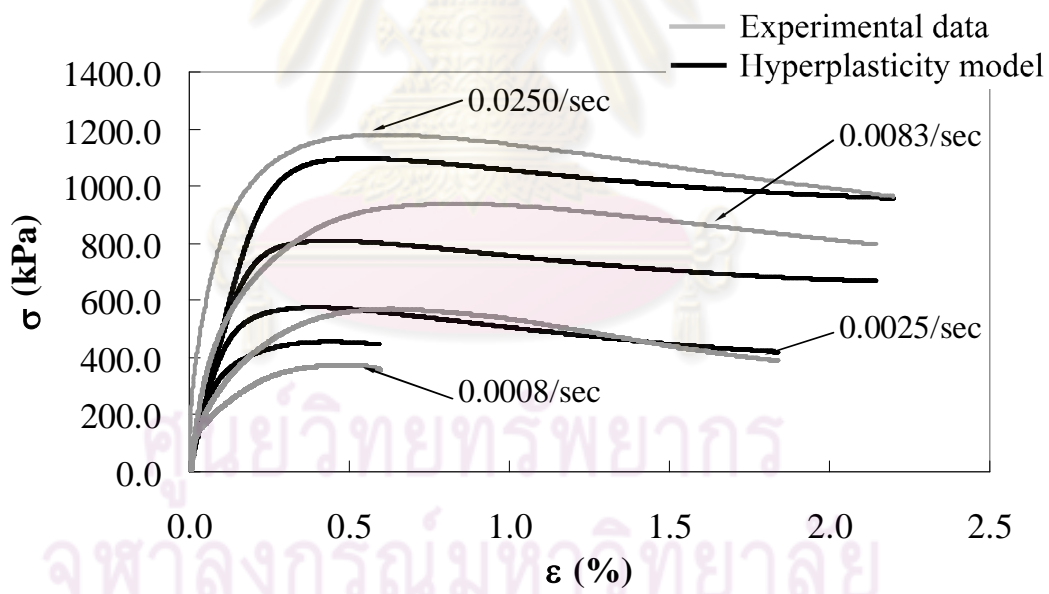


Figure 6.4 Stress-strain curves of asphaltic concrete under S-IDT test at 25°C

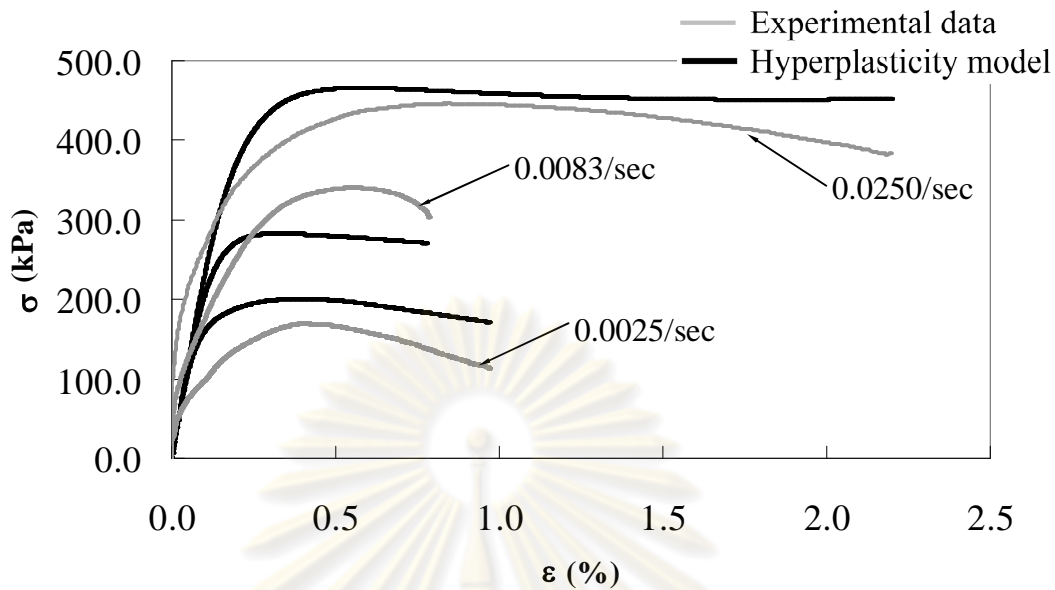


Figure 6.5 Stress-strain curves of asphaltic concrete under S-IDT test at 40°C

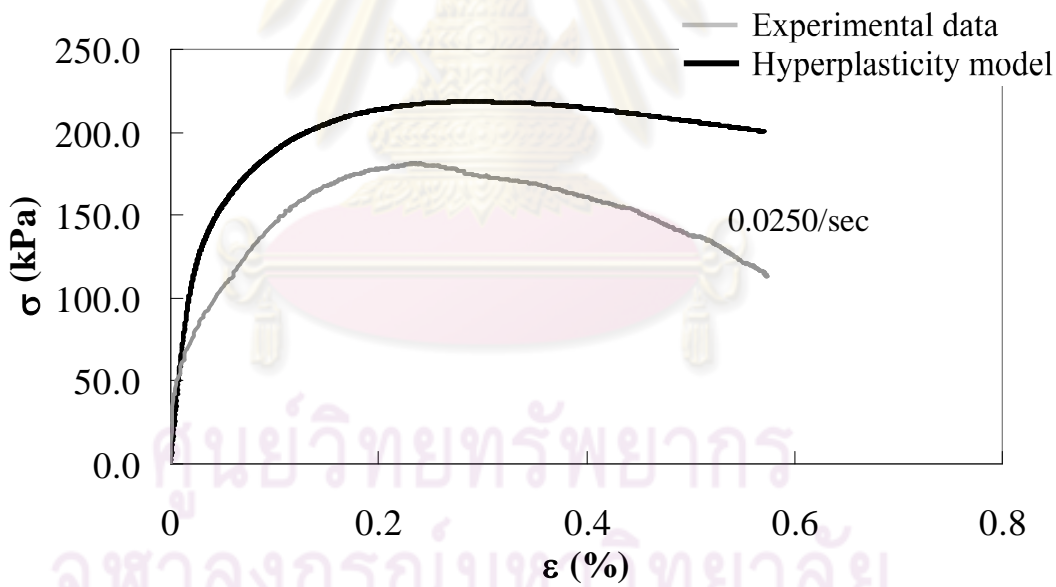


Figure 6.6 Stress-strain curves of asphaltic concrete under S-IDT test at 55°C

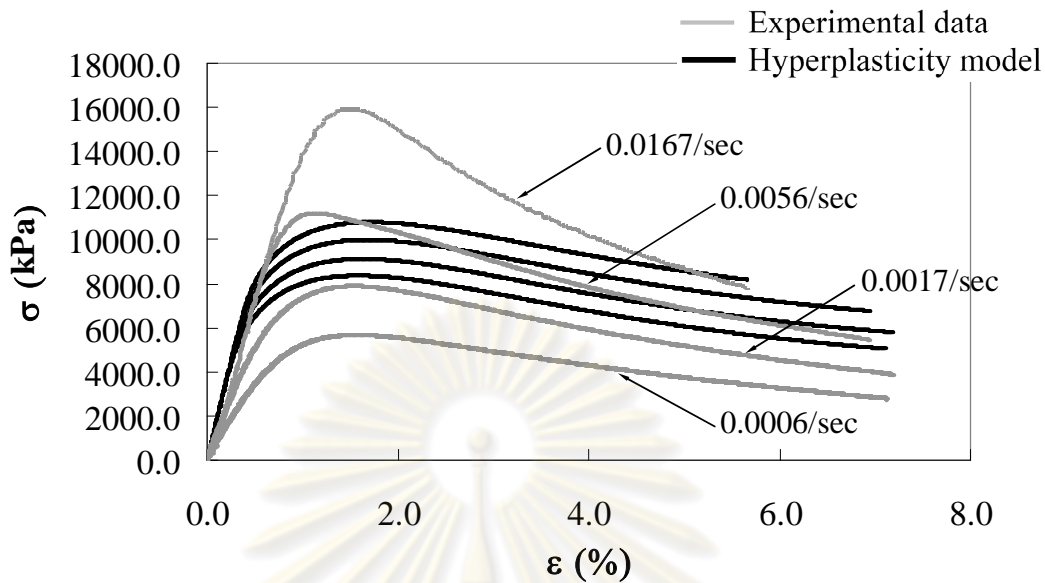


Figure 6.7 Stress-strain curves of asphaltic concrete under S-UC test at 10°C

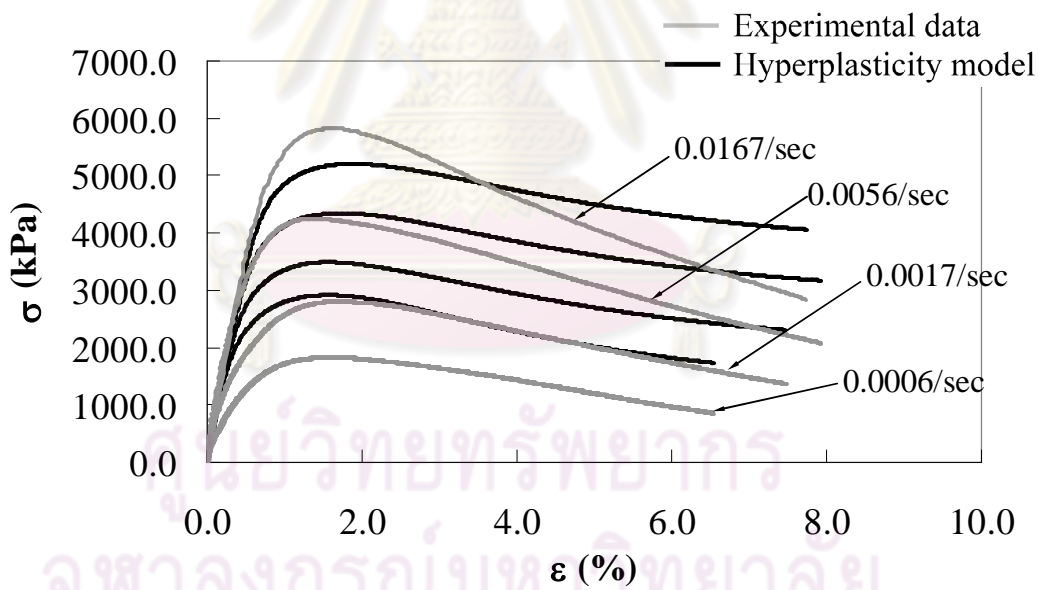


Figure 6.8 Stress-strain curves of asphaltic concrete under S-UC test at 25°C

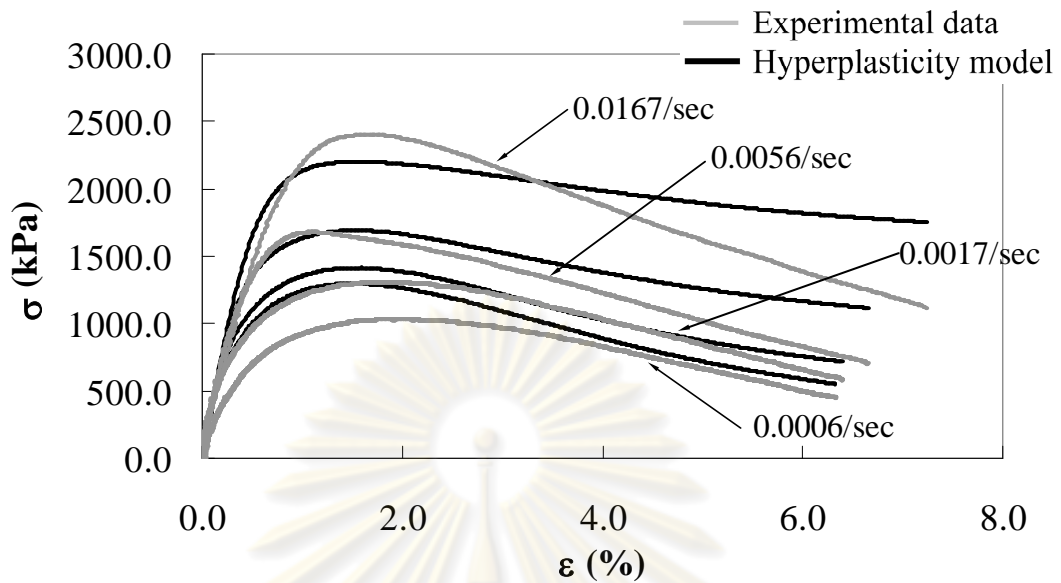


Figure 6.9 Stress-strain curves of asphaltic concrete under S-UC test at 40°C

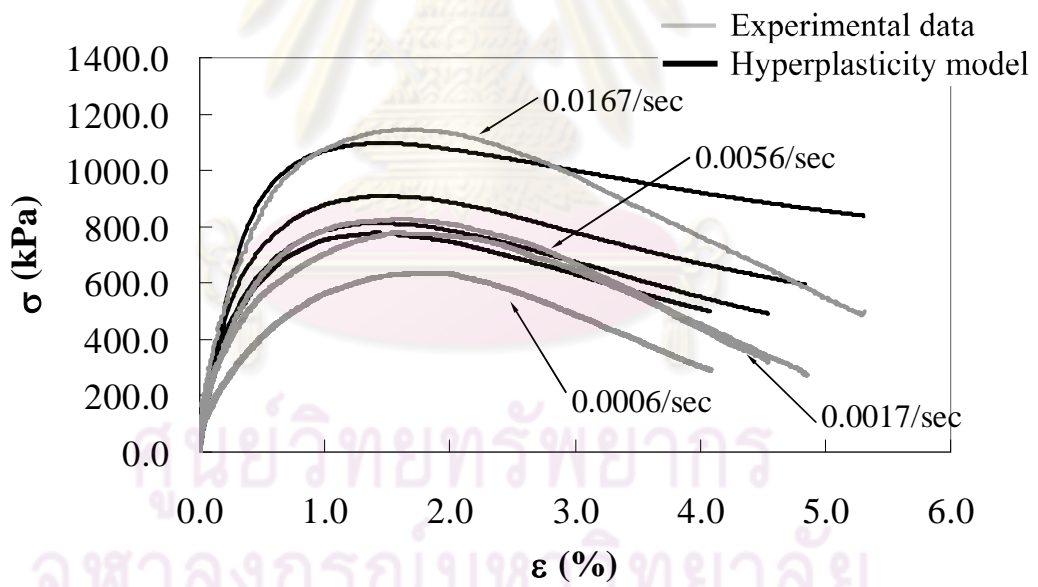


Figure 6.10 Stress-strain curves of asphaltic concrete under S-UC test at 55°C

According to the comparison between the prediction of the rate-dependent hyperplasticity model and the result of S-IDT test, the reference stiffness and strength parameters E_1 and k_1 at any temperatures are 3.10×10^{-3} GPa and 7.00×10^{-7} where E_1 and k_1 are the exponential constant. The reference temperatures for stiffness and strength θ_E and θ_k are 2.32×10^3 and 4.20×10^3 where θ_E and θ_k are the gradient of

exponential decay. The parameter of temperature and strain rate A , B , and C approximately are $9.00 \times 10^{15} \text{ s}^{-1} \cdot \text{K}^{-1}$, $1.39 \times 10^4 \text{ K}$, and $9.00 \times 10^{-4} \text{ MPa} \cdot \text{K}^{-1}$. For temperature and strain rate parameters, the only one of these constants that can be interpreted in a straightforward physical manner is B , which is equal to $\Delta F/R$, where R is the gas constant and ΔF is the activation energy for the thermally activated rate process. The estimated value of activation energy is therefore 116 kJ/mol, which compares well with values reported by Mitchell and Soga (2005) of 226 kJ/mol for concrete and 113 kJ/mol for soil asphalt. The shape controlling parameters of stress-strain graph α_0 and a are 1.00×10^{-2} and 4.0. As for parameter a it slightly affect to the rate-dependent hyperplasticity model.

Following the comparative relation between the predicting and S-UC test, the values of the E_1 and k_1 at any temperatures are $2.00 \times 10^{-5} \text{ GPa}$ and $6.00 \times 10^{-6} \text{ MPa}$. The values of θ_E and θ_k for reference strength parameters are $3.91 \times 10^3 \text{ K}$ and $4.07 \times 10^3 \text{ K}$. Following the values of temperature and strain rate A , B , and C , they approximately are $9.00 \times 10^{18} \text{ s}^{-1} \cdot \text{K}^{-1}$, $1.55 \times 10^4 \text{ K}$, and $2.70 \times 10^{-3} \text{ MPa} \cdot \text{K}^{-1}$ respectively. The estimated value of the activation energy is 128 kJ/mol. As for the shape controlling parameter of stress-strain graph α_0 and a moreover are 3.50×10^{-2} and 4.0.

6.4 Model prediction of cyclic condition

The prediction of rate-dependent hyperplasticity model is also presented comparing with the sets of C-IDT test. The series of testing are operated under the various temperatures. The conditions of temperature in this C-IDT test are also controlled to be 10°C, 25°C, 40°C, and 55°C. The format of this load duration is 1 by 9 according to ASTM D 4123. In C-IDT test, the model parameters are summarised in Table 6.2. These parameters are well agreed by the least square method. The predicted results of model compared with the last five cycles of C-IDT test result under the changing of temperature are shown in Figure.5.11 to 5.14.

Table 6.2 Summarised parameters of the rate-dependent hyperplasticity model for C-IDT and S-IDT tests

| Parameters | Unit | C-IDT test | S-IDT test |
|------------|-----------------------|------------------------|-----------------------|
| E_1 | GPa | 1.00×10^{-11} | 3.10×10^{-3} |
| θ_E | K | 7.99×10^3 | 2.32×10^3 |
| k_1 | MPa | 7.00×10^{-7} | |
| θ_k | K | 4.20×10^3 | |
| A | $s^{-1} \cdot K^{-1}$ | 4.88×10^7 | 9.00×10^{15} |
| B | K | 6.68×10^3 | 1.39×10^4 |
| C | MPa. K^{-1} | 4.88×10^{-2} | 9.00×10^{-4} |
| α_0 | - | 1.00×10^{-2} | |
| a | - | 4.0 | |

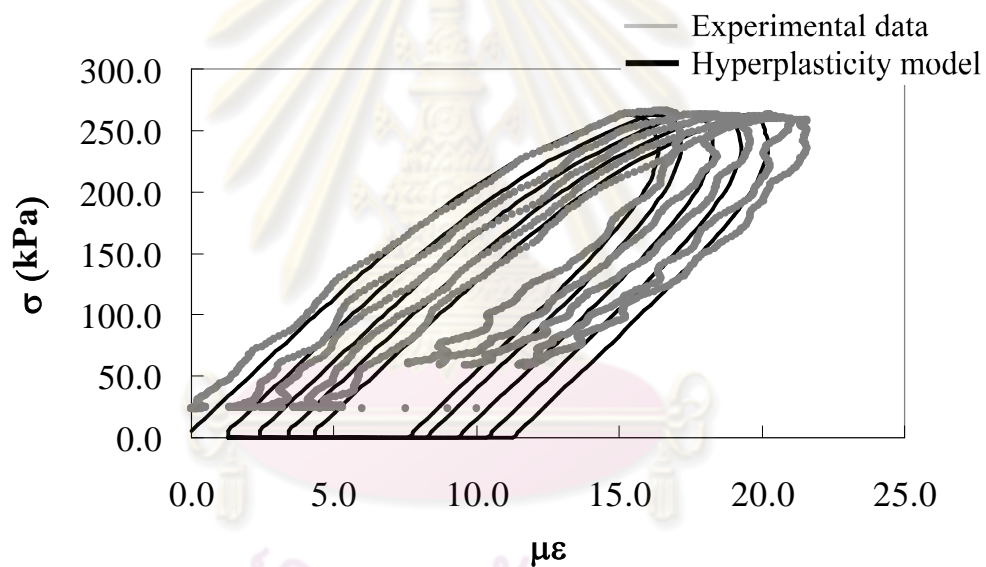


Figure 6.11 Stress-strain curves of asphaltic concrete under C-IDT test at 10°C

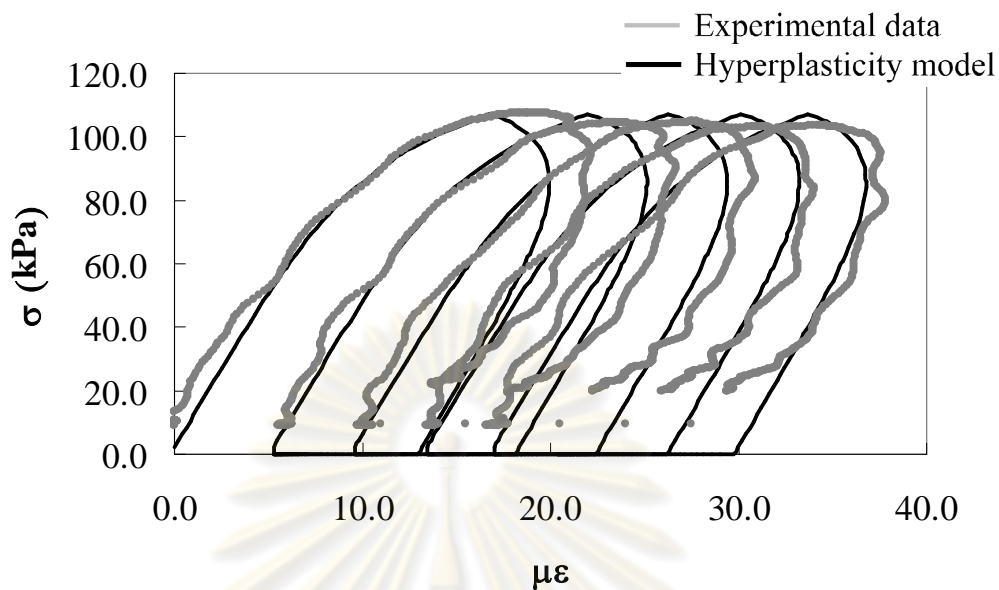


Figure 6.12 Stress-strain curves of asphaltic concrete under C-IDT test at 25°C

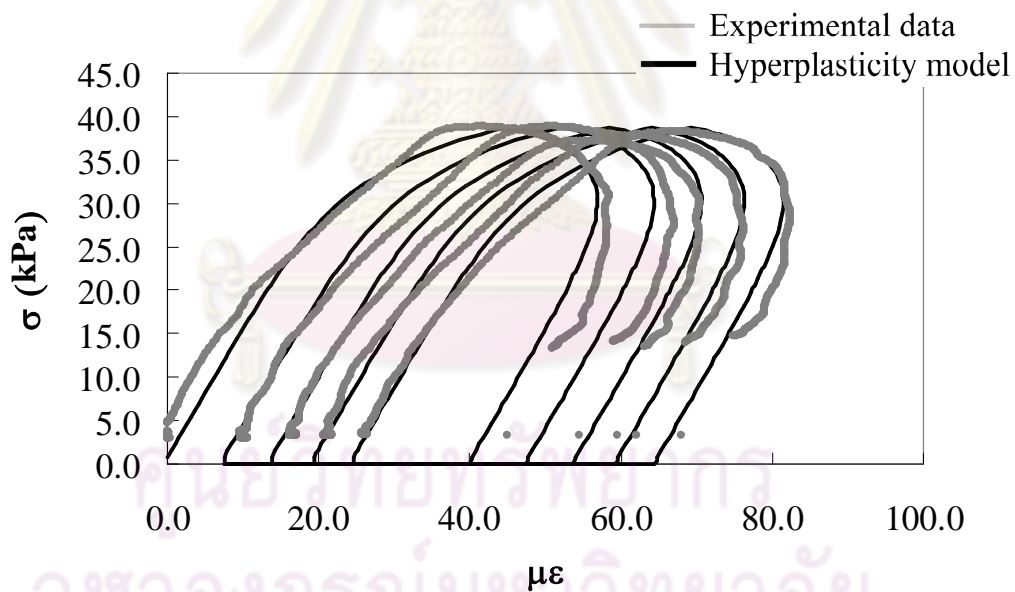


Figure 6.13 Stress-strain curves of asphaltic concrete under C-IDT test at 40°C

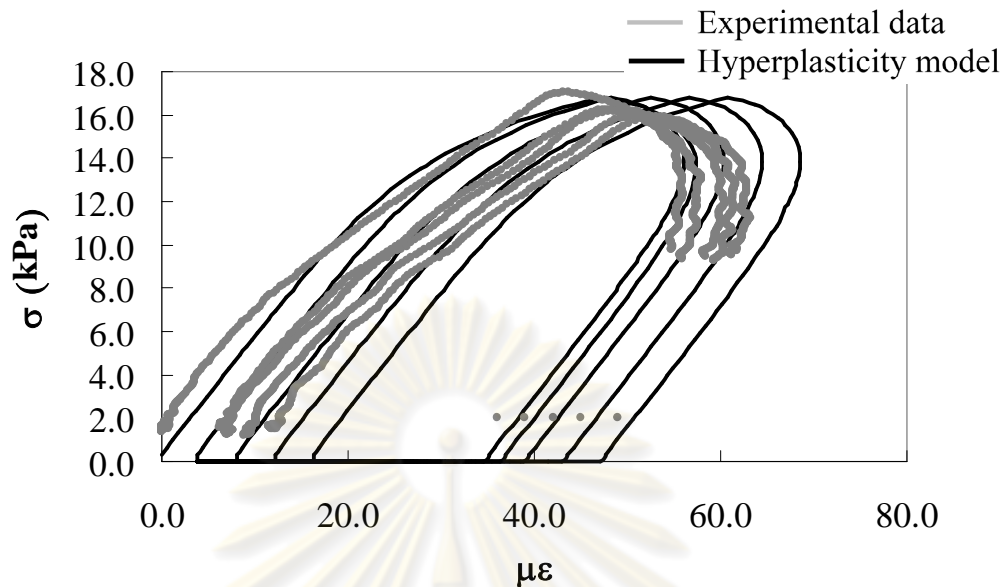


Figure 6.14 Stress-strain curves of asphaltic concrete under C-IDT test at 55°C

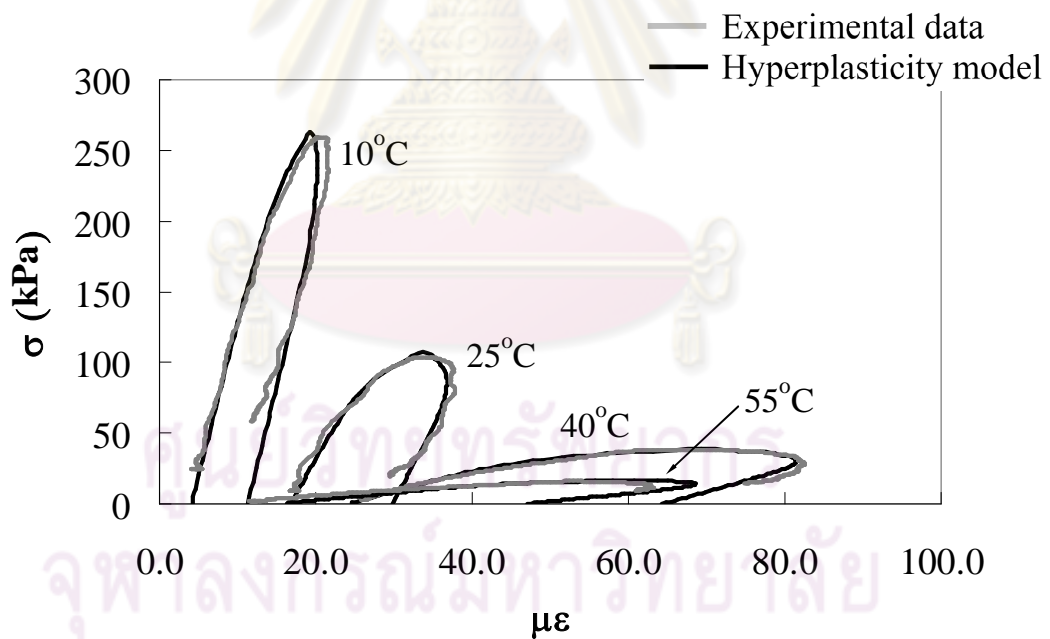


Figure 6.15 Comparison of stress-strain curve between experimental test and rate-dependent hyperplasticity model in the last cycle

The prediction of rate-dependent hyperplasticity model against the C-IDT test shows that E_I and k_1 are 1.00×10^{-11} GPa and 7.00×10^{-7} MPa. As for reference temperature θ_E and θ_k are 7.99×10^3 K and 4.20×10^3 K. From the parameter in term

of E , E_I in the cyclic condition is smaller than E_I in the static condition, yet θ_E of cyclic condition is higher than θ_E of static condition. For the parameters of k term (k_1 and θ_k) of both conditions, they are equal because the values of k_1 and θ_k do not influence to the stress-strain response. The parameter of temperature and the strain rate A , B , and C approximately are $4.88 \times 10^7 \text{ s}^{-1}\text{K}^{-1}$, $6.68 \times 10^3 \text{ K}$, $4.88 \times 10^{-2} \text{ MPa.K}^{-1}$. The estimated value of the activation energy is 55 kJ/mol. Finally, the shape controlling parameters of stress-strain graph of cyclic condition are equal to their values in static condition as α_0 is 1.00×10^{-2} and a is 4.0. This model used the same parameters as S-IDT are k_1 , θ_k , α_0 , and a . Figure 6.15 shows the last cycle of model comparing with experimental data. An investigation of this figure expresses that the model can predict the cyclic stress-strain curve at any temperature well.

6.5 Summary

In the predicting between the constitutive model and the experimental test, three sets of suitable parameter acquired from S-IDT, S-UC, and C-IDT tests are arisen. For comparison with S-IDT test, the model predictions at 10°C and 25°C show the good result as illustrated in the stress-strain curve. Nonetheless, the results at 40°C and 55°C are not quite good. For comparison with S-UC test, the stress-strain behaviour is predicted not well only at 10°C and high strain rates at 0.0167 and 0.0056 s^{-1} . Due to the fact that the brittle behaviour (stress-strain curve suddenly drop after peak) cannot be well predicted by rate-dependent hyperplasticity model, the model result does not match the test result. For comparison with C-IDT test, although the stress-strain curve at 55°C of both model and test result are slightly different, it is obvious that the model predictions show quite perfect result.

CHAPTER 7

Concluding Remarks

7.1 Introduction

The research finding can be pointed out into four points i.e. a numerical implementation, an experimental testing, a time-temperature superposition, and a future study.

7.2 Numerical implementation

This section indicates the practical use of constitutive model for predicting the asphaltic concrete behaviour. The model used in this research is the rate-dependent hyperplasticity model developed by Likitlersuang *et al.* (2009). The model was developed for predicting the shear behaviour of asphaltic concrete under different strain rate and temperature. The key feature of developed model can be summarized as follows:

In a static condition, the model prediction is compared with the data of S-IDT and S-UC tests. The result of model predicting shows that the model can be used to predict the asphaltic concrete behaviour at the wide range of changed temperatures and strain rates. In a cyclic condition, the rate-dependent hyperplasticity model is expressed to fit the cyclic loading same as traffic load effectively.

An advantage in using the rate-dependent hyperplasticity model is found that two potential equations can be employed to define the stress-strain relation. It is convenient and concise to apply the model to the numerical method comparing with other model in pavement engineering. Since this model can be used to examine the stress-strain behaviour well, they are possible to be developed for structural analysis of flexible pavement. There are few limitations in the development of rate-dependent hyperplasticity model. The model describes shear behaviour, and it displays in terms of one-dimensional variables (σ, ε) . The Gibbs free energy function does not contain

the terms which would correspond to thermal expansion or to heat capacity (see Houlsby and Puzrin (2006)). Furthermore, the behaviour of asphaltic concrete, in common with other geomaterials, includes important shear-dilatancy effects (especially at high shear stress levels) which are not taken into account here.

7.3 Experimental tests

The research demonstrates an investigation of strain rate and temperature effect on a crack propagation as well as a stress-strain-strength characteristic of asphaltic concrete both an indirect tensile mode and an unconfined compression mode by varied four strain rates and temperatures. The experimental data shows that the effects of strain rate and temperature strongly influence the mechanical behaviour of asphaltic concrete. Both Young's modulus and peak load of indirect tensile mode and unconfined compression mode rise following the increase of strain rate and the decrease of temperature. For the indirect tensile test, at the low temperature and high strain rate the asphaltic concrete obviously shows the brittle behaviour. At the high temperature (i.e. 55 °C), the pure tensile mode could not be observed, since the asphaltic concrete no longer behave as a brittle material. Finally, it can be concluded from this study that the strain rate and the temperature considerably affect to the measured peak strength and the stiffness of asphaltic concrete.

The testing result can prove that a temperature obviously affects to a resilient modulus (M_r) and a constitutive behaviour. The resilient modulus is decreasing when the temperature increases. The permanent strain or plastic strain of asphaltic concrete rises when the temperature is higher.

The test result verifies that the temperature change evidently influences the value of permanent deformation. The flow number (FN) is reducing when the temperature increases. However, at the low temperature (10°C) the permanent deformation cannot be observed in the first 40,000 cycles. This is because a material perfectly displays the purely elastic behaviour. At 25°C the asphaltic concrete can not be observed a failure in the creep rupture. The analysis of C-UC test results can be employed to evaluate the properties of AC 60/70 mixed material used in the flexible

pavement construction. This result of C-UC test furthermore demonstrates that the asphaltic concrete mixture produced by means of this research might not be suitable for the road in very hot condition.

7.4 Time-temperature superposition

The time-temperature superposition principle is selected to explain the effect of temperature and strain rate. The outstanding of this research is to prove that both a compressive and a tensile mode can be modelled with the single temperature shift function. Therefore, the master curve and the temperature shift parameter produced from both test series can be established. In accordance with both analysis results, the master curve and the temperature shift parameter are beneficial for evaluating the visco-elastic property of pavement design in Thailand.

The analysis of time-temperature superposition shows that it is very useful for estimating the strength value at the various temperatures and the strain rates. This time-temperature superposition analysis is also beneficial to solve the complication that only the loading rate controlling can be used without temperature controlling to study the stress-strain-strength characteristic of asphaltic concrete.

For limitation, the results of this research can be practically employed in the pavement research in Thailand or other tropical countries, and the results must be viewed with some cautions as they are based on temperature at 10°C to 55°C and dense grade mixture.

7.5 Future study

Because this research presents only the one-dimensional rate-dependent hyperplasticity model for the prediction of asphaltic concrete, to predict the practical behaviour truly occurred in the road this model need to be developed into two-dimension or three-dimension. To explain the pavement engineering problem happened in the real field, either two-dimensional model or three-dimensional model is then applied to the finite programme.

Due to the fact that most database system of asphaltic concrete which is available in Thailand is still not complete enough, this may because the apparatuses for studying the asphaltic concrete are very expensive. Besides, the pavement design in Thailand is depended on the empirical formula/chart instead of studying the real properties of asphaltic concrete. Consequently, the asphaltic concrete study is expanded. For an experimental test, the completed set of laboratory test of dense grade asphaltic concrete should be studied by changing the type of its asphalt cement such as AC 40/50 and AC 85/100 and also changing the aggregate type such as the limestone, granite and the basalt.



ศูนย์วิทยทรัพยากร
จุฬาลงกรณ์มหาวิทยาลัย

REFERENCES

- Annual Book of ASTM Standards. 1995. 1st ed. Vol 04.03. Detroit: American Society for Testing and Materials.
- Asphalt Institute. 1995. Superpave level 1 mix design. Superpave series No. 2 (SP-1). Kentucky.
- Chompoorat, T., and Likitlersuang, S. 2009. Temperature shift function of asphaltic concrete for pavement design in tropical countries. The IES Journal Part A: Civil and Structural Engineering Vol. 2 No. 3: 246-254.
- Chompoorat, T., Likitlersuang, S., and Legkanai, N. 2009. Temperature effect on permanent deformation of asphaltic concrete Proceeding of National Civil Engineering Conference 14th. Thailand. (In Thai)
- Chompoorat, T. and Likitlersuang, S. 2008. Effects of strain rate and temperature in the indirect tensile test of asphaltic concrete. Proceeding of KKCNN Symposium on Civil Engineering 21st. Singapore.
- Chompoorat, T. and Likitlersuang, S. 2008. Constitutive models for asphaltic concrete Proceeding of National Civil Engineering Conference 13rd. Thailand. (In Thai)
- Chompoorat, T., Likitlersuang, S., and Pumeer, K. 2008. Temperature effect on resilient modulus of asphaltic concrete Proceeding of National Transport Conference (NTC) 5th. Thailand. (In Thai)
- Houlsby, G.T. and Puzrin, A.M. 2000. A Thermomechanical Framework for Constitutive Models for Rate-Independent Dissipative Materials. An International Journal of Plasticity. 16(9): 1017-1047.
- Houlsby, G.T. and Puzrin, A.M. 2002. Rate-Dependent Plasticity Models Derived from Potential Functions. Proceeding of Rheology. 46(1): 113-126.
- Houlsby, G.T. and Puzrin, A.M. 2006. Principles of hyperplasticity (an approach to plasticity theory based on thermodynamics principles). 1st ed. London: Springer Verlag.
- Huang, Y.H. 2004. Pavement analysis and design. 2nd ed. New Jersey: Pearson Prentice Hall.

- Jahromi, S.G. and Khodaii, A. 2008. Carbon fiber reinforced asphalt concrete. The Arabian Journal for Science and Engineering Vol. 33 No. 2B: 355-364.
- Likitlersuang, S., Houlsby, G.T., and Chompoorat, T. 2009. A model for shear response of asphaltic concrete at different shear rates and temperatures. Proceeding of ASCE Journal of Engineering Mechanics (In pressed).
- Likitlersuang, S. and Houlsby, G.T. 2007. Prediction of a continuous hyperplasticity model for Bangkok Clay. An International Journal of Geomechanics and Geoengineering Vol. 2 No. 3: 147-157.
- Meor, O.H. and Teoh, C.Y. 2008. Effects of temperature on resilient modulus of dense asphalt mixtures incorporating steel slag subjected to short term oven ageing. Proceedings of world academy of science, engineering and technology Vol. 36: 221-225.
- Mitchell, J.K. and Soga, K. 2005. Fundamentals of soil behavior. 3rd ed. New Jersey: Wiley.
- Park, S.W., Kim, Y.R., and Schapery, R.A. 1996. A viscoelastic continuum damage model and its application to uniaxial behavior of asphalt concrete. Mechanics of materials Vol. 124 No. 1: 241-255.
- Park, S.W. and Kim, Y.R. 2001 Fitting prony-series viscoelastic models with power-law presmoothing. Journal of Materials in Civil Engineering Vol. 13 Issue 1: 26-32.
- Phromsorn, C., Anuvadesirikeart, S., Sirarom, P., and Gatenuiti, V. 2003. Properties on indirect tensile strength and resilient modulus of asphalt concrete utilized in Thailand. Report No. RD 204 Bureau of Road Research and Development. Department of Highway. Thailand. (In Thai)
- Puzrin, A.M. and Houlsby, G.T. 2001. A Thermomechanical Framework for Rate-Independent Dissipative Materials with Internal Functions. An International Journal of Plasticity. 17: 1147-1165.
- Puzrin, A.M. and Houlsby, G.T. 2003. Rate dependent hyperplasticity with internal functions. Proceedings of ASCE Journal of Engineering Mechanics Vol. 129 No. 3: 252-263.
- Schapery, R.A. 1999 Nonlinear viscoelastic and viscoplastic constitutive equations with growing damage. An International Journal of Fracture Vol. 97: 33-66.

- Schwartz, C.W., Gibson, N., and Schapery, R.A. 2002. Time-temperature superposition for asphalt concrete at large compressive strains. Transportation Research Record No. 1789: 101-112.
- Thammavong, A and Lavansiri, D. 2003. Stabilization of reclaimed asphalt pavement using foamed asphalt. Proceeding of Technology and Innovation for Sustainable Development Conference 1st. Thailand.
- Witczak, M.W., Kaloush, K., Pellinen, T., El-basyouny, M., Tempe, A.Z., and Von quintus, H. 2002. Simple performance test for superpave mix design (NCHRP report 465). Washington, DC: National Cooperative Highway Research Program (NCHRP).



ศูนย์วิทยทรัพยากร
จุฬาลงกรณ์มหาวิทยาลัย



APPENDIX

ศูนย์วิทยทรัพยากร
จุฬาลงกรณ์มหาวิทยาลัย

TECHNICAL NOTE

Temperature shift function of asphaltic concrete for pavement design in tropical countries

Thanakorn Chompoorat and Suched Likitlersuang*

Department of Civil Engineering, Faculty of Engineering, Chulalongkorn University, Phayathai Road, Bangkok 10330, Thailand

(Received 22 December 2008; final version received 28 April 2009)

Pavement design in many tropical countries like Thailand refers to the standard of America or Europe. These quoted standards were produced from experimental database of cold climate zone which is totally different from database collected in tropical area. To directly employ the design standard from one place to another may not be always appropriate. One way is to transform the database to check for important factors such as temperature, where cold climate countries environment is significantly differently from those in the tropical zone. The objective of this article is to evaluate the behaviour of asphaltic concrete under the varying temperature and strain rate by using the principle of time–temperature superposition both in compressive and tensile modes. A series of unconfined compression and indirect tensile tests were performed to failure or at large strain level. For both test series, the temperature was varied from 10 to 55°C and four different loading rates were applied. The constitutive results of two tests were cross-plotted to produce the master curve and temperature shift function.

Keywords: asphaltic concrete; unconfined compression test; indirect tensile test; strain rate; temperature; time–temperature superposition

1. Introduction

In general, the method that has been selected for the structural design of pavement in Thailand is analytical, based on the standard of the Asphalt Institute (AI) or AASHTO. Because this method depends on the database of each locality or country where the test outcome from one zone might not be appropriate for another zone, due diligence is needed. When the pavement design in Thailand is translated using research articles from America which are not calibrated with database or test results of Thai local materials, the applicability becomes questionable. This might be one of the causes of permanent deformation or rutting as generally detected on the roads of Thailand. According to the analytical method, the asphaltic concrete was assumed to be visco-elastic. However, the asphaltic concrete may show a plastic or irreversible behaviour. For example, in the case of the cycle carriage load occurred on the road, although the stress is lower than the yield strength of asphaltic concrete, irreversible strain takes place leading to failure. This irreversible strain signifies the plastic behaviour.

Many researches tried to prove that the asphaltic concrete exhibits thermo-visco-elasto-plastic behaviour. This is because the stress–strain–strength characteristic of asphaltic concrete will be changed when the temperature and/or strain rate are

transformed. At any temperature, the asphaltic concrete will deform slowly and permanently if the load is slowly applied. On the other hand, if a higher rate of loading is applied, the asphaltic concrete will behave much stiffer and might exhibit a fracture or crack. In addition, the asphaltic concrete will relax differently when there is the temperature variation at various strain rates. To define the effects of temperature and strain rate, Kim (2009) presented the qualitative strain rate versus stress-free temperature behaviour, as illustrated in Figure 1. This relation can be used to explain the mode of damage of asphaltic concrete. For instance, the asphaltic concrete specimen will collapse with the fracture (tensile) mode at high strain rate and low temperature conditions. However, the asphaltic concrete will fail by plastic flow at low strain rate and high temperature condition. Another possible failure mode is through microcracking at intermediate strain rate and low temperature condition.

In theory, the asphaltic concrete can be simply assumed as a thermo-rheologically simple (or linear visco-elastic) material. This material can be characterised in terms of a common time and temperature parameter, a so-called reduced time and then the time–temperature superposition can be applied. Schwartz *et al.* (2002) demonstrated a simple technique to explain the time–temperature superposition with growing damage based on the uniaxial compression

*Corresponding author. Email: fceslk@eng.chula.ac.th

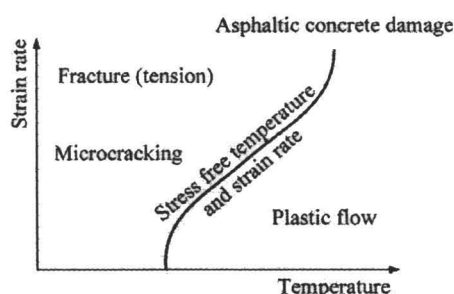


Figure 1. Effect of temperature and strain rate on asphaltic concrete.

constant rate test. They concluded that the master curve and temperature shift parameter can also be obtained from the uniaxial compression test.

This research aims to study the time-temperature superposition of asphaltic concrete, which is extended from the previous work reported by Schwartz *et al.* (2002). A series of unconfined compression (UC) and indirect tensile tests (IDT) each were used to evaluate the time-temperature superposition of asphaltic concrete. These two test series were carried out under wide ranges of temperatures and strain rates. The temperature conditions of both tests were varied at 10°C, 25°C, 40°C and 55°C, such as that experienced in practice on the pavement layer in tropical countries like Thailand. The loading rates were applied to the UC test at 0.0006, 0.0017, 0.0056 and 0.0167 s⁻¹, and to the IDT test at 0.0008, 0.0025, 0.0083 and 0.0250 s⁻¹, which was presented by Chompoorat and Likitlersuang (2008). The strain rates of both tests are commonly found in the traffic loads which are also specified by AASHTO T 283 (AASHTO 2001).

2. Theoretical background

2.1. Elasto-visco-plastic model

The characteristic of asphaltic concrete not only shows a completely elastic behaviour, but also shows plastic behaviour beyond first yield (or at large strain level). For instance, when the asphaltic concrete is loaded until it reaches the first yield and then is reloaded back to the original condition, the loading path will return to the origin. This shifted deformation comes from plastic strain or permanent strain. Apart from the plastic behaviour at large strain, it is well-known that the asphaltic concrete also shows the viscous behaviour such as time-delayed response from the traffic load.

Therefore, elasto-visco-plastic (EVP) theory is generally applied to the stress-strain analysis of pavement engineering. EVP theory can be described by the mechanical model as shown in Figure 2. This model is composed of three basic elements which are a

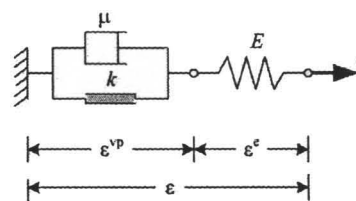


Figure 2. Elasto-visco-plastic model.

linear spring with spring constant (E), a slip friction with coefficient of friction (k) and a dashpot (pistons moving in a viscous fluid) with coefficient of viscosity (μ).

2.2. Time-temperature superposition

The properties of viscous material, for example, asphaltic concrete can be assumed to be a function of time and temperature. In general, it is difficult to describe the mechanic behaviour of asphaltic concrete under previous two functions. Fortunately, asphalt binder is thermorheologically simple material, which means that the effect of time can be replaced by the effect of temperature, and vice versa. The asphaltic concrete property as a function of time (or frequency) such as the complex modulus (E^*) or shear dynamic modulus (G^*) at various temperatures can be shifted along the horizontal log time (or log frequency) axis to form a single characteristic master curve. The E^* and G^* can be estimated following the dynamic modulus test (AASHTO TP 62) and the shear dynamic modulus test (AASHTO TP 7). For example in Figure 3, the modulus at any temperature can be modelled with a single curve at reference temperature named as a master curve. All curves are shifted by means of the temperature shift parameter ($a_T(T)$) which is defined:

$$a_T(T) = \frac{t}{t_R} \quad (1)$$

where, t is time (before shifting), and t_R is reduced time or time at reference temperature (after shifting) (see Figure 3).

Schapery (1999) developed the Schapery continuum damage model which explains the concept of the visco-plasticity with growing damage. This model consists of the visco-elastic correspondence principle, microstructure damage, and strain hardening visco-plastic behaviour. Schapery's continuum damage model is the separation of total strain ϵ_t into its components:

$$\epsilon_t = \epsilon_{ve} + \epsilon_d + \epsilon_{vp} \quad (2)$$

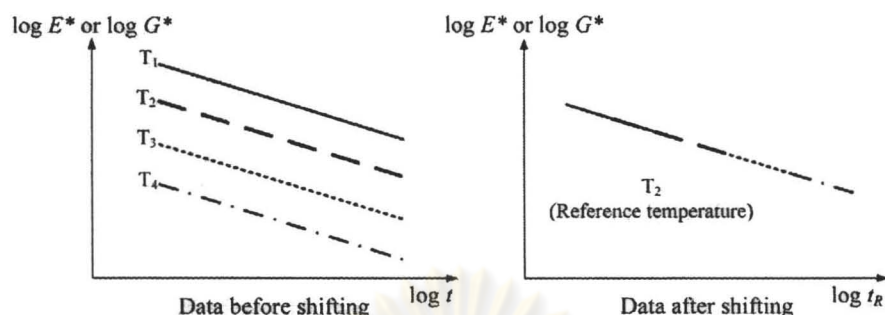


Figure 3. Data shifting to construct master curve.

where, ε_{ve} is the linear visco-elastic strain, ε_d is the strain due to microstructure damage, and ε_{vp} is the visco-plastic strain. For calculation of the temperature shift parameter corresponding to the total strain ε_t , Schapery (1999) concluded the components of ε_t may be interchanged using the time-temperature superposition.

$$a_{Tve}(T) = a_{Td}(T) = a_{Tvp}(T) \quad (3)$$

where, $a_{Tve}(T)$, $a_{Td}(T)$ and $a_{Tvp}(T)$ are temperature shift parameter for visco-elastic, microstructure damage, and visco-plastic behaviour, respectively.

Schwartz *et al.* (2002) presented the time-temperature superposition with growing damage, which it was verified by the uniaxial compression constant strain rate tests at large-strain values. According to the uniaxial compression test results, the master curves (stress vs. reduced time) and corresponding time-temperature shift functions curve are obtained. The procedure producing both curves falls under the cross-plot method. Note that since the strain value is fixed, this plot is similar to a modulus versus log time curve. The procedure of cross-plot is schematically illustrated in Figure 4 and can be explained as follows. First, a given magnitude of strain reference is selected. For this strain at a given temperature, the magnitude of stress and time are determined for each strain rate. Secondly, the relation of log stress and log time for the given strain magnitude are constructed. Finally, the log stress and log time curves for each temperature are shifted to produce the master curve, and the temperature shift function is constructed by the same procedure as the dynamic modulus test and shear dynamic modulus test.

3. Experimental programme and result

The materials employed in this study are designed according to the Marshall method. The grade of asphalt cement is AC 60/70 and the nominal maximum

size of aggregate is 12.5 mm. All of these materials are practically used for road construction in Thailand. These selected materials are designed with a mix of 5.5% by weight of AC 60/70. The specimen dimension used is 100 mm diameter with 65 mm height for the IDT test. On the other hand, the specimen of 100 mm diameter with 150 mm height is prepared for the UC test. The asphaltic concrete mixtures are compacted by Superpave Gyrotory Compactor (SGC) which is controlled by computer. The mould of SGC is rotated through a 1.25 ± 0.02 degree pivot angle. While the mould is being rotated at 30 rev/min, a 600 ± 18 kPa static load is placed on the specimen through the use of a ram. The density of $2400\text{--}2450$ kg/m³ (based on Marshall mixed design) and air void content of 3–5% were achieved after compaction using SGC.

The universal testing machine with static loading condition is employed in this study. The UC specimen is loaded along the specimen height in static condition; on the other hand, the IDT specimen is loaded across its diametric plane in static condition. The radial and axial strains are measured by means of four strain gauges (two for radial strain and two for axial strain). To investigate the effect of loading rate on the development of micro-cracking until failure, four different strain rates which are 0.0006, 0.0017, 0.0056 and 0.0167 s⁻¹ for UC test and 0.0008, 0.0025, 0.0083 and 0.0250 s⁻¹ for IDT are applied. The temperatures selected in this study are 10°C, 25°C, 40°C and 55°C.

Figures 5 to 8 summarise the measured stress and strain responses of the UC tests for all four temperatures. At 10°C (Figure 5), the maximum stress typically occurred at the strain value of $\sim 1.5\%$. The magnitude of maximum stress increased with increasing strain rate; however, the strain rate hardly influenced the peak strain. The overall characteristic and quality of the data from 25°C, 40°C, and 55°C are similar to those from 10°C. Nevertheless, there are evident anomalies in the data of 40°C and 55°C at the rate of 0.0056 s⁻¹. The curves are slightly flatter and the maximum stress values are smaller than expected.

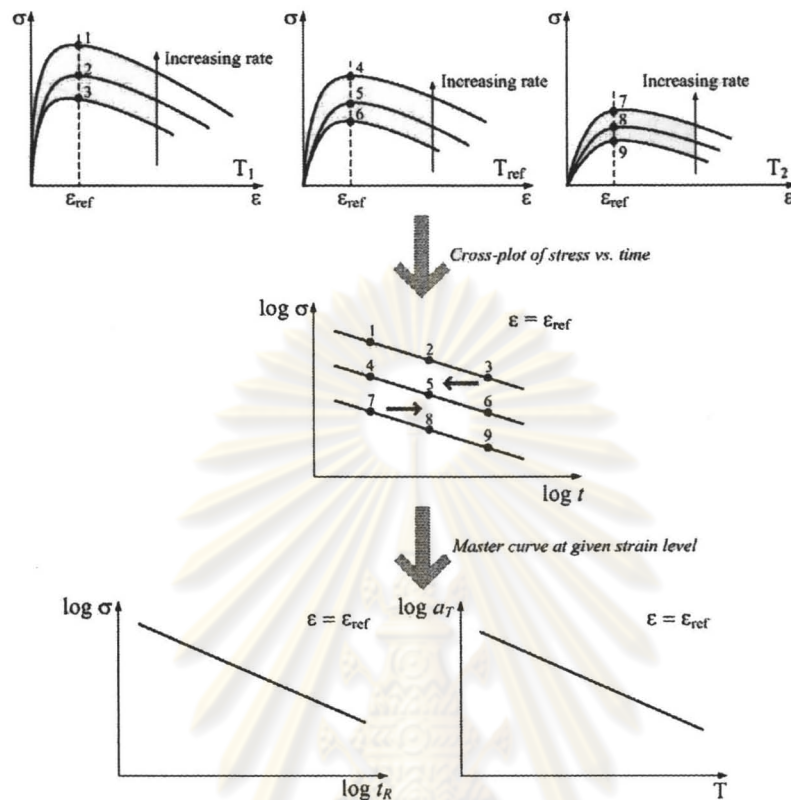


Figure 4. Schematic of time-temperature superposition principle using cross plot.

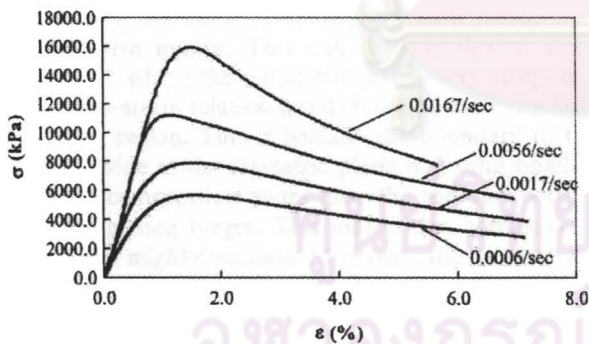


Figure 5. Stress-strain behaviour of UC tests with different strain rates at 10°C.

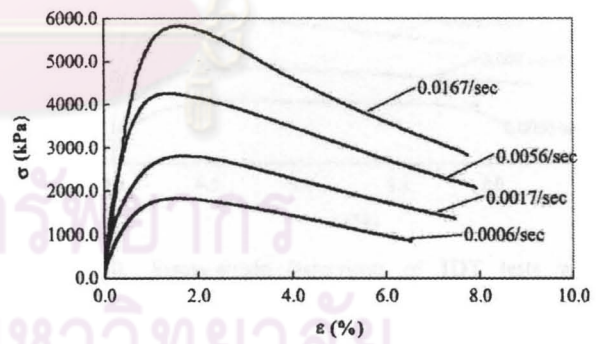


Figure 6. Stress-strain behaviour of UC tests with different strain rates at 25°C.

In the UC mode, all of the specimens tested failed perfectly in compression mode. The typically failure mode observed is shown in Figure 9.

The mechanical responses of all four temperatures during the IDT tests are shown in Figures 10 to 13. At the lowest temperature (Figure 10), the asphaltic mixture has the highest peak stress, and it effectively shows the tensile behaviour. It can be observed the

strength suddenly drops after peak due to the fact that at low temperature, the asphaltic concrete behaves as a brittle material especially for the fastest test (0.0250 s^{-1}). The failure mechanism exhibits almost pure tensile mode as shown in Figure 14.

At standard temperature (25°C), the IDT behaviour can be competently expressed similarly as at 10°C, but for the stress-strain curve of the lowest

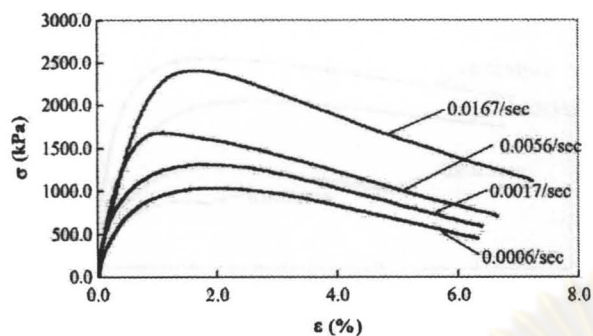


Figure 7. Stress-strain behaviour of UC tests with different strain rates at 40°C.

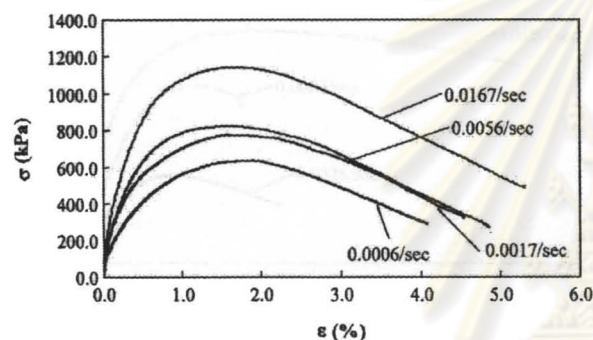


Figure 8. Stress-strain behaviour of UC tests with different strain rates at 55°C.

strain rate (0.0008 s^{-1}), it displays both tensile and compressive modes. This can be investigated from Figure 11 where the initial stiffness is very steep, but the stress-strain relation trends rebound after reaching the peak region. This is because the boundary of the tension zone at the diametric plane is getting smaller, and the compression zones near the top and bottom cap are getting bigger. This means that compression behaviour might dominate. Moreover, the stress-strain behaviour of specimens at 40°C (Figure 12) is similar to those at 25°C. The effect on compression zones around the top and bottom cap is more obvious especially at the slowest test (0.0008 s^{-1}).

At the highest temperature (55°C), the stress-strain behaviour can be measured only by the fastest test (0.0250 s^{-1}); nevertheless, its behaviour is not in purely tensile mode. There is also no the tensile behaviour observed at the other strain rates (see Figure 15).

4. Analysis of experimental results

The analysis can be separated into two parts: (i) the strength and stiffness, (ii) and the time-temperature

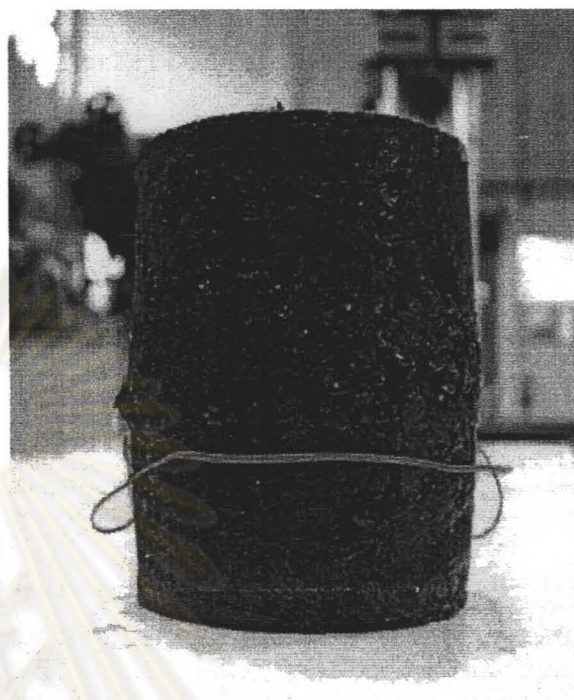


Figure 9. Typical failure mechanism of asphaltic concrete under UC test.

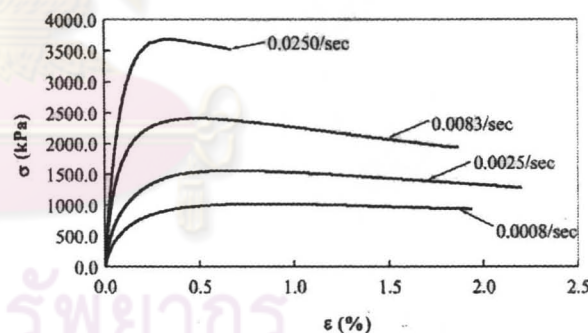


Figure 10. Stress-strain behaviour of IDT tests with different strain rates at 10°C.

superposition. Firstly, we focus on the strength and stiffness of asphaltic concrete both compression and tension mode. The maximum stress (σ_{max}) and the secant Young's modulus at 50% of maximum stress (E^{50}) of UC and IDT tests are measured as presented in Tables 1 and 2, respectively. Figures 16 to 19 show the variation of E^{50} and σ_{max} with temperature from the UC and IDT tests. It can be concluded that both E^{50} and σ_{max} roughly increase with the strain rate and temperature. However, there are evident anomalies of E^{50} under the UC condition at the strain rate of 0.0167 and 0.0056 s^{-1} data and at temperature of 25°C and

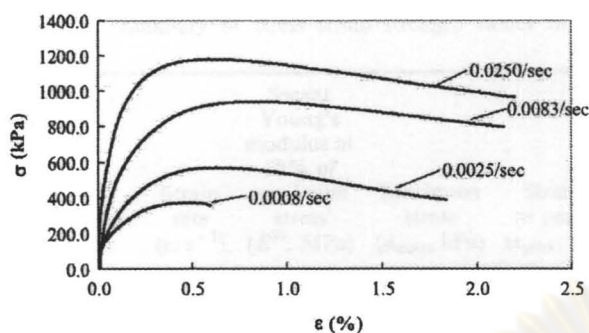


Figure 11. Stress–strain behaviour of IDT tests with different strain rates at 25°C.

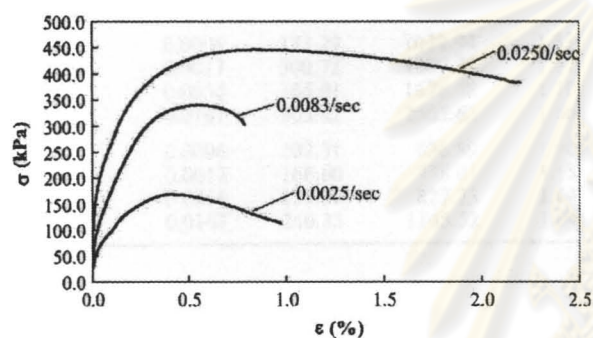


Figure 12. Stress–strain behaviour of IDT tests with different strain rates at 40°C.

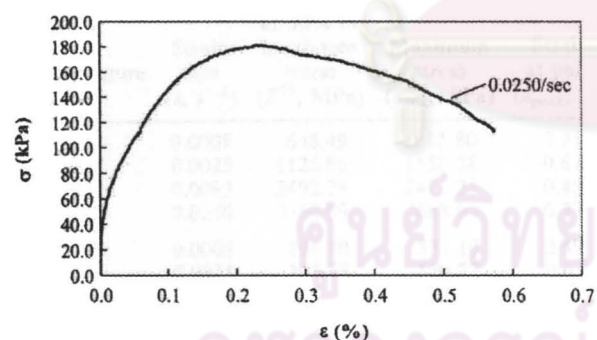


Figure 13. Stress–strain behaviour of IDT test at 55°C.

40°C (see Figure 16). This is because it is difficult to control the first contact between the specimen and the loading plate perfectly. Resulting from those, there is a slight effect at the beginning of loading at the highest strain rate. The strain at peak is measured as presented in Tables 1 and 2 for the UC and IDT tests, respectively. The range of peak strain from the UC tests scattered around 1.10–1.90% (average 1.50%) between upper and lower bound as shown in Figure 20. This value is smaller than what is typically found in

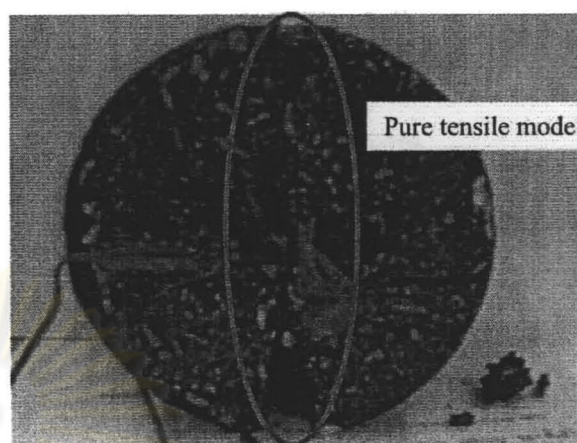


Figure 14. Example of failure mechanism of asphaltic concrete under IDT test at 10°C and strain rate of 0.0083 s^{-1} .

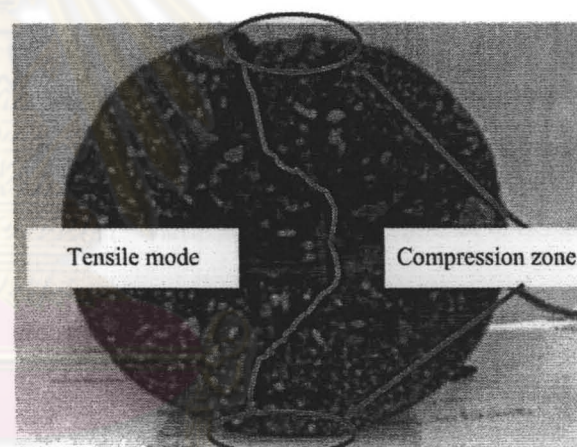


Figure 15. Example of failure mechanism of asphaltic concrete under IDT test at 55°C and strain rate of 0.0008 s^{-1} .

concrete (the compressive strain before failure of concrete is around 3%). The data of strain at peak of IDT tests are even more scattered to form any useful conclusion as shown in Figure 21. The range of peak strain from the IDT tests is 0.23–0.91% (average 0.5%) which matches that of concrete which has the tensile strain before failure around 0.8–1.0%.

Secondly, the time–temperature superposition of asphaltic concrete at large strains can be analysed based on the same framework of Schwartz *et al.* (2002). However, the analysis is extended to both the UC and IDT tests. The reference strain of UC and IDT tests are selected at 1.5% and 0.5% as they represent the average peak strain of the compression and tension

Table 1. Summary of stress-strain-strength values from UC tests.

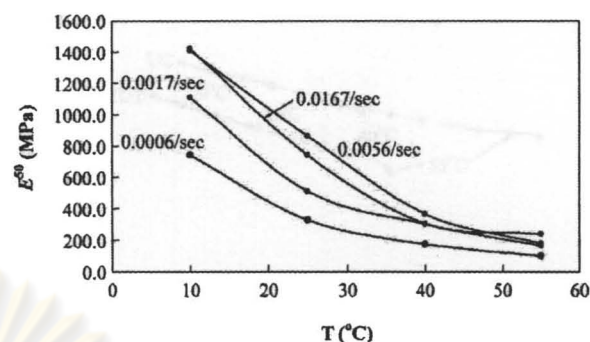
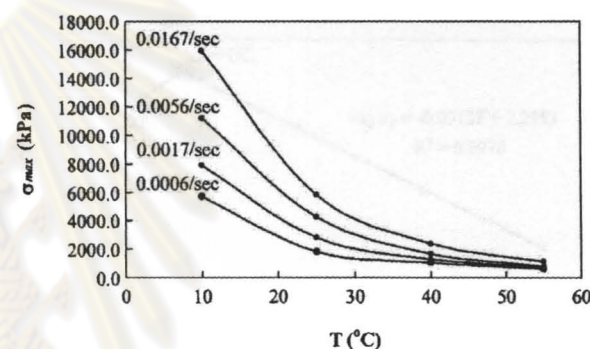
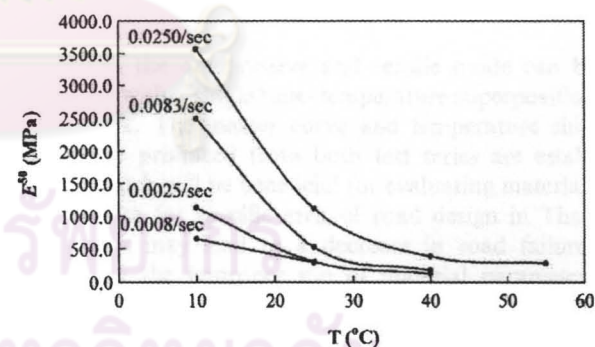
| Temperature (T, °C) | Strain rate ($\dot{\epsilon}$, s ⁻¹) | Secant Young's modulus at 50% of maximum stress (E^{50} , MPa) | Maximum stress (σ_{max} , kPa) | Strain at peak (ϵ_{peak} , %) |
|---------------------|--|---|--|---|
| 10 | 0.0006 | 742.84 | 5685.64 | 1.58 |
| | 0.0017 | 1107.29 | 7894.84 | 1.53 |
| | 0.0056 | 1409.99 | 11202.93 | 1.13 |
| | 0.0167 | 1419.54 | 15910.43 | 1.52 |
| 25 | 0.0006 | 325.71 | 1827.37 | 1.57 |
| | 0.0017 | 508.35 | 2807.38 | 1.68 |
| | 0.0056 | 864.86 | 4251.71 | 1.36 |
| | 0.0167 | 741.44 | 5824.72 | 1.64 |
| 40 | 0.0006 | 172.29 | 1032.94 | 1.83 |
| | 0.0017 | 300.72 | 1307.77 | 1.67 |
| | 0.0056 | 365.01 | 1678.48 | 1.10 |
| | 0.0167 | 303.62 | 2405.62 | 1.66 |
| 55 | 0.0006 | 102.31 | 636.89 | 1.90 |
| | 0.0017 | 166.60 | 778.01 | 1.58 |
| | 0.0056 | 179.99 | 827.23 | 1.64 |
| | 0.0167 | 240.33 | 1145.52 | 1.64 |

Table 2. Summary of stress-strain-strength values from IDT tests.

| Temperature (T, °C) | Strain rate ($\dot{\epsilon}$, s ⁻¹) | Secant Young's modulus at 50% of maximum stress (E^{50} , MPa) | Maximum stress (σ_{max} , kPa) | Strain at peak (ϵ_{peak} , %) |
|---------------------|--|---|--|---|
| 10 | 0.0008 | 646.49 | 1015.80 | 0.91 |
| | 0.0025 | 1126.86 | 1558.38 | 0.67 |
| | 0.0083 | 2492.28 | 2411.35 | 0.48 |
| | 0.0250 | 3560.99 | 3688.94 | 0.32 |
| 25 | 0.0008 | 294.80 | 372.10 | 0.49 |
| | 0.0025 | 305.78 | 570.27 | 0.63 |
| | 0.0083 | 525.04 | 938.89 | 0.81 |
| | 0.0250 | 1117.31 | 1180.08 | 0.59 |
| 40 | 0.0008 | N/A | N/A | N/A |
| | 0.0025 | 168.96 | 168.96 | 0.55 |
| | 0.0083 | 180.38 | 340.67 | 0.55 |
| | 0.0250 | 393.07 | 446.27 | 0.85 |
| 55 | 0.0008 | N/A | N/A | N/A |
| | 0.0025 | N/A | N/A | N/A |
| | 0.0083 | N/A | N/A | N/A |
| | 0.0250 | 280.24 | 181.29 | 0.23 |

N/A, not available (test cannot be performed).

test, respectively. The relation between stress at the reference strain (σ_{ref}) and reduce time (t_R) of both the UC and IDT tests can be approximated as a simple

Figure 16. Variation of E^{50} with temperature of UC tests.Figure 17. Variation of σ_{max} with temperature of UC tests.Figure 18. Variation of E^{50} with temperature of IDT tests.

linear relationship as shown in Figure 22. The relationship between temperature shift parameter (a_T) and temperature can be concluded:

$$\log a_T = -0.0913T + 2.2353 \quad (4)$$

where, T is the temperature in °C. The regression analysis illustrated that the Equation (4) has $R^2 = 0.9978$ as shown in Figure 23.

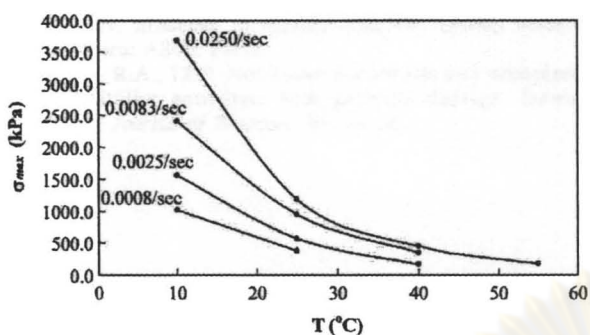


Figure 19. Variation of σ_{max} with temperature of IDT tests.

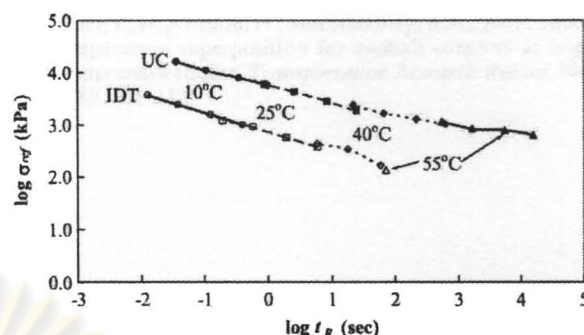


Figure 22. Stress-reduce time master curve from UC and IDT tests.

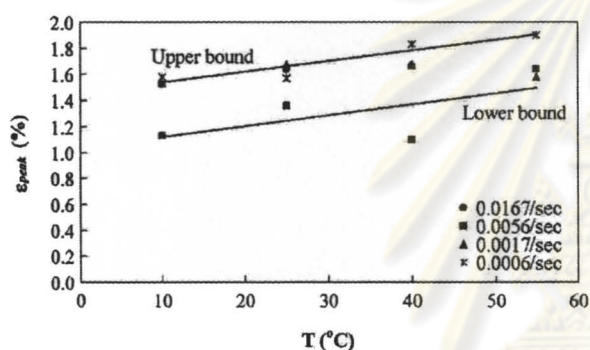


Figure 20. Variation of ϵ_{peak} with temperature of UC tests.

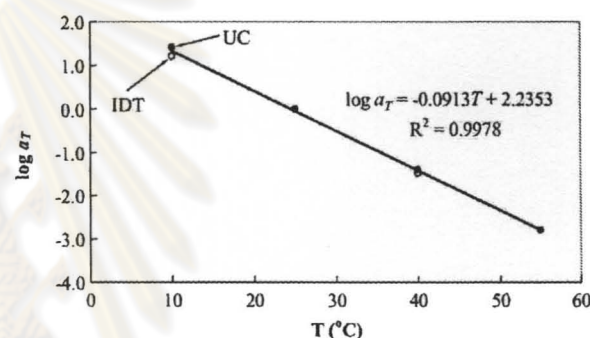


Figure 23. Time-temperature shift function from UC and IDT tests.

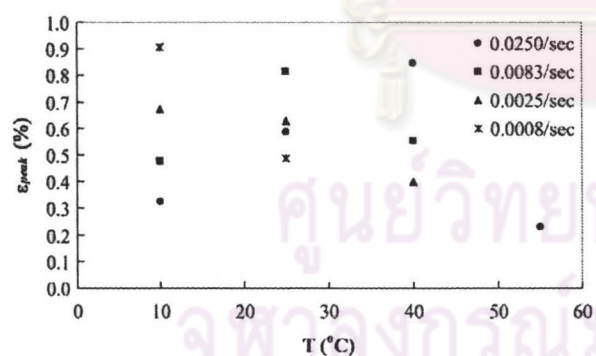


Figure 21. Variation of ϵ_{peak} with temperature of IDT tests.

5. Conclusions

This research presents the stress-strain behaviour of asphaltic concrete under wide range of temperatures and strain rates by means of the unconfined compression and indirect tensile tests. The time-temperature superposition principle is selected to explain the effect of temperature and strain rate. This research proves

that both the compressive and tensile mode can be modelled with a single time-temperature superposition framework. The master curve and temperature shift parameter produced from both test series are established, which will be beneficial for evaluating materials appropriate for specific area of road design in Thailand. This may lead to a decrease in road failures caused by the improper use of material parameters such as temperature. The results of this study may be useful for pavement research in Thailand or other tropical countries. However, the results must be viewed with some caution as they are based on temperature at 10°C to 55°C and dense grade mixture.

References

American Association of State Highway and Transportation Official (AASHTO), 2001. *Standard specifications for transportation material and method of sampling and testing*. 19 ed. Washington, DC: United State of America.
 Chompoorat, C. and Likitlersuang, S., 2008. Effects of strain rate and temperature in the indirect tensile test of asphaltic concrete. *In: The Twenty-First KKCNN Symposium on Civil Engineering, Singapore, 25-28.*

Kim, 2009. *Modeling of asphalt concrete*. United State of America: ASCE Press.

Schapery, R.A., 1999. Nonlinear viscoelastic and viscoplastic constitutive equations with growing damage. *International Journal of Fracture*, 97, 33–66.

Schwartz, C.W., Gibson, N., and Schapery, R.A., 2002. Time-temperature superposition for asphalt concrete at large compressive strains. *Transportation Research Record*, No. 1789, 101–112.



ศูนย์วิทยทรัพยากร
จุฬาลงกรณ์มหาวิทยาลัย

BIOGRAPHY

On August 4th, 1980 I was born in Bangkok, Thailand. I attained my Bachelor of Engineering in Civil Engineering from Srinakharinwirot University in 2002. I furthered my study to earn a Master of Engineering in Civil Engineering (Geotechnical Engineering) from Chulalongkorn University in 2003. With my intention of graduation in Ph.D., I started studying at Department of Civil Engineering (Geotechnical Engineering), Chulalongkorn University in 2006. During studying in Ph.D. Degree, I held the TA scholarship and the scholarship of Professor Dr. Supradit Bunnag funds on supporting the research expenses. I was also selected to be a representative of civil engineering graduate student. All semesters I attended at Chulalongkorn University, my progress both in education and in life experience has been smoothly expanded by the great advisor of my dissertation, Assistant Professor Dr. Suched Likitlersuang. The main theme of my research is an experimental and a numerical study of asphaltic concrete under tropical environments. I moreover took an opportunity to be a part of four projects which are under the cooperation of professors of Civil Engineering Department and other firms. Those four projects are Analysis of Land Subsidence in Bangkok Metropolitan and its Vicinity Area, Evaluation of porous asphalt pavement performance, Study of soil settlement affected to PTT gas pipeline, and Developing the flexible pavement material for road construction in Thailand using the analytical method. While studying the Ph.D. program, ten papers of mine had been already submitted to International Conference on Soil Mechanics and Geotechnical Engineering 17th (1 paper), The 20th, 21st, and 22nd KKCNN Symposium on Civil Engineering (3 papers), The 13th and 14th National Civil Engineering Conference (4 papers), and The 5th National Transport Conference (2 papers). An article, Constitutive Models for Asphaltic concrete, written by me and my advisor were selected by Roads Association of Thailand on the honourable mention of technical paper award. Before I finished my Ph.D., my devotion and working hard on my study enabled me to be accepted from both The IES Journal Part A: Civil and Structural Engineering, and Journal of Engineering Mechanics, ASCE to publish two international academic journals provided by me and my advisor.